Cartilage Stress Relaxation Induced by Intra-tissue Transport of Cationic Nanoparticles: Implications for Post-traumatic Osteoarthritis Drug Delivery

by

Whitney Terese Young

B.S. Bioengineering
University of Toledo, 2011

Submitted to the Department of Mechanical Engineering in
Partial Fulfillment of the requirements for the degree

Master of Science in Mechanical Engineering

at the

Massachusetts Institute of Technology

June 2016

Signature of Author: _____
Department of Mechanical Engineering
May 20, 2016

Certified by: _____
Alan J. Grodzinsky
Professor Biological, Electrical and Mechanical Engineering
Thesis Advisor

Accepted by: _____
Rohan Abeyaratne
Professor Mechanical Engineering
Chairman, Committee on Graduate Students

Cartilage Stress Relaxation Induced by Intra-tissue Transport of Cationic Nanoparticles: Implications for Post-traumatic Osteoarthritis Drug Delivery

by

Whitney Terese Young

Submitted to the Department of Mechanical Engineering
on May 20, 2016 in Partial Fulfillment
of the Requirements for the Degree of
Master of Science in Mechanical Engineering

ABSTRACT

Avidin has previously been proposed as a drug carrier molecule for intra-articular injection of osteoarthritis (OA) therapeutics. Its nanoscale size and net positive charge make it a viable candidate for transport into and through articular cartilage, one of the most affected tissues in OA. Avidin has been shown to have a high uptake into and long retention time within cartilage, and is also non-toxic to chondrocytes. The goal of this thesis was to assess whether avidin has any deleterious effects on the mechanical properties of cartilage as it moves into and through the tissue.

Using cartilage explants in vitro, mechanical stress relaxation experiments were performed at two ionic strengths (low = 0.015 M NaCl and physiologic = 0.15 M NaCl) in the presence and absence of added avidin. After an initial set of compressive strain ramps and relaxations, 100 μM avidin was added to the test chamber to determine whether additional changes in the stress relaxation behavior occurred. The stress was monitored for 18 hours after the addition of avidin. In addition, real-time one-dimensional transport experiments were performed to estimate the diffusivity of avidin within cartilage. Experiments were conducted using both immature (2 – 3 weeks old) bovine and adult (26 – 62 years old) human cartilage.

Avidin was found to have effects on the mechanical properties of cartilage in certain environmental conditions. At the lower ionic strength, avidin caused both the bovine and human cartilage to relax to a lower final equilibrium stress. Addition of avidin to bovine cartilage disks in physiologic ionic strength caused a faster stress relaxation and an increased tissue Young's modulus. However, in the most clinically relevant condition tested—adult human cartilage in physiologic ionic strength—no differences were observed in the mechanical properties when avidin was added. Diffusive transport times for avidin through cartilage were found to be ~4-fold faster in immature bovine cartilage compared to adult human cartilage.

The results of these studies suggest that avidin does not adversely affect the mechanical strength of cartilage in clinically relevant conditions, a critical requirement of any drug delivery vehicle to cartilage. Although this study focused on avidin as a potential drug-carrying nanoparticle, the protocols and analysis methods developed can be used to study other candidate drug carriers in the future.

Thesis Supervisor: Alan J. Grodzinsky
Title: Professor Biological, Electrical and Mechanical Engineering

ACKNOWLEDGEMENTS

I would like to start by thanking my advisor, Alan Grodzinsky, for his constant support, enthusiastic encouragement and unmatched optimism. I can't count the number of times Al assured me that my *next* attempt was going to be the one that worked. That kind of unwavering confidence kept me going when I felt like everything was working against me. I also greatly appreciated Al's genuine open-door policy. There was never a time I stopped by his office to ask a question that I didn't get his full attention and a detailed explanation. Al's enthusiasm for facilitating the learning of his students is remarkable. I could not have done this without him and learned so much from him along the way.

I would also like to thank all members of the Grodzinsky lab for their friendship and the welcoming environment they have created; it was truly a pleasure working in this group. In particular, I have to say that Han-Hwa Hung's help with day-to-day lab-related issues was instrumental to the progress of my experiments. Also, Eliot Frank's deep understanding of everything technical was so helpful in troubleshooting my experiments and protocols. Working in collaboration on experiments and modeling with Yamini Krishnan was not only helpful and informative, but also enjoyable. I would also like to thank Paul Liebesny, my desk and lab mate, for the numerous coffee runs, experimental troubleshooting chats and general life conversations to break up the workload!

This endeavor also would not have been possible without the support (financial and otherwise) of MIT Lincoln Laboratory. My group and leadership (Jeff Palmer, Catherine Cabrera and Paula Collins) there have been nothing but supportive of my graduate studies and I cannot thank them enough for that. Finally, I would like to thank my friends and family for their support and encouragement over the last 2 years, the journey would not have been as enjoyable without them.

TABLE OF CONTENTS

GLOSSARY

ACL	anterior cruciate ligament
Da	dalton (= 1 g/mol)
Dex	dexamethasone
DMEM	Dulbecco's modified eagle medium
DMMB	dimethyl-methylene blue
DMOADs	disease modifying osteoarthritis drugs
DZ	deep zone
ECM	extracellular matrix
EDC	EthylDiaminopropylCarbodiimide
FITC	fluorescein isothiocyanate
GAG	glycosaminoglycan
HA	hyaluronic acid
IA	intra-articular
IL-1	interleukin 1
kDa	kilo Dalton
LME	linear mixed effects
MDa	mega Dalton
MMP	matrix metalloprotease
MW	molecular weight
MZ	middle zone
NEAA	non-essential amino acids
NHS	N-Hydroxy Succinimide
NSAIDs	non-steroidal anti-inflammatory drugs
OA	osteoarthritis
PBS	phosphate buffered saline
PEG	polyethylene glycol
pI	isoelectric point
PTOA	post-traumatic osteoarthritis
RRx	Rhodamine Red
SEM	standard error of the mean
SF	synovial fluid
sGAG	sulfated glycosaminoglycans
SZ	superficial zone
TNF-α	tumor necrosis factor-α
TxR	TexasRed

LIST OF FIGURES

LIST OF TABLES

1 INTRODUCTION

1.1 Problem Statement

Osteoarthritis (OA) is one the most common joint diseases and is increasing in prevalence. Of the top 30 diseases and injuries that contribute to disability-adjusted life-years in the United States, OA is one of 10 that increased by more than 30% from 1990 to 2010[1]. OA is a progressive disease that affects diarthrodial joints (e.g., knee, hip, wrist) and is characterized by articular cartilage loss, increased bone density and formation of osteophytes (spurious bone growths)[2]. Other tissues in the joint—ligaments, synovium, etc.—are also susceptible to the disease through degradation and/or inflammation. OA has several risk factors, one of which is joint trauma. OA that occurs after a traumatic joint injury, such as an ACL tear, is a subset of OA called post-traumatic osteoarthritis (PTOA) and accounts for 12% of the disease burden[3]. Unlike most types of OA, PTOA has the unique feature of knowing the time of disease onset—the time of the injury. This presents a unique opportunity for early intervention in the progression of the disease[4].

Although several therapeutic options exist to manage pain, decrease inflammation and increase joint lubrication, no disease modifying osteoarthritis drugs (DMOADs) exist. Preventing or delaying the degeneration of articular cartilage is a major focus of current OA therapeutics research. Articular cartilage is a specialized tissue that provides compressive strength in joints and also allows for near frictionless articulation of the bones. Its degeneration in OA leads to decreased compressive loading abilities and eventually to painful bone-on-bone contact.

Systemically delivered drugs struggle to reach articular cartilage because it is an avascular tissue. Combined with the fact that OA is a localized disease, intra-articular (IA) injection of therapeutics is thought to be a better delivery method for OA drugs, especially when cartilage is the target. Injecting the drug directly into the joint reduces systemic side effects and increases the concentration of drug seen by the target. With these benefits come the difficulties of rapid clearance from the joint by the lymphatic system and potentially harmful effects to joint tissues due to the increased drug concentration[5]. In addition to the

research focusing on DMOADs, OA therapeutics research is also focused on reducing the challenges associated with IA injection.

Dexamethasone (dex), a small, synthetic glucocorticoid drug, is currently used in treatment of late-stage OA to reduce joint inflammation and pain. Recent studies have shown dex's potential as an inhibitor of cartilage degradation, particularly in the case of PTOA[6,7,8,9]. Recent work by Bajpayee has focused on developing a delivery method for dex that would increase its residence time in the joint and uptake into cartilage without causing harm to any of the joint tissues[10,11]. She developed an avidin-based delivery system that has been shown to have high specificity and retention time in cartilage and is not toxic to chondrocytes. An additional measure that needs to be investigated for safety, and the focus of this work, is the effect of avidin itself on the mechanical integrity of cartilage. Cartilage provides the majority of the compressive strength in joints. If injection of an avidin-dex drug delivery system adversely affects the mechanical properties of cartilage due to the properties of avidin (e.g., physicochemical), the joint as a whole could be weaker and susceptible to further damage. Understanding the effect, if any, and its timeline could guide the recommendations of clinicians for post-injection activity.

1.2 Specific Aims

The primary goal of this work was to assess the effects, if any, that avidin has on the mechanical properties of articular cartilage as measured by stress relaxation. Additionally, this work aimed to create a framework that can be used for testing the effects of future drug delivery systems on the mechanical, transport and biological properties of articular cartilage. Finally, this work sought to compare the aforementioned effects on immature bovine cartilage to adult human cartilage.

1.3 Scope of Report

One main type of experiment run for this work was long-term mechanical stress relaxations. Small[†], cylindrical disks of articular cartilage with the superficial zone (SZ) intact were loaded into an unconfined compression chamber, bathed in testing solution and compressed to a specified strain. The strain was maintained for 12-24 hours and stress

[†] 3 mm diameter x 1 mm thick
[‡] 6 mm diameter x ~500 μm thick
[§] Formulation for medium in Appendix 8.1 (pg. 73)

measurements were continuously collected. For baseline, negative control samples, nothing was done to the sample during the strain hold. These runs established the natural behavior of cartilage over this extended time period. The only difference for samples measuring the effects of avidin was the addition of 100 μM of avidin to the chamber after the first two hours. Low (0.015 M) and physiologic (0.15 M) ionic strength testing solutions were used and samples from both immature bovine and adult human were tested. Exponential curves were fit to the relaxations and the fitted parameters of the negative control samples were compared to the samples in which avidin was added.

Previous work[12] has shown that the rate limiting process in stress relaxation induced by changes in bath salt concentration is the diffusion of ions into and through the cartilage. Hypothesizing that the diffusion of avidin through cartilage may influence the mechanical stress relaxation, real-time transport experiments were run to determine the diffusivity of avidin in cartilage. Larger, thinner[‡] disks of cartilage with the SZ intact were sandwiched between two chambers such that the only path of transport from one to the other was through the cartilage. The movement of fluorescein isothiocyanate (FITC) labeled avidin from the upstream chamber through cartilage and into the downstream chamber was monitored by circulating the downstream liquid through a spectrofluorometer that continuously measured the fluorescence. The resulting curve of increasing fluorescence over time was used to determine the diffusivity of avidin by fitting the data to a linearized diffusion model. Transport was measured in both immature bovine and adult human.

Due to the length of both the mechanical and transport experiments (24-48 hours), there was concern about loss of cartilage matrix throughout the duration, which could affect the mechanical and transport properties being measured. To address this concern, control experiments that measured matrix loss in a variety of conditions were run to determine suitable storage and running conditions. Other experiments to characterize the experimental setups were also run including noise assessment, temperature monitoring and concentration dependent signal response.

‡ 6 mm diameter x ~500 μm thick

1.4 Summary of Results

Experiments assessing the loss of cartilage matrix in multiple salt concentrations, protease inhibitor concentrations, temperatures and storage conditions were run to select conditions for the mechanical and transport tests. In all of the conditions tested, no samples had greater than 10% GAG loss over 24 hours. There was a significant increase in GAG loss at room temperature as the salt concentration of the test solution increased from 0.015 M to 1 M. The inclusion of protease inhibitor in the testing solutions didn't have a significant effect on GAG loss. Increasing the temperature during the test showed a trend toward increased GAG loss, however, storing the samples in a solution containing protease inhibitor at -20˚C provided protection from the temperature effect.

The most notable and clinically relevant finding of the mechanical stress relaxation experiments was that adding avidin to human cartilage at physiologic ionic strength had no measurable effects on the mechanical properties under study. Avidin did have effects in other test conditions. At low ionic strength (0.015 M), both human and bovine cartilage relaxed to a lower final equilibrium stress in the presence of avidin. Bovine cartilage in physiologic salt with avidin relaxed more quickly, had an increased Young's modulus and had a lower wet weight than samples not exposed to avidin. Additional findings, related to the salt concentration of the test solutions were also observed. At the lower salt concentration, bovine samples had an increased Young's modulus. In physiologic salt, relaxation of bovine cartilage occurred more quickly and relaxation of human cartilage proceeded to lower final equilibrium stress.

The real-time, one-dimensional diffusive transport experiments provided estimates of the steady-state diffusion coefficient (coupled to the porosity (ϕ) and partition coefficient (K)) of avidin in bovine and human articular cartilage. In human cartilage, the estimated value of $\phi K D_{ss}$ was 2.67×10^{-8} cm^2/s and in bovine was 1.02×10^{-7} cm^2/s. A correlation between the proteoglycan concentration and diffusivity was observed in the human samples. As the GAG concentration increased, so did the rate of diffusion.

2 BACKGROUND

2.1 Synovial Joints and Hyaline Cartilage

Synovial joints, also as known as diarthrodial joints, are the most abundant and most mobile joints in the body. Examples of synovial joints include the knee, hip and ankle. The main components of a synovial joint (Figure 1) are the (1) articular capsule, (2) joint cavity and (3) articular cartilage. The articular capsule forms a continuous and sealed sac enclosing the surfaces of the two articulating bones. The outer surface of the capsule is a fibrous network integrated with the periosteum of the bones and the inner surface contains the synovial membrane. The synovial membrane acts like a sieve, allowing an ultrafiltrate of nutrient-carrying plasma to pass through and enter the joint space. Additionally, the capillary and lymph systems of the synovial membrane allow for continual turnover of molecules[13]. Inside the articular capsule, the space between the surfaces of the two bones is called the joint cavity. Synovial fluid (SF), secreted from the synovial membrane, fills the synovial cavity and is essential for joint lubrication, shock absorption and nutrition[14,15]. The final major component of a synovial joint is the hyaline cartilage that forms a thin layer on the surfaces of the articulating bones. This provides an additional layer of separation between the bones and helps with shock absorption and reduction of friction.

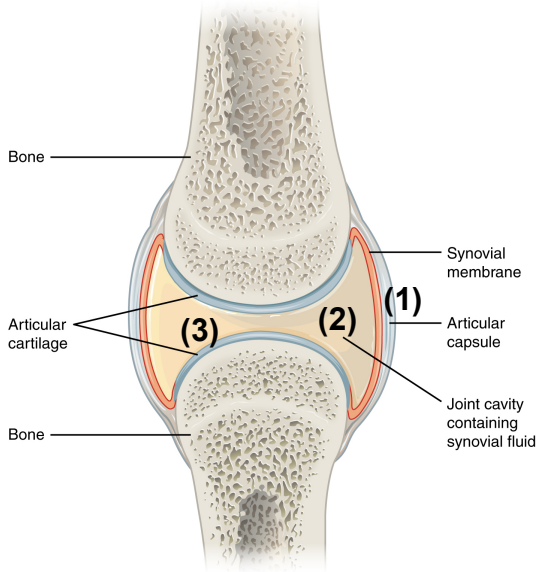

Figure 1. Synovial joint anatomy. The three main components of a synovial joint are the (1) articular capsule, (2) joint cavity and (3) articular cartilage. (Image credit: OpenStax CNX[16])

Hyaline cartilage is a unique and complex biological tissue that provides mechanical strength and lubrication in synovial joints. Cartilage is avascular, aneural and alymphatic, requiring it to rely on diffusion of molecules through the SF both for nutrition and clearance. It is also highly hydrated with 70-85% of its wet weight being attributed to water[17]. The dry weight of cartilage is 50-60% collagen fibrils, 30-35% aggrecan proteoglycans, 1-5% chondrocytes and 1-10% other proteins. The collagen in cartilage is mostly type II and the fibrils provide the tensile and shear strength for the tissue. Aggrecan is a bottlebrush shaped proteoglycan with a long (400 nm[18]) core protein and glycosaminoglycan (GAG) side chains. The GAG side chains are either keratan sulfate or chondroitin sulfate and are ~40 nm in length, but only separated on the core protein by 2-3 nm[18]. Both types of GAGs carry a negative charge at physiologic pH because of their sulfate and carboxyl groups, which creates electrostatic repulsion between molecules, giving cartilage high compressive strength.

Cartilage can be divided into four zones (Figure 2) based on organization and concentration of the main components[19]. Facing the synovial fluid, the uppermost layer is called the superficial zone (SZ) and accounts for 10-20% of the total thickness. In this layer, the collagen fibrils are oriented parallel to the articular surface as are elongated chondrocytes and the aggrecan concentration is at its lowest. Just below the SZ is the middle zone (MZ), where collagen is randomly oriented, chondrocytes are round and at a higher density and aggrecan concentration is increased. The MZ is 40-60% of the thickness. Next is the deep zone (DZ), making up 30-40% of the thickness. Collagen fibrils are aligned perpendicularly to the underlying subchondral bone and the density of chondrocytes and concentration of aggrecan are both at their highest. The final zone is the calcified region, which provides a transition from the soft cartilage to the stiff subchondral bone. As the density of cells and concentration of proteoglycans increase with depth, the pore size and water content both decrease.

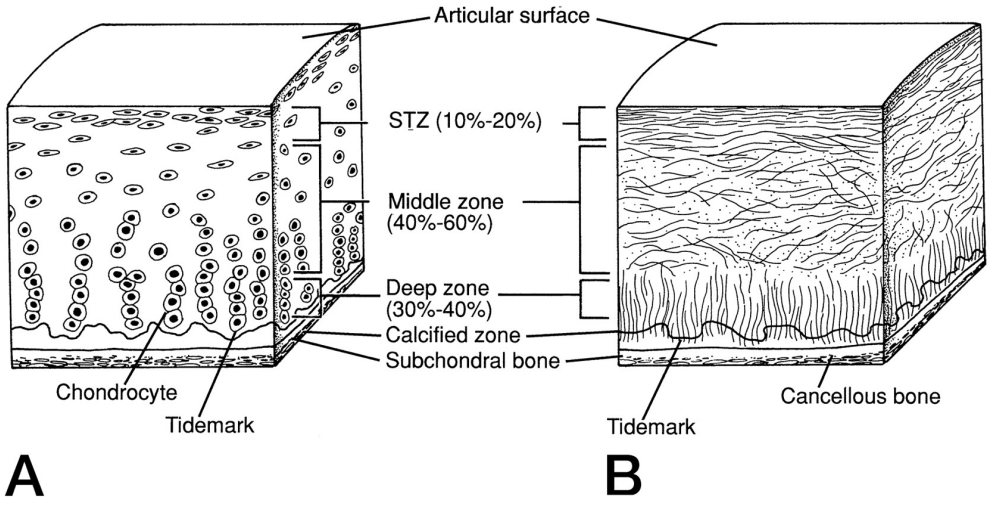

Figure 2. Zones of articular cartilage. The structure and organization of articular cartilage changes with depth. Part **A** in the figure shows how the shape and orientation of chondrocytes changes from the superficial zone to the deep zone. At the articular surface, the chondrocytes are elongated and aligned parallel to the surface. In the deep zone, the chondrocytes are rounded and stacked perpendicular to the subchondral bone. Part **B** shows how the density and orientation of collagen and proteoglycans changes. The concentration of the molecules increases with depth and orientation changes from being parallel to the surface to perpendicular to the subchondral bone. (Image credit: Buckwalter et al 1994[20])

2.2 Osteoarthritis Pathology and Traumatic Joint Injury

Osteoarthritis is a disease of synovial joints, now known to eventually affect all the joint tissues—cartilage, bone, ligaments, menisci, joint capsule, synovium, muscles and neural tissue[21,22]. The main characteristics associated with OA joints are (1) loss of articular cartilage leading to joint space narrowing, (2) subchondral bone remodeling and (3) osteophyte formation[23]. The loss of articular cartilage is multifaceted. Micro-cracks and fissures at the surface result in loss of extracellular matrix (ECM) and hypertrophy of the chondrocytes. Loss of proteoglycans in the ECM reduces the load-bearing capacity of the joint, making it more susceptible to further damage and cartilage loss. Overtime, the hypertrophic chondrocytes undergo apoptosis, which releases the intracellular contents. Some of released contents are proteinases that cause further degradation of ECM and an inflammatory response in the SF of the joint. Not only does apoptosis of the chondrocytes release deleterious products, it also reduces the number of available cells that can produce new ECM. This imbalance of degradation and synthesis contributes to the overall loss of articular cartilage[2]. Subchondral bone in OA joints undergoes remodeling, primarily

sclerosis, that results in a stiffer, thicker tissue[23]. Bony outgrowths and protrusions, called osteophytes, also form within the joint.

Although the exact causes of OA are not fully understood, several risk factors have been identified. The Centers for Disease Control and Prevention (CDC) have separated the risk factors into two main categories: non-modifiable and modifiable[24]. Risk factors that are out of person's control include genetics, gender and age. OA is more common in women and people over age 65. A number of genes have been implicated in OA and it has been estimated that the hereditability of OA is 50%[25]. Modifiable risk factors include weight, occupation and injury. Being overweight or obese can lead to early onset or faster progression of OA. Occupations that require repetitive motion of a joint may lead to formation of OA in that joint. Injury to a joint, as discussed below, increases the risk of developing OA as well.

Suffering a traumatic joint injury causes an increased risk of developing OA. Traumatic joint injuries are acute injuries to an articular joint often caused by a sudden mechanical impact. Examples of such injuries include ligament tears, articular fractures, bone fractures and soft tissue damage. The force with which the impact is applied affects the level of damage to the joint, ranging from nanoscale cell and matrix damage up to macroscopic damage of the articular surface[26,27,28,29]. The combined results of several studies have shown that a major ligament or capsular injury increases the risk of OA by 10 times and an articular fracture increases the risk by more than 20 times[26,30,31,32,33,34]. After an acute joint injury, there is a sudden increase in levels of inflammatory cytokines (IL-1, IL-6, TNF-α) in the synovial fluid which can diffuse into cartilage, initiating proteolysis and matrix degradation[35]. The combination described here of traumatic joint injury followed by up-regulated joint degradation is a subtype of OA called post-traumatic osteoarthritis (PTOA) and accounts for 12% of the overall disease burden[3].

After a traumatic joint injury occurs, methods of assessing joint damage and monitoring the development of PTOA are not yet well defined[4]. Images can be taken of the joint to assess damage, but agreement on the relationship between image and damage is not unanimous[36,37,38,39]. Samples of synovial fluid show clear signs of a biological response and

in vitro models are being used to discover novel biomarkers[8]; however, none exist yet to track the progression of the disease or assess the efficacy of treatments[40,41].

Some hypotheses about the cause of the injury-induced biological degeneration include release of oxygen free radicals from chondrocytes[42,43], release of fibronectin fragments[44] and increased levels of pro-inflammatory molecules in the synovium such as TNF-α, IL-1, IL-6, nitric oxide and MMPs[8,28,45,46,47]. As compared to OA, PTOA provides a unique opportunity for treatment. In the case of OA, pain and other symptoms often do not manifest themselves until significant damage has already occurred in the joint. This leads to treatment occurring in the later stages of the disease[48,49]. PTOA, on the other hand, has a known time-zero, the traumatic injury, which provides an opportunity for earlier intervention in the progression of the disease.

PTOA is a disease of the whole joint, but one of the most affected tissues is cartilage, making it a popular target for drug treatments. Several studies have been focusing on post-injury treatments that could prevent or slow the progression of cartilage degeneration and thus PTOA. Results suggesting that biological interventions post-injury, such as inhibition of proteolytic enzymes or inflammation pathways, can decrease chondrocyte death and matrix degeneration have been reported for in vitro experiments as well as for animal models[28,42,45,50,51,52]. Another study considered joint loading post-injury and found that decreasing early loading of an injured joint might minimize the extent of tissue damage by limiting the inflammatory response[46]. Several investigators have also taken a synergistic approach to the intervention, combining inhibition of death and degradation with promotion of growth and matrix production[8,53,54,55,56].

2.3 Drug Treatment Options for Osteoarthritis

OA treatment is highly variable and includes options such as lifestyle changes, physical activities, drug administration and surgery, if the disease progresses far enough. Within drug treatment, there are again multiple options both in terms of delivery method and purpose. Medications can be administered systemically, topically or locally via injection. Types of medications include analgesics, for pain relief; non-steroidal anti-inflammatory drugs (NSAIDs), for reducing inflammation and pain; corticosteroids, for reducing

inflammation and pain; and hyaluronic acid, for aiding in joint lubrication with the hope of reducing pain[57]. Because OA is a localized disease, confined to one or more joints, systemic delivery of medication is not optimal. Using local delivery of the drug, such as intra-articular (IA) injection, provides many advantages over systemic: (1) reduced unintended, off-target systemic binding, (2) more controllable drug dosing for a specific joint, (3) increased bioavailability, (4) smaller required dose, (5) lower overall drug cost and (6) less concern with patient compliance[5]. Although IA injection is preferable to systemic delivery, it comes with its own set of challenges, most notably rapid clearance from the joint.

To combat the issue of clearance, several researchers are focused on finding better delivery systems than injection of the free drug molecule. Good delivery systems increase the residence time of the drug in the joint, but not at the cost of making the drug biologically inaccessible or toxic. Liposomes have been used to encapsulate hydrophobic drugs, providing a sustained release of the drug as the liposome dissolves, extending drug activity in the joint by up to 14 days[58,59,60]. For non-hydrophobic drugs, another option is to use synthetic (or natural) biodegradable nano- and microparticles. In the joint space, the drug is released by diffusion out of the particle or degradation of the particle and animal studies have shown residence times of up to 21 days[61,62,63,64]. Although there are not currently any liposome or particle based delivery systems approved for IA injection in the United States, FX006 (Flexion Therapeutics, Burlington, MA), a microparticle PLGA-encapsulated triamcinolone acetonide, is in Phase III clinical trials[65]. A third option is to directly modify the drug. Adding PEG to hydrophobic drugs can increase their bioavailability and molecular weight (MW)[5]. Conjugating elastin-like polypeptide to protein drugs can decrease their clearance, but can also change the pharmacokinetics compared to the unmodified protein[66,67,68,69].

OA is a disease of the whole joint and drug therapies have a variety of targets within the joint. Of interest for this thesis is cartilage as a target. IA injection is particularly useful for cartilage because it is avascular, making systemic drug delivery very difficult. When a drug is injected into an articular joint, it enters into the joint capsule. To reach cartilage, the drug must diffuse through the viscous synovial fluid and penetrate the dense ECM of cartilage,

all the while competing against clearance by the lymphatic system and synovial capillaries. Recent work by Bajpayee et al. has focused on improving delivery of dexamethasone (dex) to cartilage in IA injection[10]. In this work, dex, a small molecule drug, was conjugated to a larger carrier molecule, avidin, and showed increased joint residence times of 7 days in rat studies.

2.4 Dexamethasone and Avidin

Dexamethasone is a small, (MW = 392.46 Da) synthetic glucocorticoid (subclass of corticosteroids) drug used for its anti-inflammatory and immunosuppressant effects. Intra-articular injections of corticosteroids, including dex, are commonly used to manage pain in OA patients[70]. On the potency scale, dex ranks high among other glucocorticoids[71] and has been the focus of research recently for OA indications other than anti-inflammation[7,8,72,6,73]. Recent studies suggest that dex could be effective as a preventative treatment for PTOA patients[6,7,8]. Like other small molecule drugs, dex faces the problem of rapid clearance from the joint space upon IA injection. Because of its effectiveness in recent studies, additional research is being done to improve the delivery and retention of dex in cartilage for treatment of OA and PTOA[74].

Avidin, shown in Figure 3, is a tetrameric or dimeric[75] glycosylated protein that is naturally produced by birds, reptiles and amphibians and found in the whites of their eggs. The tetrameric version has a molecular weight of 66 – 69 kDa[76] and a basic isoelectric point (pI ~ 10.5), meaning it carries a positive charge at neutral pH. Avidin is perhaps best known for its high affinity and specificity to biotin. The avidin-biotin linkage is one of the strongest known non-covalent bonds[77]. This extremely strong and specific binding is exploited all across biology, in applications ranging from assays to purification to drug delivery.

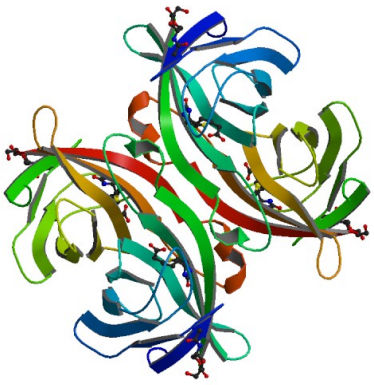

Figure 3. Structure of avidin. Avidin is a tetrameric protein with a molecular weight of 66-69 kDa. It has a basic isoelectric point (pI ~ 10.5), making it positively charged at physiologic pH. (Image credit: The Protein Data Bank[78])

The nanoscale size (diameter ≈ 7 nm) and positive charge at physiologic pH of avidin has made it the target of recent research in the field of drug delivery for OA. Degradation of cartilage in articular joints is one of the main manifestations of OA and thus makes cartilage a popular target for drug therapies. The ECM of cartilage contains a large number of sGAGs, which are negatively charged at physiologic pH, giving cartilage a net negative charge. The potential for electrostatic interactions between positively charged avidin and negatively charged cartilage was the driving factor behind the dissertation work of Bajpayee[79].

In her work, Bajpayee showed that particles with diameters less than 10 nm are able to penetrate the dense ECM of cartilage. Her work also showed that avidin has a partition coefficient greater than 1 for cartilage, meaning the concentration of avidin is higher in cartilage than it is in the surrounding solution. Not only does avidin partition up into cartilage, it is also able to penetrate the full depth and be retained in the tissue for times on the order of days. Bajpayee hypothesized that these results suggest electrostatic interactions between the avidin and cartilage and that there is weak 'binding' occurring between avidin and the matrix of cartilage. Additionally, avidin was shown to be non-toxic to immature bovine chondrocytes at concentrations up to 1 μM, a concentration much higher than would be need for IA injection.

The work of this thesis aimed to investigate an additional measure of safety of avidin in cartilage—the effect on mechanical properties. One of the main functions of cartilage in an

articular joint is to provide compressive mechanical strength. It is important that IA injection of avidin conjugated to dex does not compromise the mechanical integrity of cartilage. A decrease in mechanical strength post-injection could put the tissue and joint at risk for further damage.

2.5 Temperature in the Knee

Several studies have measured the intra-articular temperature of knee joints in healthy and diseased patients. The studies have primarily been conducted to compare healthy to diseased knee temperature as well as to determine how different physical modalities (icing, heating, etc.) affect joint temperature. In these studies, the baseline IA temperature of healthy knee joints has been reported to vary between 29.4 and 35.1˚C [80,81,82,83,84]. The variations in temperature can be attributed to factors such as method of measurement, activity level of the subject and environmental conditions[81,85]. Interestingly, one study reported that the volume of synovial fluid in the joint did not affect the temperature value, but rather only its rate of change[81]. Several studies have also shown that OA joints have an increased baseline temperature as compared with healthy joints[81,86]. This increased temperature is thought to contribute to the enzymatic activity that causes degradation of cartilage in OA joints. The experiments conducted for this thesis were performed at or near room temperature (21.2 – 26.7˚C) and the variation in temperature during any given experiment was within the range of variation seen in a human knee joint (Δ 2.8˚C).

2.6 Mechanical Properties & Stress Relaxation in Cartilage

The mechanical properties of articular cartilage are determined by the structure of the extracellular matrix. The two main contributors to the mechanical strength are collagen type II and aggrecan. Collagen type II forms long fibrils that are aligned differently throughout the depth of cartilage. From SZ to MZ to DZ, the fibrils transition from being parallel to the articulating surface to randomly oriented to perpendicular to the subchondral bone[19]. Collagen contains amine (NH_3^+) and carboxyl (COO^-) groups in approximately equal numbers[87], which leads to an overall neutral charge of the fibrils at physiologic pH. Aggrecan contains a long core protein with two different types of glycosaminoglycan (GAG) side chains, both of which are polysaccharides made up of repeating disaccharide units. Chondroitin sulfate, the more prevalent of the GAGs, contains one carboxyl and one

sulfate (SO_3^-) group per disaccharide, giving a charge of –2 per disaccharide at physiologic pH. Keratin sulfate contains one sulfate group per disaccharide, giving it a charge of –1 per disaccharide at physiologic pH. Summing the concentrations of all the ionizable groups (amine, carboxyl, sulfate) multiplied by their respective charge, gives rise to a property called the fixed charge density (FCD), shown below in Equation 1, where the FCD (ρ_m) is normalized by Faraday's constant (F) to give units of concentration to match the right hand side. Because the number of negatively charged ionization groups is higher than the positively charged groups, articular cartilage has a net negative FCD. Although the FCD is a function of ionization, which in turn depends on pH, the FCD has been shown to remain mostly unchanged from pH 5 – 7[88], relevant pH values for physiologic implications.

$$\frac{\rho_m}{F} = [NH_3^+] - [COO^-] - [SO_3^-] \qquad (1)$$

The overall negative charge of articular cartilage has implications for the mechanical compressive strength on both the nano- and macroscales. The GAG chains of aggrecan are separated by 2 – 3 nm[18], which is on the order of a Debye length. Debye length refers to the distance at which electrostatic effects persist and can be perceived by other adjacent charged molecules. Because of the close spacing, the negative charges on one GAG chain are felt by the GAG chains located nearby, which results in electrostatic repulsion at the nanoscale. At the macroscale, more positively charged ions (H^+, Na^+, etc.) diffuse into the tissue to balance out the negative fixed charges and satisfy electroneutrality[89,90]. This uneven distribution of ions is known as Donnan equilibrium. When the positive ions diffuse into the tissue, at the nanoscale they shield the fixed negative charges on the GAG chains, increasing the effective Debye length and thus decreasing the amount of repulsion. The unequal partitioning of H^+ and OH^- into the tissue can create a different pH value inside the tissue as compared to outside, which can affect the ionization state of the ionizable fixed groups. To balance out the concentration gradient created by more positive ions entering the tissue, water enters, causing the cartilage to swell and creating a swelling pressure[90,91]. The tensile strength of collagen acts to restrain this swelling pressure, creating equilibrium. Overall, the nanoscale repulsion of GAGs and the macroscale swelling of the tissue provides cartilage with its compressive strength.

Some of the major factors that affect the compressive properties of cartilage are (1) the FCD of the matrix, (2) the pH of the tissue and (3) the ionic strength of the surrounding environment. Increasing the FCD of cartilage, either by increasing the GAG concentration or decreasing the water volume[89], results in an increase in the compressive strength because of more GAG chain repulsion and tissue swelling. Changing the pH inside the tissue, which is a function of the surrounding pH, affects the ionization state of the amine, carboxyl and sulfate groups. As pH increases, more carboxyl and sulfate groups lose an H^+ ion and become negatively charged, which means more repulsion, swelling and compressive strength[92,93,94,95,96]. The ionic strength (salt concentration) of the surroundings affects the shielding of GAG chain repulsion. A decrease in salt concentration of the surrounding liquid means there are fewer positive ions available to diffuse into cartilage and shield the fixed negative charges, so compressive strength increases[95,97,98,99,100,101,102,103].

One measure of the mechanical strength of cartilage and how it changes is stress relaxation. During a stress relaxation test, the tissue is strained to a fixed value and then maintained at that deformation until stress equilibrium is reached. When the cartilage is compressed, reaching the equilibrium stress is governed by three main mechanisms: (1) electrical re-equilibration of the ions shielding the fixed charges, (2) mechanical, poroelastic rearrangement of fluid (i.e., flow of water)[104,105] and (3) chemical diffusion of ions and other chemical species. The electrical re-equilibration of ions takes on the order of 1 nanosecond and can be considered to be in quasi-equilibrium at all times[106]. Eisenberg and Grodzinsky[12] (1987) performed a slight variation on the typical stress relaxation test. After straining the cartilage and letting it come to equilibrium, they rapidly increased the salt concentration of the surrounding bath and monitored the change in stress over time. They found that the mechanical rearrangement of fluid occurs on a faster time scale than the diffusion of ions through the tissue, leading to ion (or other species) diffusion being the rate limiting process of ionic strength perturbation-induced stress relaxation.

The experimental protocols and results from Eisenberg and Grodzinsky[12,97] were driving factors behind the work of this thesis. Their work focused on the diffusion of small ions through cartilage and how that impacted the mechanical properties and time scales of stress relaxation. They found that the diffusion time for small ions within cartilage explained the

time scale of stress relaxation in the tissue. As the ions diffuse throughout, they shield more of the fixed charges and thus decrease the repulsion of the GAG chains. This thesis has focused on the effects of avidin, a high molecular weight, multi-charged cationic protein, on the mechanical properties of cartilage as measured by stress relaxation. It was hypothesized that the positive charge of avidin may have a similar effect on shielding repulsion of GAGs as positive ions and could lead to a decrease in overall stress and thus tissue compressive strength in cartilage. Unknown, however, is the complicating effects of avidin size and valence compared to that of small ions.

2.7 Diffusive Transport in Cartilage

Much research has been conducted to characterize the transport properties of different solutes in cartilage. The two main parameters that are studied are the diffusion and partition coefficients. The diffusion coefficient [*units:* area/time] provides a measure of the rate that a solute moves through a given area. The partition coefficient [*unitless*] describes how a solute is taken up into the tissue relative to the surroundings. A partition coefficient > 1 indicates a higher volumetric concentration of the solute inside the tissue compared to the surroundings. Understanding how molecules are taken up by and move through the tissue is important because cartilage is avascular, so the chondrocytes rely on diffusion and fluid transport to receive their nutrition. These parameters are particularly interesting for applications of drug delivery to cartilage for OA treatment when chondrocytes are the intended target of the therapy.

Several different methods have been used to estimate the diffusion and partition coefficients of solutes in cartilage. Methods vary in their ability to measure one or both of the parameters and their dimension of measurement. An incubate and slice technique (1D)[107,108,109], absorption/desorption bath series (3D)[110,111] and a microscope equipped with a photometer (1D and 3D)[112,113,114] can all provide estimates of both parameters. Fluorescence recovery after photobleaching (2D)[115,116], inline downstream bath signal measurement (1D)[117,118,119] and nuclear magnetic resonance (1D and 3D)[120,121] methods all only provide estimates of solute diffusivity. Equilibrium uptake experiments, in which cartilage samples are incubated with varying amounts of solute and the concentration in the bath is measured before and after incubation, are often used to provide a measure of the

partition coefficient and supplement the diffusion-only methods. More detailed descriptions of these techniques can be found in Appendix 8.9 (pg. 96).

Partitioning and diffusivity of solutes in cartilage has been found to vary based on several different factors. Diffusion has been found to be anisotropic[122], meaning the diffusivity of a solute depends on its direction of movement through the tissue. Additionally, diffusivity varies with the zones of cartilage due to the differing compositions of the ECM[112,123]. GAG concentration in the tissue has been found to affect the uptake of charged solutes, but not neutral ones[112,118]. Both the diffusivity and partition coefficient are inversely proportional to solute size [10,109,112,116]. Solutes that carry a net charge can experience enhanced or inhibited partitioning and diffusion due to electrostatic attraction or repulsion with the cartilage matrix[10,112]. Environmental factors of the surroundings have been found to impact the parameters as well. Temperature increases the diffusivity as predicted by the Stokes-Einstein relation for spherical particles in low Reynolds number liquids, shown in Equation 2, where k_B is Boltzmann's constant, T is absolute temperature, η is dynamic viscosity and r is particle radius[108,111]. When the tissue is subjected to dynamic loading, the transport of large molecules is increased, while the transport of small molecules appears to be unaffected[122,124,125,126,127,128,129]. This suggests that the transport of small molecules is diffusion controlled and that fluid convection is important for the movement of large molecules. Diffusivity decreases with increasing static, volumetric compression because of the effective increase in matrix density[112,113,126]. Conflicting findings on the effects of solute concentration have been reported. Some studies found that the rate of diffusion decreased over time[109,120,130], implying a reliance on concentration, while other studies found that bath concentration had no affect on diffusion[108,131].

$$D = \frac{k_B T}{6\pi\eta r} \qquad (2)$$

Transport properties differ in diseased (OA) tissue as compared to healthy. One hallmark of OA cartilage is decreased GAG content. This has been found to speed up the diffusion of large molecules[108,116,132] and reduce the uptake and retention of positively charged solutes[10]. Mechanical injury to the articular surface can speed up the diffusion rate through

the superficial zone, but doesn't typically affect partitioning[133]. Fissured versus intact cartilage surfaces absorb solutes differently[134,135].

The work of this thesis sought to estimate the diffusivity of avidin in cartilage to supplement the mechanical tests being conducted. The setup of the mechanical experiments involved the transport of avidin into cartilage while the tissue was under static strain. It was hypothesized that avidin's transport rate into the cartilage would be the governing time scale for changes seen in the mechanical measurements. Independent measurements of the diffusion rate could prove or disprove this hypothesis when combined with the mechanical results.

3 METHODS

3.1 Cartilage Explant Harvest

Explants of cartilage were obtained from either immature bovine or adult human donor knee joints (the latter having modified Collins Grade 0 or Grade 1 cartilage (i.e., normal or at most limited regions of early surface fibrillation))[136]. Harvesting methods for the two types vary and are each described below.

3.1.1 *Bovine*

Cartilage explant samples used in mechanical, transport and biochemical experiments were harvested from immature (2-3 weeks old) bovine (Research 87, Boylston, MA) femoropatellar grooves and/or condyles. Biopsy punches 3 or 6 mm in diameter were used to punch disks of cartilage from the groove. During the harvesting process, sterile technique was used to minimize the potential of contamination and later bacterial growth in samples that were kept in culture. Disks that had been cut out of the joint were placed into a well of a plate containing 1x sterile PBS to maintain hydration while all disks were removed.

After being removed from the joint, the cartilage disks underwent one of the following processes depending on the final use in experimentation. Trimming of the disks to specified thicknesses was done using a custom template and razor blade, as previously

described[8], for all processes and the superficial zone was always left intact as a part of the final sample.

3 mm biopsy punches

(1) Trimmed to 1 mm thick and transferred to a well in a new plate containing medium[§] and stored at 37˚C. The medium was changed every 2-3 days until used in an experiment.

(2) Trimmed to 1 mm thick and transferred to a 2 mL tube containing 1x PBS + protease inhibitor (Roche Life Sciences, Indianapolis, IN) and stored at -20˚C until used in an experiment.

6 mm biopsy punches

(1) Trimmed to ~500 μm thick and transferred to a 2 mL tube containing 1x PBS + protease inhibitor and stored at -20˚C until used in an experiment.

3.1.2 *Human*

Cartilage samples from postmortem human knee joints were obtained as previously described[8,137]. The human joints were obtained from the Gift of Hope Organ and Tissue Donor Network (Ithasca, IL) and all procedures for obtaining the cartilage were approved by the Rush University Medical Center Institutional Review Board (ORA Number: 08082803-IRB01-AM01) and the Committee on Use of Humans as Experimental Subjects at MIT. At the time of donor tissue harvest, the joint surfaces were assessed by a forensic pathologist and scored on the modified Collins grading system[136]. All joints used for this work were either Collins Grade 0 or 1. Three joints from three donors, both male and female and ranging in age from 26 to 62 years old, were used for this work. Full thickness (~1 – 2 mm) disks of cartilage, 3 or 6 mm in diameter, were cored from the tibial plateau or distal femur of the knees. Samples were harvested 24-72 hours after time of death of the donor and only normal (unfibrillated) cartilage was used. After removal from the joint, explants were stored in 1x PBS + protease inhibitor at -20˚C until used in an experiment. A summary of the joints used is shown in Table 1 below.

§ Formulation for medium in Appendix 8.1 (pg. 73)

	Gender	Age	Modified Collins Grade[136]
1	Male	26	1
2	Female	62	0
3	Male	32	0

Table 1. Human donor knee joint information.

3.2 Mechanical Stress Relaxation

All mechanical tests were conducted with 3 mm diameter by approximately 1 mm thick disks of cartilage with the superficial zone intact.

3.2.1 *Sample preparation*

Samples were thawed/equilibrated at room temperature for ≥ 30 minutes. After equilibration, sample thickness was measured using a current sensing micrometer or digital calipers. Measurements were taken at 3 different locations and the average thickness was used to calculate strain percentages in mechanical testing.

3.2.2 *Mechanical protocol*

Unconfined compression stress relaxation tests were performed using a Dynastat mechanical spectrometer (IMASS, Hingham, MA). A cartilage disk was loaded into an unconfined compression chamber (10 x 32.4 x 14.5 mm (w x l x h)) and a 9.5 mm diameter platen was lowered to the height of the disk. Then 2.5 mL of testing liquid was added and the experimental protocol started. Testing liquid was either 0.1x PBS or 1x PBS, with ionic strengths (due predominantly to the NaCl concentration) of 0.015 and 0.15 M, respectively. The PBS used did not contain Ca^{2+} or Mg^{2+}. The top of the chamber was covered with parafilm to reduce evaporation during the course of the experiment. A tubing and pump system was used to circulate the fluid in the chamber continuously to avoid the formation of stagnant films. The experimental setup is shown in Figure 5.

Initially, the sample was allowed to swell/equilibrate in the testing solution for 20 minutes. Following this, the sample was subjected to four rounds of 4% compressive strain, achieving a final compression of 16%. The strain steps were applied over 60 seconds and the sample was then allowed to relax and equilibrate for nine minutes before the next strain ramp. After the fourth strain ramp, the sample was maintained at

16% strain for two hours, fifteen minutes to allow for any residual relaxation that the sample might undergo from the strain ramps. For negative control samples, nothing additional was done at this point and the strain was maintained for another 18 hours. For samples being tested, 167 µL of 100 mg/mL avidin (ThermoFisher Scientific, Waltham, MA) was added to the test chamber, giving a final concentration of 100 µM, and the strain was maintained for 18 hours. After the long static hold, the strain was reduced to 8% and the sample was allowed to equilibrate. Then another set of four strain ramps, like those at the beginning of the protocol, was applied. Figure 4 shows a timeline of the mechanical protocol.

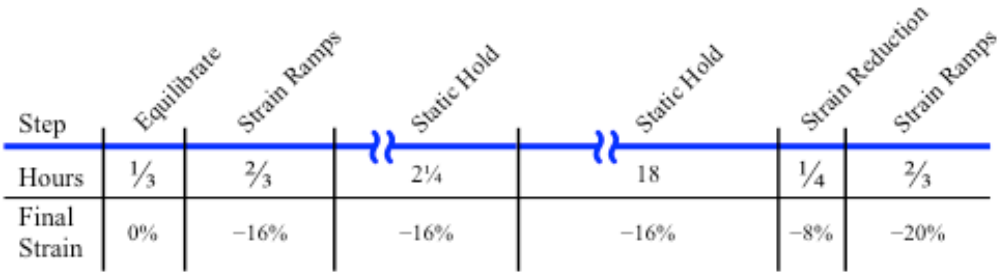

Figure 4. Mechanical protocol timeline. This figure gives a visual representation of the timing of the different pieces of the mechanical protocol. The (–) in front of the strain values indicates compression (rather than tension).

Stress was measured continuously throughout the protocol at a frequency of 0.156 – 10 Hz. For some of the tests, a HOBO data logger and temperature probe[**] (Onset, Bourne, MA) was used to monitor the temperatures both in the testing room as well as inside the chamber.

At the conclusion of the experiment, the test liquid was collected and saved at -20˚C, the wet weight of the cartilage explant was measured and then the sample was digested in proteinase-K[††] (Roche Life Sciences, Indianapolis, IN) at 60˚C overnight. The digest was subsequently stored at -20˚C and later assayed for GAG content using the dimethyl-methylene blue (DMMB) assay[138].

[**] HOBO 4-Channel Thermocouple Data Logger with a Type K 6-ft Beaded Thermocouple Sensor
[††] Formulation for proteinase-K in Appendix 8.1 (pg. 73)

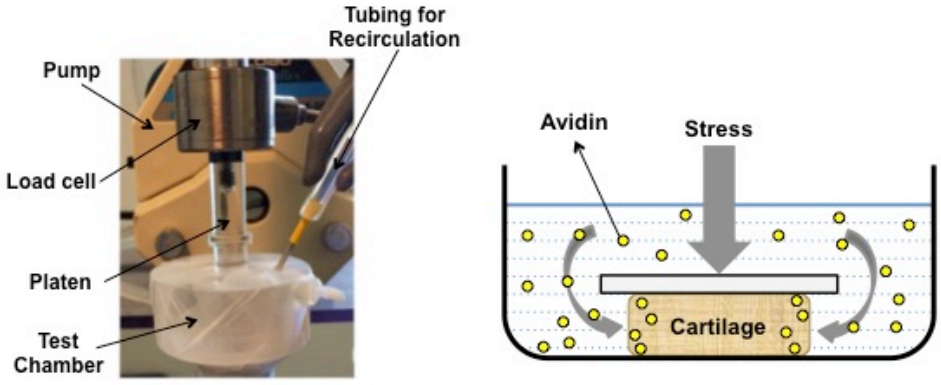

Figure 5. Mechanical stress relaxation experimental setup. The photo on the left shows the actual experimental setup. The cartilage sample is located inside the test chamber, under the platen. The test chamber is covered with parafilm to minimize evaporation of the test liquid over the course of the experiment. The platen that compresses the cartilage disk is attached to a load cell, which measures the grams required to compress the cartilage by a specified strain. Tubing connects to a port on the left side of the chamber, is fed through a pump and re-enters the chamber on the other side. This provides recirculation of the test solution, which minimizes the chance of formation of films at the surface of the cartilage and also ensures a well-mixed bath. The cartoon on the right (not to scale) depicts what happens inside the test chamber when avidin is added. While the cartilage is held at a fixed strain, avidin molecules in solution partition into the tissue and diffuse radially into the cartilage disk.

3.2.3 *Data analysis*

The data were processed differently depending on where in the protocol they were collected. For all the data, the recorded values were converted from load (grams) to stress (Pascals) using Equation 3. The sets of strain ramps from the beginning and end were used to calculate the Young's modulus of the tissue before and after the long, static hold. An exponential decay model (Eqn. 4) was fit to the stress relaxations of each strain ramp to find the equilibrium stress (a) and characteristic relaxation time (τ). The slopes from the corresponding stress/strain curves provided the moduli. An example of the strain ramps and stress relaxations is shown in Appendix 8.6 (pg. 85).

$$stress\ [Pa] = \frac{load\ [g]}{area\ [m^2]} \times \frac{9.8\ N}{1000\ g} \qquad (3)$$

$$a + be^{-t/\tau} \qquad (4)$$

The data from the long, static hold was analyzed as a stress relaxation curve after undergoing pre-processing. First, a new time zero was set in order to be able to

differentiate relaxation in the long hold from that induced by the 4th strain ramp. Using the characteristic relaxation time of the 4th ramp from the beginning of the protocol (τ_4), the new starting point was set at $5\tau_4$ away from the peak stress of the 4th ramp. Next, all the values were divided by the stress at the new starting point in order to normalize the data to range between 0 and 1. The absolute stress values from sample to sample varied significantly, so normalizing the values allowed for comparisons between samples. The data were then spilt into two parts—before avidin and after avidin. All samples were divided this way regardless of whether or not avidin was added during the experiment. Finally, exponential models were fit to both sets of data to obtain the parameters shown in Equation 4 (a, b, τ). Appendix 8.6 (pg. 85) shows an example of where $5\tau_4$ is located, what a normalized long hold stress relaxation curve looks like and exponential fits of data before and after the addition of avidin.

The measured GAG content was normalized by the wet weight of each sample to account for variations in size from sample to sample. This provided a $\mu g\ GAG/mg\ of\ tissue$ value that could then be compared between samples within and between sample types (bovine and human).

Linear mixed-effects models were used to analyze the wet weight, GAG content, modulus difference and exponential model parameter values. The effects included in the model varied depending on what set of data was being analyzed. Possible fixed effects were salt concentration, avidin concentration and the interaction of salt and avidin. Sample (animal/donor) was treated as a random effect in all models. Effect sizes, how much a factor changes the outcome, and p-values are reported when useful and appropriate.

3.3 Real-time 1D Transport

All transport tests used 6 mm diameter by approximately 500 μm thick cartilage disks with the superficial zone intact.

3.3.1 *Sample and setup preparation*

Samples were thawed at room temperature for ≥ 30 minutes, allowing them to equilibrate. While the sample equilibrated, all interior surfaces of the transport

chamber and gaskets (Figure 6) were coated with SuperBlock™ Blocking Buffer (ThermoFisher Scientific, Waltham, MA) and allowed to sit for ≥ 30 minutes. The thickness of the cartilage explant was measured in three locations, using digital calipers, and then averaged and recorded.

The explant was then loaded into a custom-built transport chamber, shown in Figure 6. The upstream and downstream sides of the chamber were secured together, effectively sandwiching the explant between them. Test liquid (2 mL) was added to the downstream side of the chamber first and the explant was checked for a secure seal. If no leakage was observed, test liquid was then added to the upstream as well.

3.3.2 *Transport*

Once the explant was secured and the test liquid added, magnetic stir bars were placed in each side of the chamber and the transport chamber was connected to a SPF-500™ Spectrofluorometer (SLM Instruments, Urbana, IL) via a tubing and pump system that continually circulated the liquid in the downstream through a cuvette in the instrument. The signal of just the test liquid in the downstream was monitored for ≥ 20 minutes to make sure that a stable baseline signal could be achieved. After establishing a baseline, avidin (combination of unlabeled and FITC-labeled) was added to the upstream chamber. The experiment was allowed to run for 24-48 hours and the fluorescence signal of the downstream was recorded every 3 seconds. A schematic of the experiment is shown in Figure 7.

When a linear trend in the downstream fluorescence was observed, usually 10-24 hours into the run, a small volume (e.g., 2 μL) of the upstream liquid was spiked into the downstream chamber as a calibration. The experiment was run for another several hours after the spike to make sure the slope before the calibration was recovered. For some of the tests, a HOBO data logger and temperature probe[‡‡] were used to monitor the temperatures both in the upstream chamber and the lab. At the end of a few transport runs, free fluorescein was added to the upstream chamber as a control to

‡‡ HOBO 4-Channel Thermocouple Data Logger with a Type K 6-ft Beaded Thermocouple Sensor

ensure the signal seen in the experiment was due to intact FITC-avidin and not free fluorescein that may have come off the prepared protein.

At the conclusion of the experiment, the up and downstream liquids were collected and saved at -20˚C and the cartilage sample underwent the same steps as previously described for the mechanical samples (pg. 29).

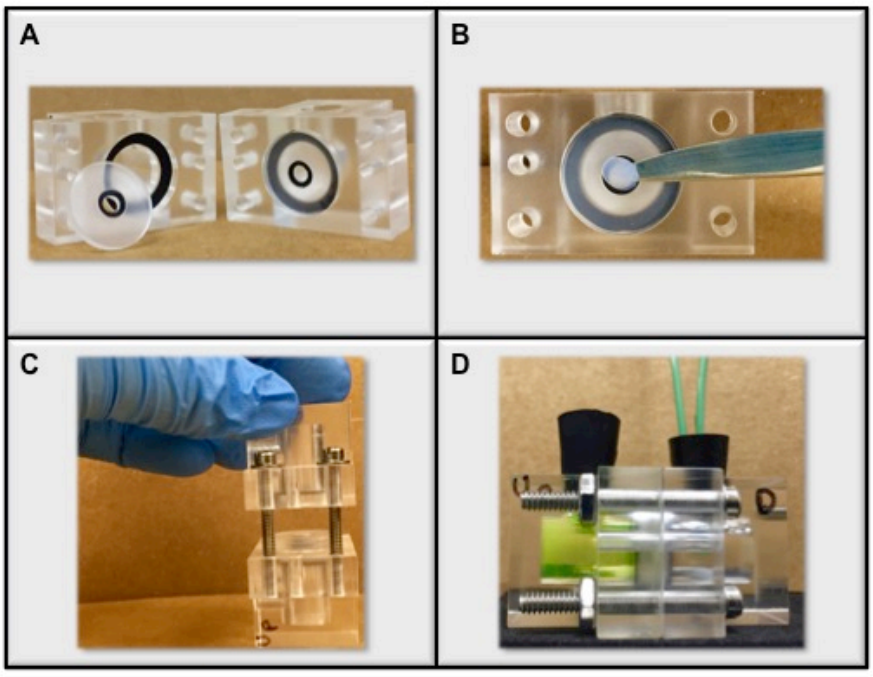

Figure 6. Images of real-time transport setup. These four images show the custom transport cell and the process for setting up a transport experiment. The transport cell, shown empty in image **A**, consists of two identical chambers—an upstream and a downstream. Each chamber has an inset ledge that holds a removable disk. The disk has a 4 mm diameter hole in the center, with an inlaid rim that holds a 6 mm diameter cartilage explant. All the pieces are first blocked with SuperBlock™ Blocking Buffer for at least 30 minutes to minimize sticking of avidin. Then the cartilage explant is placed onto the removable disk sitting inside the upstream chamber such that it covers the 4 mm hole completely, as shown in image **B**. The downstream disk and chamber are then placed on top of the upstream chamber and secured tightly with screws so as to sandwich the cartilage explant between the upstream and downstream chambers (image **C**). Image **D** shows the final experimental setup. Both chambers contain 2 mL of buffer and the upstream chamber also has FITC-labeled avidin, as is evidenced by the bright color in the chamber on the left. Rubber stoppers are used to cover the openings in both chambers to minimize evaporation during the experiment. The rubber stopper in the downstream has two tubes running through it that recirculate the downstream liquid between the bath and the detector (spectrofluorometer). The transport cell sits on top of a magnetic stir plate and small stir bars inside each chamber ensure well-mixed baths.

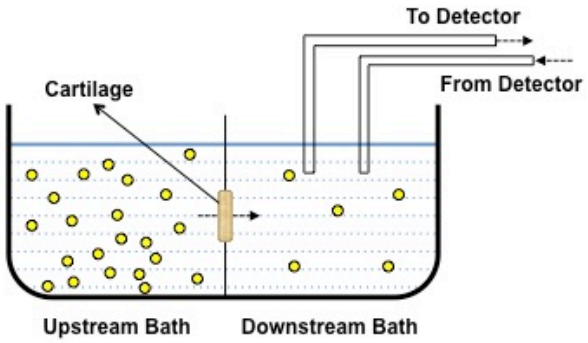

Figure 7. Real-time 1D transport experimental setup. This figure shows a schematic of the transport experiment. At the beginning of the experiment, a high concentration of FITC-labeled avidin is added to the upstream bath. The downstream liquid is continually re-circulated between the bath and the detector. Over time, FITC-labeled avidin moves from the upstream bath to the downstream bath through the cartilage, the only path between the two chambers. The detector continuously records the amount of fluorescence in the downstream bath, which is a real-time measurement of the transport of FITC-labeled avidin through cartilage.

3.3.3 *Data analysis*

The curves of fluorescence versus time were used to calculate transport parameters of avidin in bovine and human cartilage. All the curves were processed the same way, regardless of cartilage source. First, the raw signal underwent pre-processing. The t_0 for the experiment was set to the time of avidin addition by removing any data collected before that point. A calibration value was calculated using the signals before and after the small volume spike of the upstream bath into the downstream. This calibration value was used to determine the signal of the upstream bath. Assuming a constant upstream concentration throughout the experiment, the ratio of downstream to upstream was obtained by dividing the downstream signal at each time point by the calculated upstream signal. The associated equations for these steps are shown below (Eqns. 5 – 7).

$$calval = signal_{after} - signal_{before} \quad (5)$$

$$signal_{up} = \frac{signal_{cal} V_{down}}{V_{cal}} \quad (6)$$

$$\frac{C_{down}}{C_{up}} = \frac{signal(t)_{down}}{signal_{up}} \quad (7)$$

After pre-processing, the linear region of the curve was used to calculate avidin's steady-state diffusivity (D_{ss}). A linearly increasing signal is representative of a steady-state flux (Γ), which can be expressed in terms of D_{ss} and other tissue characteristics, shown in Equation 8, where ϕ is the porosity of the cartilage, K the partition coefficient of avidin into the tissue and δ the thickness of the sample. The time derivative of the C_{down}/C_{up} ratio, which is the slope of the transport curve, is related to steady-state flux, the downstream volume (V_{down}) and the surface area of transport (A) (Eqn. 9). Therefore, using the slope of the linear region and Equation 9, a value for D_{ss} can be calculated. For this work, the value that was calculated actually represents $\phi K D_{ss}$, where ϕ is the porosity of the cartilage and K the partition coefficient of avidin into the tissue. The work done for this thesis did not explicitly measure these values, so they were assumed to be coupled to D_{ss} in the initial calculation. Because they are scalar multipliers of D_{ss}, values can be plugged in for them to isolate D_{ss}.

$$\Gamma = \phi K D_{ss} \frac{C_{up} - C_{down}}{\delta} \cong \phi K D_{ss} \frac{C_{up}}{\delta} \quad (8)$$

$$\frac{\partial}{\partial t}\left(\frac{C_{down}}{C_{up}}\right) = \frac{\Gamma A}{V_{down} C_{up}} \cong \frac{\phi K D_{ss} A}{\delta V_{down}} \quad (9)$$

Previous work in this lab modeled the transport of avidin through cartilage as having an effective diffusivity that includes a binding term[10]. The hypothesis was that the positively charged avidin was undergoing first order, reversible, bimolecular binding with the fixed negative charges of the cartilage matrix. Values for the binding site density of the fixed negative charge groups (N_T) and the equilibrium binding constant between avidin and the matrix (K_D) were determined using equilibrium uptake experiments. The transport curves produced in this work were used to calculate an effective diffusivity $\left(D_{eff}\right)$ and a ratio of N_T/K_D. Extrapolating the linear region to the time axis provided a value for the time lag $\left(\tau_{lag}\right)$, which is related to the effective

diffusivity by Equation 10. Assuming that D_{eff} includes the effects of first order, reversible, bimolecular binding, the ratio of binding site density to the equilibrium binding constant is related to D_{ss} and D_{eff} as shown in Equation 11. An additional assumption of this equation, which linearizes the diffusion equation, is that the concentration of free avidin inside the tissue is much, much lower than the equilibrium binding constant[106].

$$\tau_{lag} = \frac{\delta^2}{6D_{eff}} \qquad (10)$$

$$D_{eff} \cong \frac{D_{ss}}{1 + \frac{N_T}{K_D}} \qquad (11)$$

The wet weight and GAG content of the samples was also measured and analyzed. Comparisons between the bovine and human samples were made using two-sample t-tests. The correlation between GAG content and diffusivity was investigated individually for bovine and human cartilage.

4 RESULTS

4.1 Mechanical Stress Relaxation

Mechanical tests were conducted in either 0.1x or 1x PBS, resulting in ionic strengths of approximately 0.015 M or 0.15 M, respectively. Samples of both bovine and human cartilage were tested. The bovine samples came from five different animals and the human from three different donors (Table 1). Negative control samples for these tests had no avidin added; they measured the natural response of cartilage in the given salt solution for the protocol. Test samples had 100 μM of avidin added. In addition to the mechanical tests, wet weight and GAG content of the cartilage was measured.

The results below outline the effects of salt concentration and presence of avidin on the wet weight, GAG content, modulus and stress relaxation parameters for bovine and human cartilage. General comparisons between bovine and human cartilage for these different measurements are also reported. Unless otherwise stated, these data were analyzed using a

linear mixed-effects (LME) model with animal (bovine) or donor (human) as a random effect. Fixed effects included salt concentration and/or avidin concentration, depending on the data being analyzed. Reported effect sizes indicate by how much an outcome changed due to a give factor and p-values indicate how significant a factor was in the model. For a detailed breakdown of animal-by-animal and donor-by-donor results, see the table in Appendix 8.2 (pg. 74).

	Total		**0.015 M Salt**		**0.15 M Salt**		**0 µM Av**		**100 µM Av**	
Type	*N*	*S*	*N*	*S*	*N*	*S*	*N*	*S*	*N*	*S*
Bovine	21	5	9	3	12	3	8	5	13	5
Human	17	3	9	2	8	2	6	3	11	3

Table 2. Number of replicates and sample types for each mechanical test condition. This tables outlines the number of replicates in each experimental condition (*N*) and from how many different sources (*S*) those samples came from. For example, at 0.015 M salt, 9 bovine samples coming from 3 different animals were tested.

4.1.1 *Wet Weight, Modulus & GAG*

This section first describes the effects of salt and avidin on the wet weight, modulus and GAG content for bovine and human separately and then concludes by comparing the characteristics of the different cartilage sources.

The wet weight of each sample was measured at the conclusion of the mechanical protocol before the explant was digested for GAG measurements. In the LME model for wet weight, the fixed effects were salt concentration and avidin concentration. For both bovine and human cartilage, wet weight varied greatly from animal-to-animal and human donor-to-donor ($p < 0.0001$ for both). Additionally, for the bovine samples, explants that had avidin added during the mechanical protocol had ~1.47 mg lower wet weights compared to those that received no avidin ($p = 0.0142$) (Figure 8). This trend was not seen in the human cartilage, nor was salt a significant factor for either bovine or human wet weight.

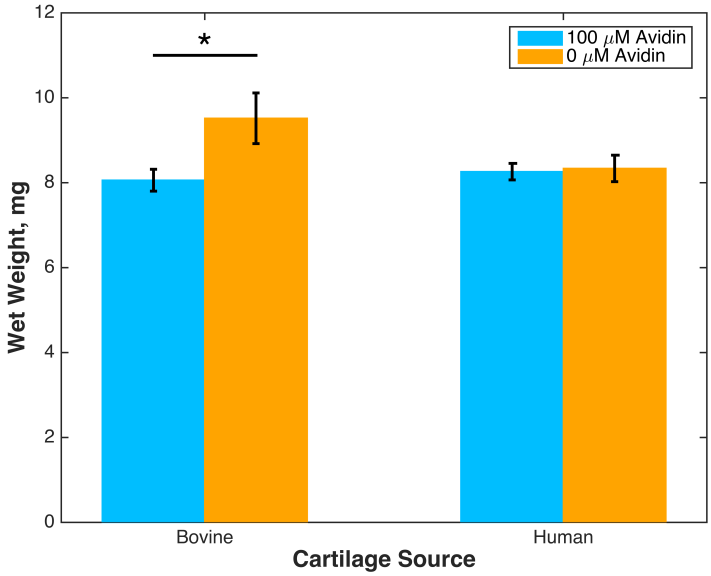

Figure 8. Wet weight of immature bovine and adult human cartilage explants after long-term (18 hours) stress relaxation with and without avidin. The blue bars (left-hand bar in each group of two) in the figure represent the average wet weight of samples that had avidin added during the mechanical protocol, while the orange bars (right-hand bar in each group of two) show the average wet weight of samples never exposed to avidin. The error bars in the figure represent the standard error of the mean (SEM). A horizontal line with a star between bars indicates a significant difference between them. This data was analyzed using a linear mixed effects model with animal/donor (bovine/human) as a random effect and salt concentration and avidin concentration as fixed effects. For the bovine data, n = 13 for the 100 μM condition and n = 8 for the 0 μM condition, all from the same 5 animals. For the human data, n = 11 for the 100 μM condition and n = 6 for the 0 μM condition, all from the same 3 donors. The addition of 100 μM of avidin to bovine samples, resulted in a ~1.47 mg decrease in wet weight (p = 0.0142).

The modulus of each sample was measured twice during the protocol—once at the beginning and again at the end. In addition to the time separating the measurements, the initial modulus was determined before any avidin would have been added, while the final modulus was measured after the time that avidin would have been added. Initial moduli were therefore only analyzed for effects of salt concentration, while the final moduli were assessed for effects of salt and avidin concentrations.

For both bovine and human, when all the initial moduli were compared to the final using a two-sample t-test, there were no significant differences (p = 0.228 for bovine and p = 0.085 for human). However, differences were seen when the data were separated into sub-groups. Bovine samples tested in 0.015 M salt had higher moduli than their counterparts tested in 0.15 M salt, both for the initial (increase of ~1 MPa)

and final (increase of ~ 0.57 MPa) moduli ($p < 0.0001$ for both). This result is shown in Figure 9A. As is seen in Figure 9B, those salt-dependencies were not observed for human cartilage. The effect of avidin was investigated by looking at each salt concentration for the final modulus within bovine and human (Figure 9C and D, respectively). At 0.15 M salt in bovine, cartilage that received avidin had a higher modulus than tissue that didn't ($p < 0.0001$). No other significant effects of avidin were seen.

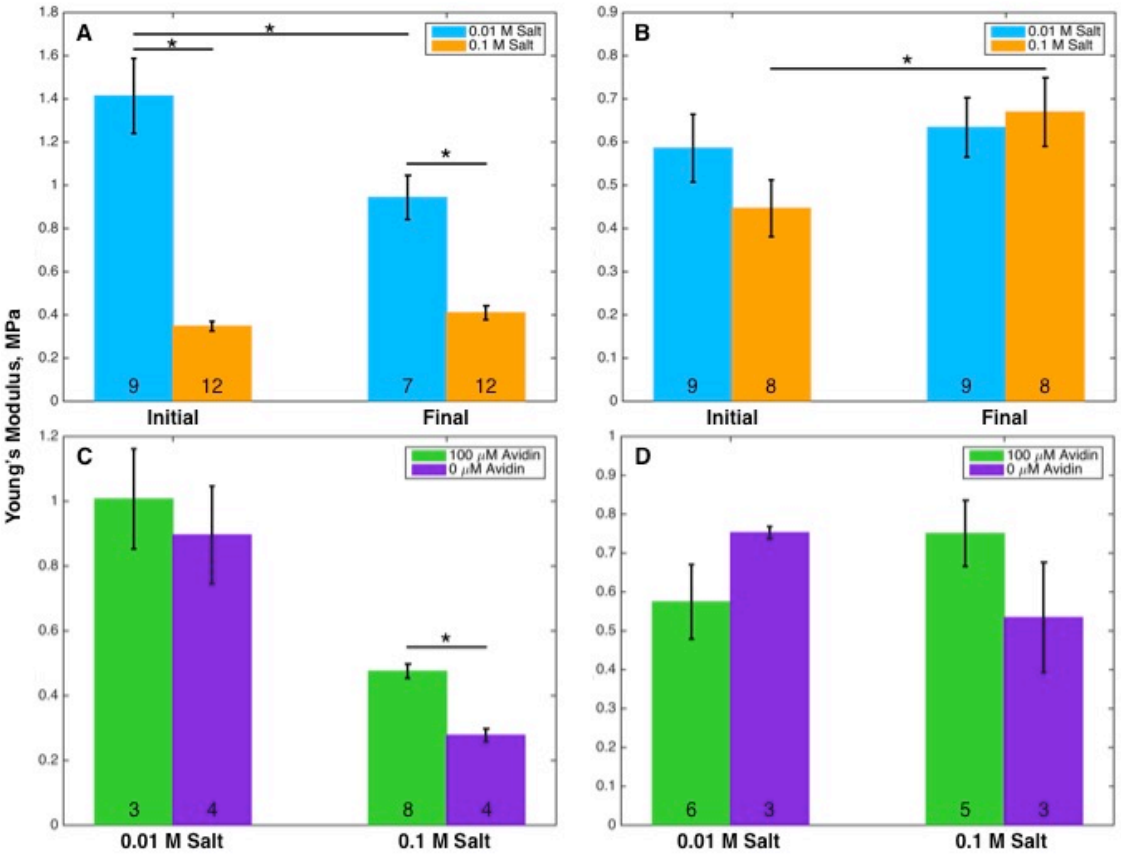

Figure 9. Young's modulus of immature bovine and adult human cartilage at different salt concentrations and with or without avidin. Bars in each figure represent the average value and error bars the SEM. The number at the bottom of each bar represents the number of replicates averaged for that bar value. The data were analyzed using linear mixed effects models and horizontal lines with stars between bars indicate significant differences. Figures **A** and **B** show the initial and final moduli of bovine and human cartilage, respectively, tested in 0.015 M salt (blue bars) and 0.15 M salt (orange bars). For bovine, samples in 0.015 M salt had higher moduli than those in 0.15 M salt both in the initial and final moduli ($p < 0.0001$ for both). Salt concentration did not have a significant effect on the moduli of the human cartilage. Figures **C** and **D** consider only the final moduli of the bovine and human cartilage, respectively, and compare the effects of avidin at each salt concentration. Green bars (left-hand bars in the groups of two) represent samples that received 100 μM of avidin and purple

bars (right-hand bars in the groups of two) represent samples that received no avidin. At 0.15 M salt, bovine samples that received avidin had a higher final modulus than those that didn't ($p < 0.0001$). The final human moduli were not significantly affected by avidin.

The GAG content of each sample was normalized by its wet weight to give a measurement of *μg GAG/mg of tissue*. This was done to account for the size variation from sample to sample. The normalized GAG content within each cartilage source depended only on the animal/donor that the explant came from and not on the salt or avidin concentrations. There was a significant different between the GAG content of the bovine samples as compared to the human, with bovine having more GAG per wet weight of tissue ($p = 0.0001$), shown in Figure 10.

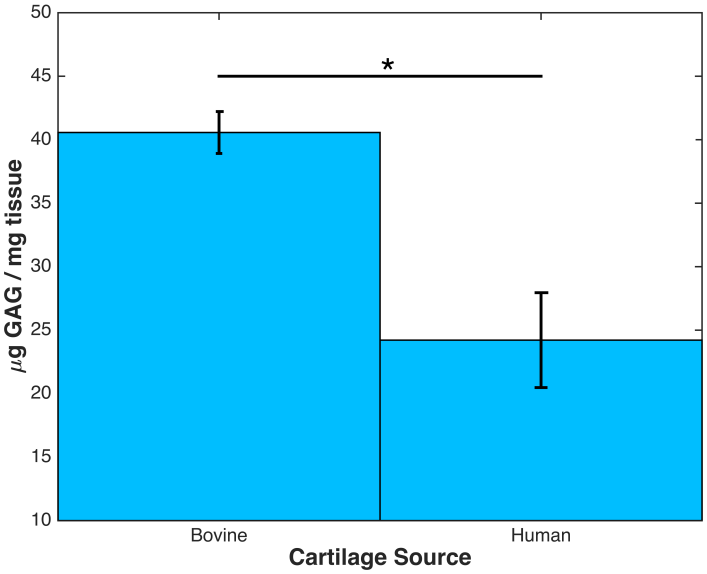

Figure 10. GAG content per wet weight of tissue for immature bovine and adult human cartilage. The bars in the figure represent the average GAG content normalized to tissue wet weight (error bars are SEM). A two-sample t-test was used to compare the bovine and human normalized GAG values. The horizontal line with the star between the two bars indicates a significant difference. The bar for the bovine data represents 21 samples from 5 different animals and the human data represents 17 samples from 3 different donors. The GAG content in the bovine samples was significantly higher than that in the human samples ($p = 0.0001$).

In addition to the GAG content, significant differences between bovine and human were seen for the initial and final moduli at 0.015 M salt and the final modulus at 0.15 M salt. The wet weight and initial modulus at 0.15 M salt did not show significant differences. Table 3 below summarizes the average values for wet weight, GAG

content and moduli for bovine and human and the p-values of a two-sample t-test between them.

	N	Wet Weight *(mg)*	Normalized GAG *(μg GAG/mg tissue)*	Modulus *(MPa)* 0.015 M Salt		Modulus *(MPa)* 0.15 M Salt	
				Initial	*Final*	*Initial*	*Final*
Bovine	21	8.61	40.57	1.41	0.94	0.35	0.41
Human	17	8.29	24.21	0.59	0.63	0.45	0.67
P-value	--	0.391	<0.0001	0.0005	0.021	0.114	0.003

Table 3. Summary of comparison of immature bovine and adult human cartilage characteristics. This table summarizes the average values for wet weight, normalized GAG content, initial/final moduli at 0.015 M salt and initial/final moduli at 0.15 M salt for bovine and human cartilage. Two-sample t-tests were used to compare the values between the bovine and human samples and the resulting p-values are reported in the last row. There were significant differences between bovine and human for the GAG content, initial modulus at 0.015 M salt, final modulus at 0.015 M salt and final modulus at 0.15 M salt.

4.1.2 *Stress Relaxation Before Addition of Avidin*

As described in the Mechanical protocol, after the 4th strain ramp and stress relaxation, samples were held at constant strain and allowed to relax for another 135 minutes before avidin was either added or not. An exponential decay model (Eqn. 3) was fit to this relaxation data and the model parameters estimated. This section reports on the fitted parameter values (a, b, τ). Physically, a represents the final equilibrium stress level that the sample relaxed to, b the difference in stress from start to equilibrium and τ the characteristic time of relaxation. All samples were treated the same up to this point in the data collection, therefore the only fixed effect for the LME model was salt concentration. Bovine and human data were analyzed separately.

As with the wet weight, GAG content and moduli, the fitted parameters varied significantly with animal/donor (p = 0.003 for bovine and p = 0.03 for human). In addition to animal-to-animal variation, salt concentration was also significant for τ (p = 0.006) in the bovine samples. At higher salt concentration (0.15 M), τ was smaller by ~32 minutes, meaning the relaxation occurred more quickly. Salt concentration was significant for all three parameters in the human samples (p = 0.037, 0.009 and 0.039 for a, b and τ, respectively). Higher salt concentration led to faster relaxation (decrease of ~9.9 minutes for τ), lower equilibrium stress (~4.5% lower a) and a larger change in stress (increase of ~4.7% for b). Curves generated using the average

parameter values for a given sample type and salt concentration are shown in Figure 11 below.

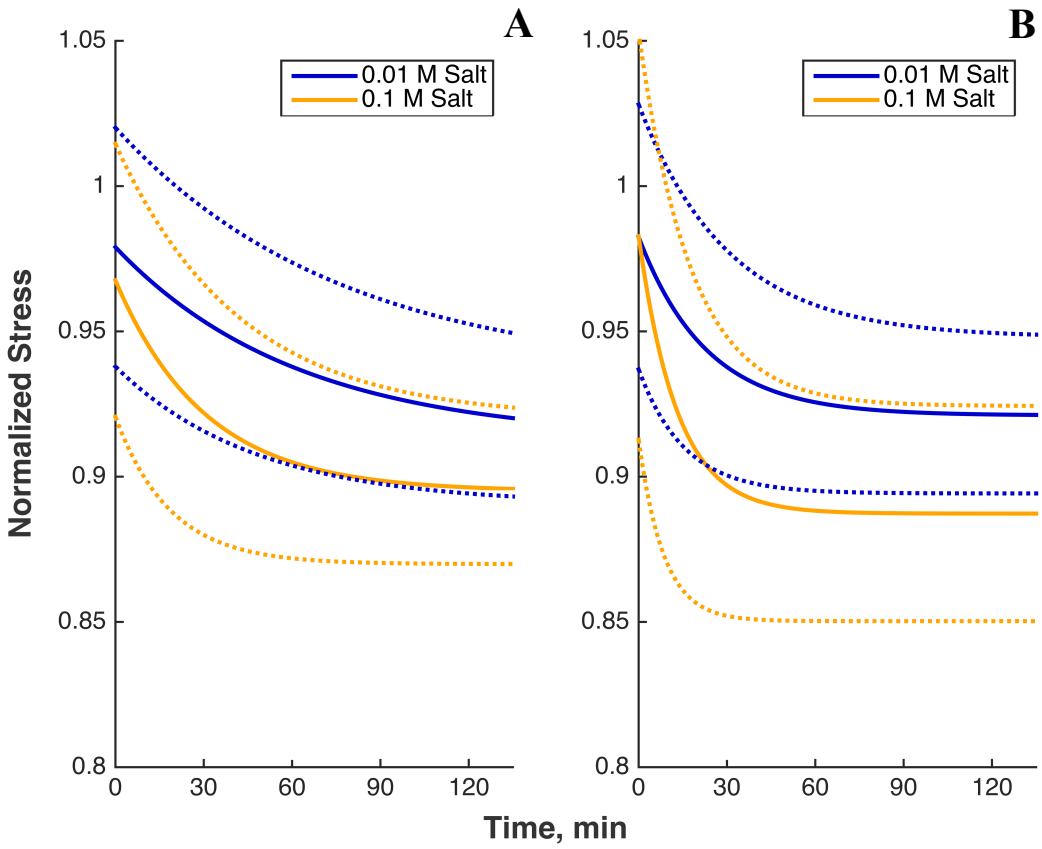

Figure 11. Stress relaxation of immature bovine and adult human cartilage equilibrated in 0.015 or 0.15 M NaCl over 135-minute strain-hold. The solid lines in each figure represent curves generated from the average exponential decay fitted parameters for samples tested in 0.015 M NaCl (blue line) and 0.15 M NaCl (orange line). The dotted lines of the same colors show 95% confidence intervals for the mean fitted parameters. The data were analyzed using LME models with animal/donor as a random effect and salt concentration as a fixed effect. Figure **A** shows the curves for bovine cartilage. The 0.015 M and 0.15 M curves represents n = 6 replicates from animals B1, B2, B5 (pg. 74) and n = 12 replicates from animals B3, B4, B5 (pg. 74), respectively. At the higher salt concentration, τ was significantly smaller (p = 0.006), leading to a faster relaxation than the lower salt concentration. Figure **B** shows the data for the human cartilage disks. The 0.015 M and 0.15 M curves represent n = 8 replicates from human donors H2, H3 (pg. 74) and n = 7 replicates from human donors H1, H3 (pg. 74), respectively. All fitted parameters were significantly different between the salt concentrations. At higher salt, the relaxation occurred faster, the equilibrium stress was lower and the change in stress was higher (p = 0.037, 0.009 and 0.039 for a, b and τ, respectively).

4.1.3 *Stress Relaxation After Addition of Avidin*

At the end of the additional 135-minute relaxation shown in the previous section, avidin was either added (test sample) or not (negative control) and the sample was allowed to relax for another 18 hours. As with the stress relaxation before the addition of avidin, an exponential decay model was fit to the data and parameters estimated. Samples were separated by salt concentration and then analyzed using a LME model with avidin as the fixed effect. Bovine and human data were analyzed separately.

Again the animal-to-animal and donor-to-donor variation was significant for all parameters at each salt concentration ($p < 0.02$ for all). At 0.015 M salt for bovine, the addition of avidin had a significant effect on parameters a and b ($p = 0.007$ and 0.044, respectively). As shown in Figure 12A, adding avidin resulted in a ~15% lower final equilibrium stress and a larger change in stress compared to no avidin. For bovine at 0.15 M salt, avidin was significant for τ ($p = 0.008$), decreasing the value by ~577 minutes when avidin was added. This can been seen in Figure 12B. Similar to the bovine, parameters a and b were significant ($p = 0.032$ and 0.003, respectively) for human at 0.015 M salt, resulting in ~8% lower final equilibrium stress when avidin was added (Figure 12C). For human cartilage at 0.15 M salt, there were no significant differences in the fitted parameters due to avidin, shown Figure 12D.

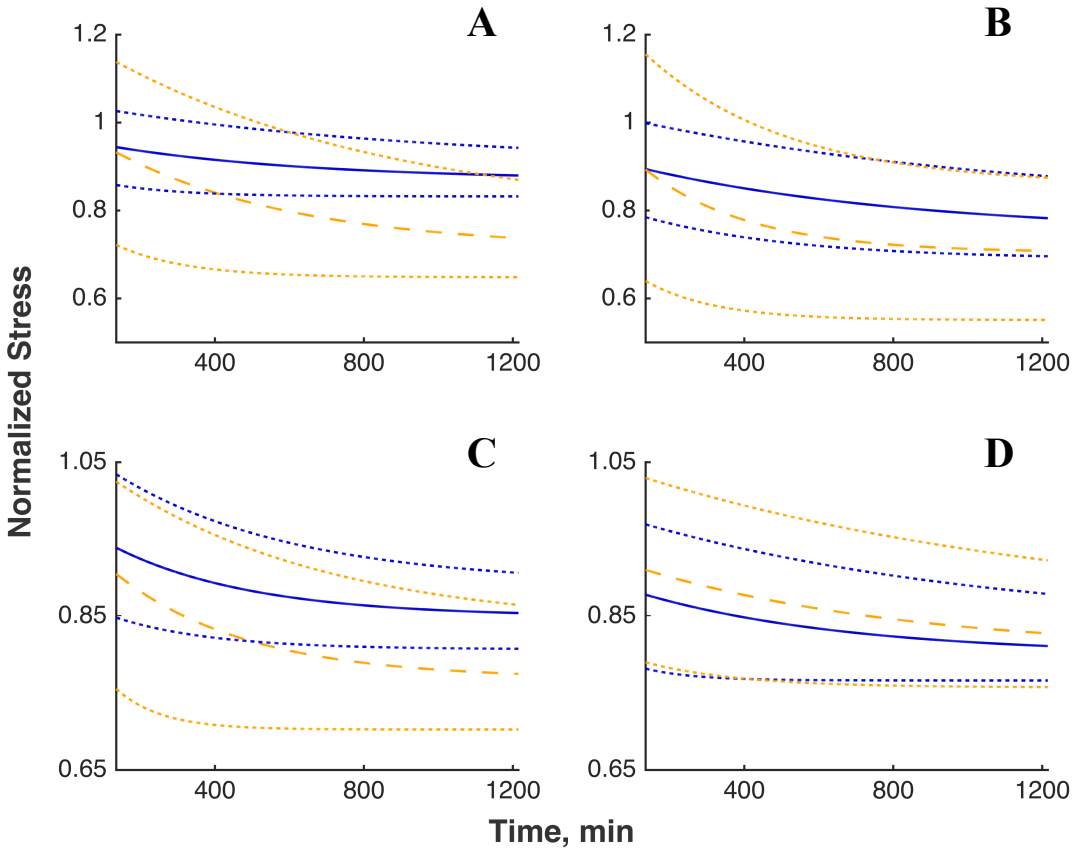

Figure 12. Long-term (18 hours) stress relaxation of immature bovine and adult human cartilage after the addition (or not) of 100 µM of avidin at 0.015 M and 0.15 M NaCl. In all figures, the solid blue lines represent curves generated from the average exponential decay fitted parameters of samples that received *no* avidin during the experiment. The same-colored dotted lines show 95% confidence intervals of the means of those same parameters. Dashed orange lines represent curves generated from the average values of the fitted parameters for samples that received 100 µM of avidin during the experiment. The same-colored dotted lines show 95% confidence intervals of the means of those same parameters. The data were analyzed using LME models with animal/donor as a random effect and avidin as a fixed effect. Figure **A** shows the curves for bovine at 0.015 M salt. At this condition, parameters a and b were significant (p = 0.007 and 0.044, respectively), with the addition of avidin leading to a ~15% lower final equilibrium stress and larger change in stress over the course of the relaxation. Figure **B** shows the curves for bovine samples at 0.15 M salt. In this case, avidin had a significant effect on τ (p = 0.008), leading to a ~577-minute faster characteristic relaxation time when avidin was present. Figure **C** shows the curves for human samples at 0.015 M salt. Avidin had a significant effect on parameters a and b for this condition (p = 0.032 and 0.003, respectively). When avidin was added at 0.015 M salt, the final equilibrium stress was ~8% lower and the change in stress higher for the human cartilage. Figure **D** shows the curves for human cartilage at 0.15 M salt. Avidin had no significant effect on any parameters for this condition. The replicates associated with each curve are as follows and reference to animal or human donor number refers to those listed in the summary table on page 74. Figure **A**: blue curve n = 3 from animals B1, B2 and orange curve n = 4 from animals B1, B2. Figure **B**: blue curve n = 4 from animals B3, B4, B5 and orange curve n = 4 from animals B3, B4. Figure **C**: blue curve n = 3 from human donors H2, H3 and orange curve n = 4 from

human donors H2, H3. Figure **D**: blue curve n = 3 from human donors H1, H3 and orange curve n = 4 from human donors H1, H3.

4.2 Real-time 1D Transport

All the transport tests were run in 1x PBS (ionic strength ~ 0.15 M) with an upstream bath concentration of 10 μM avidin. The avidin was a combination of FITC-labeled (1.9 μM) and unlabeled (8.1 μM). To ensure that the signal being measured was from the FITC-avidin complex and not free fluorescein alone, a control test was done at the end of one run in which free fluorescein was added to the upstream bath. A rapid increase in slope was observed, demonstrating that the previous fluorescent signal was from the larger FITC-avidin complex and not free fluorescein. The data from this test is shown in Appendix 8.6 (pg. 87). Because of heat generated by the magnetic stir plate used for continual mixing, the temperature inside the chamber was elevated to ~ 31˚C. See Appendix 8.4 (pg. 78) for more information about the temperature. The liquid in the downstream was constantly circulated past the detector of a spectrofluorometer, which recorded the fluorescence every three seconds over the course of the experiment. All experiments were run for at least 16 hours. At the end of the run, the wet weight of each sample was measured and subsequently its GAG content assayed after digestion.

Both bovine and human samples were tested in the real-time transport experiment. The bovine samples came from four different animals and the human from two different donors (1 & 2 in Table 1). Prior to testing, all samples were stored at -20˚C in 1x PBS+PI. Sample thickness ranged from 320 – 670 μm and all had the superficial zone intact.

The results below show the 1-D, steady state diffusion coefficient for avidin in bovine and human cartilage as calculated from the slope of the linear region of the transport curves. In addition to this calculated value, other tissue characteristic values are reported and correlations between the diffusivity and these characteristics are investigated. As mentioned in the methods section (pg. 35), the values reported here for steady-stated diffusivity (D_{ss}) actually represent the product of the porosity, partition coefficient and steady-state diffusivity ($\phi K D_{ss}$). Bovine and human samples were analyzed separately, but results for both are shown. For a detailed breakdown of animal-by-animal and donor-by-donor results, see the table in Appendix 8.2 (pg. 74).

4.2.1 *Thickness, Wet Weight & GAG*

This section briefly compares the measured thicknesses, wet weights and GAG contents of the bovine and human cartilage. Before being loaded into the transport chamber, each sample's thickness was measured with digital calipers. From a technical standpoint, slicing thin layers of the bovine explants was easier, and as a result, the bovine samples were, on average, thinner than the human samples. The explants were weighed at the end of the experiment and the human samples had a higher wet weight on average. Finally, the cartilage was digested and assayed for GAG content. The total amount of GAG in a sample was normalized by its wet weight to account for sample-to-sample size variation. This provided a measure of the $\mu g\ GAG/mg\ tissue$. The bovine and human samples were not significantly different in this measurement. A summary of the values for these measurements is shown below (Table 4) along with the p-value from a two-sample t-test comparing bovine and human samples.

	Thickness (μm)	**Wet Weight (mg)**	**Normalized GAG**
Bovine	369	8.93	34.95
Human	566	15.80	32.85
p-value	< 0.0001	< 0.0001	0.574

Table 4. Average thickness, wet weight and GAG content of immature bovine and adult human cartilage from transport experiments. This table shows the average values of 8 bovine samples from four different animals and 6 human samples from two different donors. The normalized GAG values are in units of $\mu g\ GAG/mg\ tissue$. The reported p-values are from running a two-sample t-test comparing the values of the bovine samples to the human samples.

A qualitative result of the bovine transport experiments was that uptake of the FITC-avidin could easily be seen with the naked eye at the end of the experiment. The image below (Figure 13) shows a visible green circle in the center of a cartilage explant. The uncolored rim surrounding the green is the portion of the cartilage that was clamped down, holding the sample in place for the duration of the experiment. This observation was not as easily seen in the human samples. Unlike the bovine cartilage that starts out a translucent, white color, the human cartilage is a yellowish tint at the beginning of the experiment, making it difficult to differentiate coloration due to FITC-avidin versus the natural coloring of the human cartilage.

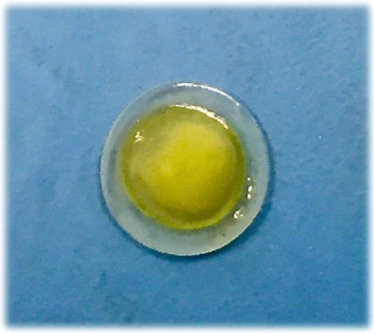

Figure 13. Image of uptake of FITC-avidin into immature bovine cartilage during transport. The green circle in the center of the image represents the available surface area of the explant during a transport experiment. The image shows that FITC-avidin is taken up into the bovine cartilage over the course of the transport experiment.

4.2.2 *Transport Curves*

The raw fluorescence signal reported by the spectrofluorometer was converted into a ratio of downstream to upstream concentration using a calibration value obtained by spiking a small volume of the upstream bath into the downstream bath part way through the experiment. An example curve of the raw signal with the calibration spike can be seen in Appendix 8.6 (pg. 87). The figures below show the relative percent in the downstream compared to the upstream over time.

Figure 14 shows curves from the 8 bovine experiments. In Figure 14A, the full-length curves are shown. The three curves from cows 1 and 2 all have two linear regions, with the second being steeper than the first. The calculated ϕKD_{ss} for the all the full-length curves, using the steeper region for cows 1 and 2, ranged from $5.65\times 10^{-8}\ cm^2/s$ to $4.36\times10^{-7}\ cm^2/s$, a difference of almost 8x. Looking at only the first 700 minutes (Figure 14B), there was only a single slope for all the curves. The range of ϕKD_{ss} values calculated using only the first 700 minutes was $5.65\times10^{-8}\ cm^2/s$ to $1.41\times10^{-7}\ cm^2/s$, a factor of 2.5x different. The average ϕKD_{ss} for the full-length curves was $2.09\times10^{-7}\ cm^2/s$ with a CV of 74.22% and for the first 700 minutes was $1.03\times10^{-7}\ cm^2/s$ with a CV of 26.26%.

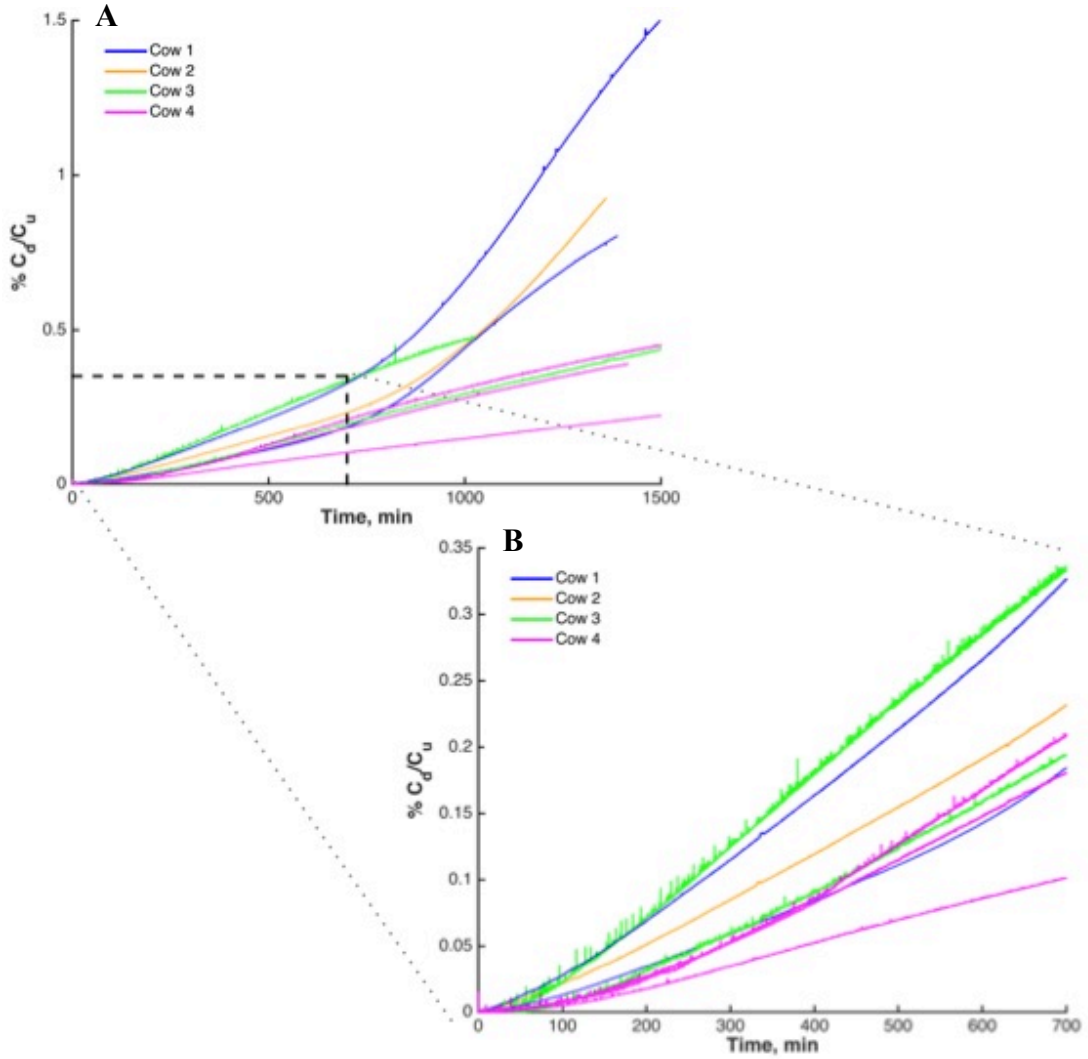

Figure 14. One-dimensional transport of avidin through immature bovine articular cartilage. These figures show the real-time transport of avidin across bovine cartilage as measured by downstream signal relative to that in the upstream (% C_d/C_u). The steady-state diffusivity of avidin is calculated using the slope of the curve and an equation for flux (Eqn. 9). Part **A** shows the full-length curves for 8 bovine samples. Three of the curves in **A** (cows 1 and 2) contain two linear regions each with their own distinct slope, while the other curves only contain a single slope. Using the steeper slope for cows 1 and 2, the average diffusivity was $2.09\times10^{-7}\ cm^2/s$ with a coefficient of variation of 74.22%. Part **B** in the figure is a zoomed in version of part **A**, looking only at the first 700 minutes. The two-slope phenomenon is not seen in this time frame. Calculating the average diffusivity using the zoomed in portion of the curves gives a value of $1.03\times10^{-7}\ cm^2/s$ with a CV of 26.26%.

The curves obtained for the human cartilage are shown in Figure 15. Although only five curves are shown, there were actually six samples run. Due to human error, the sixth sample was missing some data at the beginning of the experiment and the scale for the fluorescence reading was different than the others. For these reasons, it was not

included in the plot; however, a value for ϕKD_{ss} was still able to be determined from the linear region and calibration spike. The range of calculated ϕKD_{ss} for avidin in human cartilage was $8.53\times10^{-9}\ cm^2/s$ to $5.27\times10^{-8}\ cm^2/s$, a spread of just over 6x. The overall average was $2.67\times10^{-8}\ cm^2/s$ with a coefficient of variation of 64.25%.

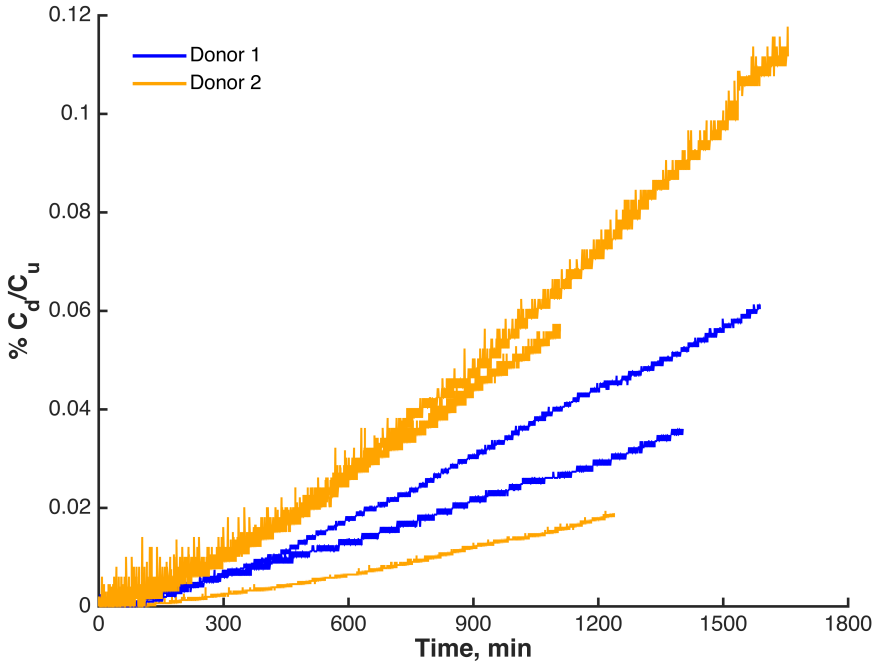

Figure 15. One-dimensional transport of avidin through adult human articular cartilage. This figure shows the real-time transport of avidin through human cartilage measured as percent signal in the downstream relative to that in the upstream. The slope of the linear region of each curve, along with an expression for flux (Eqn. 9), was used to calculate the diffusion coefficient of avidin. The average diffusion coefficient for the two human donors was $2.67\times10^{-8}\ cm^2/s$ with a coefficient of variation of 64.25%.

4.2.3 *GAG vs. Diffusivity*

The relationship between GAG content and diffusivity was investigated. The GAG chains present in the cartilage matrix provide a high concentration of fixed negative charges. Avidin is positively charged, so it was hypothesized that electrostatic interactions between the GAG molecules and avidin could affect the transport of avidin through the cartilage matrix. GAG content was again normalized by wet weight and ϕKD_{ss} was normalized by L^2, where L is the thickness of a given sample. The normalization of the diffusivity product was done because the characteristic time of diffusion is proportional to L^2/D, therefore the thickness of a sample has a large effect

on the transport. Accounting for this effect through normalization allowed for sample-to-sample comparison.

Plots of normalized GAG content versus normalized diffusivity were generated for bovine (Figure 16) and human (Figure 17) cartilage samples. The bovine data showed no clear trend for a relationship between GAG content and the diffusivity ($R^2 < 0.1$). Human cartilage, on the other hand, showed a stronger relationship between GAG content and diffusivity ($R^2 = 0.8277$). As the GAG content increased, so did the rate of diffusion.

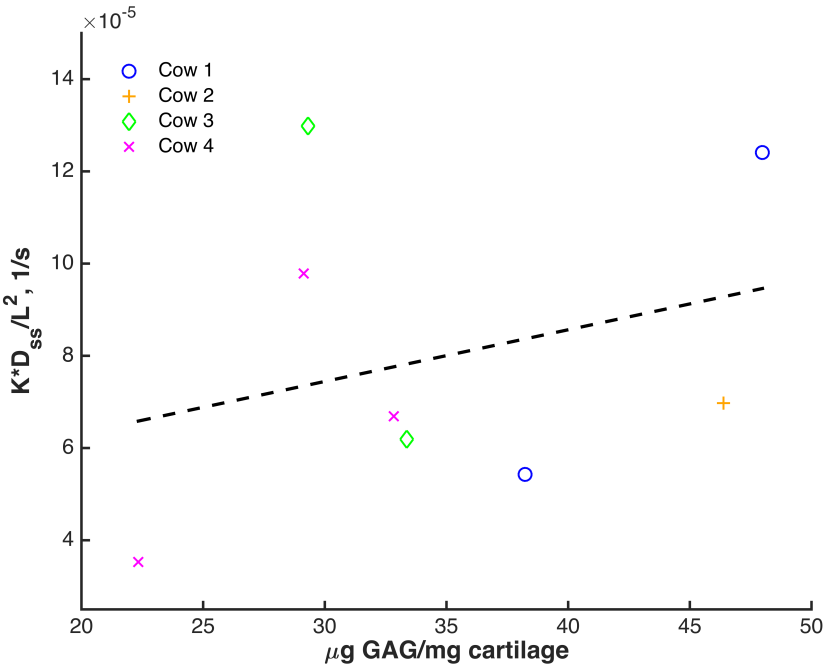

Figure 16. Normalized GAG content versus normalized diffusivity for immature bovine cartilage. This figure investigates the relationship between GAG content and diffusivity in bovine cartilage. GAG content was normalized to wet weight and diffusivity to thickness squared to account for the variations in sizes of the samples. There is no clear trend when normalized GAG content is plotted versus normalized diffusivity. The dashed line in the figure has an $R^2 < 0.1$.

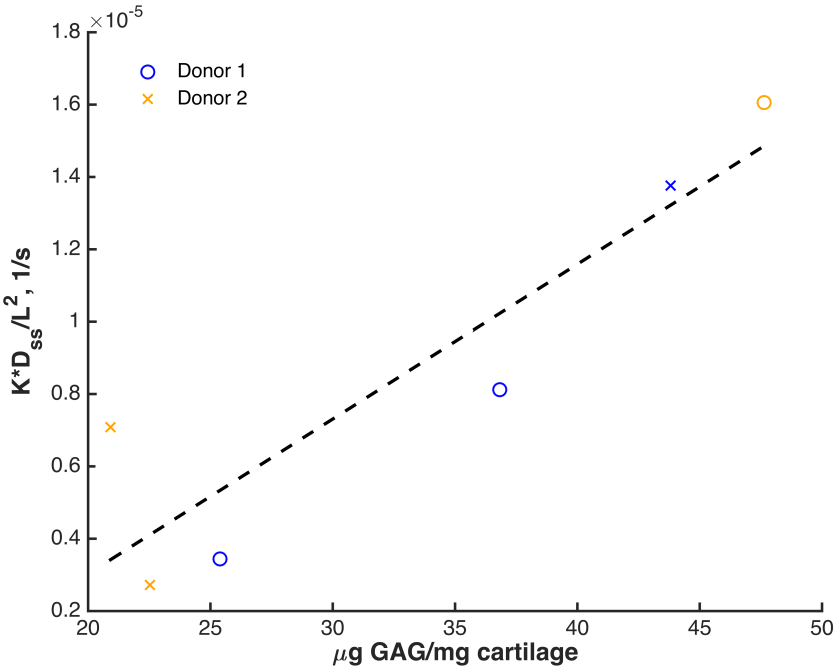

Figure 17. Normalized GAG content versus normalized diffusivity for adult human cartilage. This figure looks at the relationship between GAG content and diffusion in human cartilage. Because of sample-to-sample size variability, GAG content was normalized to wet weight and diffusivity to thickness squared. Unlike with the bovine cartilage (Figure 16), diffusion and GAG content in human cartilage is correlated ($R^2 = 0.8277$). As the GAG content increases, so does the rate of avidin diffusion.

5 DISCUSSION

5.1 Mechanical Stress Relaxation

Previous work from this lab has proposed the use of avidin as a carrier molecule to deliver drugs to cartilage for OA treatment[10]. If avidin were to be injected intra-articularly for this purpose, it would be taken up by cartilage and diffuse into the tissue. One of cartilage's main purposes in joints is to provide mechanical strength when the joint is loaded. Understanding how, if at all, the presence of avidin in cartilage affects the mechanical properties of the tissue is important in the assessment of avidin as a viable drug carrier molecule. It was hypothesized that, because avidin is positively charged and the ECM of cartilage negatively charged, the diffusion of avidin into the tissue could result in mechanical relaxation of the cartilage. The positive charge on avidin could act to shield some of the fixed negative charges in the matrix, reducing the electrostatic repulsion and effectively the mechanical strength of the tissue. The work of this thesis sought to investigate that hypothesis. The experiments that were run in 0.015 M salt were done to

maximize the likelihood of seeing a measurable effect. At low ionic strength, the GAG-GAG repulsion within the matrix of cartilage is even more accentuated due to the increase in electrical Debye length, so the shielding of these electrostatic interactions could be even more pronounced. Additionally, 100 μM of avidin is a much higher concentration than would be used clinically[139,11], but provided more molecules for potential shielding, again enhancing the effect.

Despite low N for each condition and high sample-to-sample variability, significant effects were still observed. Overall, the effects of salt and avidin were more prevalent and pronounced for the bovine samples than the human. This is likely attributable to the significantly higher GAG content of immature bovine compared to adult human that was seen (Figure 10). At physiologic ionic strength (1x PBS = 0.15 M salt (NaCl) concentration), the only significant difference observed in the human cartilage was a stiffer modulus at the end of the mechanical protocol compared to the beginning (Figure 9). Analysis of a linear mixed effects model for the initial and final moduli at 0.15 M salt with avidin as a fixed effect and human donor as a random effect, found that avidin did not have a significant effect on the modulus value ($p = 0.383$). The stiffer tissue at the end of the protocol could be due to further compaction of the tissue after complete relaxation. At 0.015 M salt, both the initial and final moduli of the bovine samples were higher than the human ($p < 0.0001$ and $p = 0.0205$, respectively). In contrast, at 0.15 M salt the human samples had higher moduli, but only the final modulus value was significantly higher ($p = 0.114$ and 0.003 for initial and final, respectively). Although the bovine samples contained more GAGs, it has been shown that the modulus of cartilage depends on more than just the electrostatic interactions between the GAG molecules[140]. It's possible that the increased modulus in human compared to bovine could be due to contributions from collagen, which forms a more integrated, mature network in adult human cartilage, and may be further stiffened by advanced glycation end products (which increase with age) compared to immature bovine. Another study that looked at modulus values for multiple sources of cartilage (human and bovine included), found that human tissue had the largest elastic modulus[141].

The effects of salt concentration were not initially the focus of this work; however, some interesting results emerged. In the lower ionic strength condition, the initial and final moduli were significantly higher for the bovine samples compared to the higher salt runs. A lower salt concentration results in an increased Debye length, consistent with a reduced shielding of, and thereby higher electrostatic repulsion between GAG molecules at the nanoscale, which can ultimately increase the modulus of the tissue. (At the macroscale, a lower bath salt concentration results in a higher difference in Donnan osmotic swelling pressure inside the tissue compared to the osmotic pressure of the bath). This effect of lower ionic strength causing the modulus to increase has been previously reported[97]. This effect was not seen in the human samples, likely because of their reduced GAG concentration as compared to the bovine.

Differences in the relaxation parameters were also seen between the salt concentrations. For both the bovine and human samples, relaxation proceeded faster at the higher salt concentration. Additionally, the human samples relaxed to a lower equilibrium stress. Cartilage inherently has a high resistance to fluid flow as is evidenced by its low hydraulic permeability $(\sim 1\times10^{-15}\, m^2/Pa\cdot s)$ [142]. A macroscale model of the electrokinetic parameters of cartilage predicts that hydraulic permeability (k) changes with pH and salt concentration[89]. Of interest for this work, the model predicts that at pH 7, the hydraulic permeability increases with increasing salt concentration. The model defines k (Eqn. 12) as being a function of fluid conductivity, σ_0, intrinsic hydraulic permeability (value if the material had zero charge), k_{11}, and fixed charge density, ρ_m, which is ultimately a function of ionic strength (and pH). Physically, as ions flow into the tissue to satisfy electroneutrality, an electrical force is generated that is directionally opposite to that of fluid flow and acts to effectively reduce the hydraulic permeability. The faster and greater relaxation seen in these experiments at higher salt could be explained by an increased hydraulic permeability, and therefore lower resistance to fluid flow, at 0.15 M salt compared to 0.015 M salt. The predicted values of k as a function of NaCl concentration are shown below in Figure 18.

$$k = k_{11}\left(1 - \frac{\rho_m^2 k_{11}}{\sigma_0 + \rho_m^2 k_{11}}\right) \qquad (12)$$

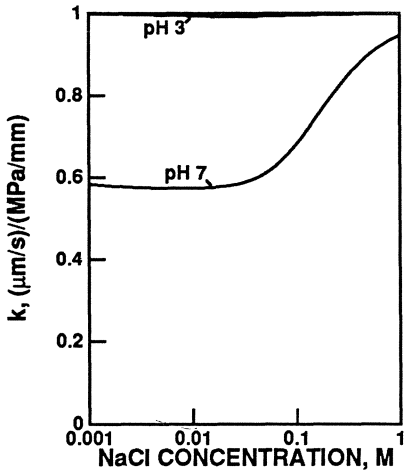

Figure 18. Hydraulic permeability as a function of NaCl concentration. This figure is a representation of the dependence of hydraulic permeability on salt concentration at pH 7 as predicted by a macro-continuum charge model. As shown in Equation 12 above, hydraulic permeability is a function of fixed charge density, which is a function of salt concentration. As the ionic strength increases (and fixed charge density decreases), the hydraulic permeability increases. (Adapted from Frank et al. 1990[89])

The main focus of this thesis was to assess the effect of avidin on the mechanical properties of cartilage as measured by stress relaxation. The addition of avidin part way through the long, constant-strain hold had significant effects at both salt concentrations for bovine cartilage and at the lower salt concentration for human. At 0.015 M salt, cartilage exposed to avidin relaxed to a lower equilibrium stress than unexposed tissue. This result supports the original hypothesis that the positive charge on avidin can shield the fixed negative charges of the ECM, causing the tissue to relax. This effect was also seen for human cartilage. At the higher salt concentration (i.e., normal physiologic ionic strength of 0.15 M), the addition of avidin resulted in faster relaxation for bovine samples. If adding avidin is thought of as simply increasing the concentration of positive ions in the bath, and therefore the ionic strength, then the theory described in the preceding paragraph about increased hydraulic permeability at higher ionic strength could explain this faster relaxation. No significant differences between +/- avidin were seen for the relaxation of human cartilage in 0.15 M salt. The increased hydraulic permeability effect may not apply for the human cartilage due to the decreased GAG content compared to bovine. The curve for predicted k values as a function of salt concentration asymptotes at very high salt.

Given that salt concentration is a proxy for FCD in the prediction of k, it's possible that the curve is shifted for human cartilage because of lower GAG content and thus smaller FCD.

Additional effects of avidin were also seen. Adding avidin caused a decrease in wet weight for bovine samples. In the context of the enhanced relaxation described above for bovine, a more relaxed tissue will have exuded more fluid by the end of the experiment, which would decrease the wet weight. This effect was not seen in human cartilage, again likely due to less GAG and overall relaxation. The final effect observed for avidin was an increase in the final modulus of bovine samples at 0.15 M salt. Intuitively this seems to be backward. If the avidin is shielding electrostatic repulsion forces, the modulus might be expected to decrease by the end of the experiment. The modulus of cartilage depends on more than just the electrostatic effects of GAGs[140], therefore this increase could be due to a different effect. If the tissue is relaxing far enough, other components of the matrix, such as collagen, could start playing a more prominent role in the stiffness. This result has been observed by other members of this lab (unpublished).

Overall, the hypothesis that avidin can induce relaxation of cartilage by shielding electrostatic effects as it diffuses into the tissue seems to be supported by the results of this thesis. Effects of avidin were seen in both human and bovine cartilage, however the effects were less pronounced for the human samples. At physiologic ionic strength in human cartilage, which is the most clinically relevant condition, avidin did not cause additional relaxation of the tissue. This is a promising result for the use of avidin as a drug carrier molecule, especially considering the 100 μM tested here is a higher concentration of avidin than would be needed clinically.

5.2 Real-time 1D Transport

The transport experiments in this thesis were run to supplement the mechanical tests. Once avidin was inside the bath of the mechanical chamber, it could enter cartilage via electrical migration, convective transport and/or diffusive transport. It was hypothesized that the process of diffusion-reaction would be the rate-limiting step of movement of avidin into cartilage and would thus be the rate-limiting process governing any avidin-induced

mechanical effects. Running transport experiments to better characterize the diffusion of avidin into and through cartilage could also shed light on to the mechanical results.

Although diffusion properties were the focus of these experiments, an interesting side result was the GAG content of the bovine samples compared to the human. In the mechanical samples, there was a significant difference in GAG content between the two cartilage sources, with bovine having more GAG per wet weight of tissue. So, it was a bit surprising to find no significant difference between the GAG per tissue-weight of bovine and human in the samples used for transport experiments. However, in considering the preparation differences of these two sample types, the lack of difference makes more sense. The bovine samples had an average thickness of less than 400 μm, meaning their composition was dominated by the superficial zone, which has the lowest GAG content as a function of depth in cartilage. The human samples, on the other hand, were closer to 600 μm thick, thus containing a considerable amount of middle and possibly even some deep zone tissue, which are more GAG-rich. This imbalance in zone distribution led to a slight over prediction of GAG for human cartilage and under prediction for bovine, ultimately resulting in their values being similar.

The main result from these transport experiments was an estimate of the steady-state diffusivity (D_{ss}) of avidin in bovine and human cartilage. Because of the way the calculation was done, the values actually represent a product of $\phi K D_{ss}$. Previous work from this lab has estimated the porosity of immature bovine cartilage (ϕ) to be 0.81 and the partition coefficient of avidin into immature bovine cartilage (K) to be 4.4 – 5.9[10]. For the sake of simplicity, the reported values were left as the product of the terms; however, an estimate of D_{ss} alone can easily be obtained by dividing the reported values by 0.81 and 4.4 – 5.9, or any other estimates for these parameters.

The average values of $\phi K D_{ss}$ for avidin in bovine and human cartilage were found to be $1.03\times10^{-7}\ cm^2/s$ and $2.67\times10^{-8}\ cm^2/s$, respectively. This suggests that the transport of avidin into and through bovine cartilage occurs ~3.9x faster than in human cartilage. Although values for ϕ and K were provided above, those were determined using immature bovine cartilage only. Due to composition differences between immature bovine and adult

human, the porosity and partition coefficient could vary greatly. For this reason, the product term was used to compare the two cartilage types. One hypothesis for the increased transport in bovine could be higher GAG content, like what was seen in the mechanical samples, which means more fixed negative charges that could attract and interact with avidin. Because the GAG content of the bovine and human samples used in the transport experiments was not significantly different, this hypothesis doesn't seem to explain the difference in this particular dataset. Another possibility is that the bovine samples contained some larger pore-like openings that artificially increased the diffusion rate. Immature bovine cartilage hasn't become fully avascular and as a result can have blood vessels reaching almost all the way to the articular surface. Although care was taken in the preparation of samples to obtain thin slices that would exclude such openings, it is possible that some samples contained remnants of blood vessels.

A previous study measured the diffusivity of ovalbumin, a negatively charged globular protein of molecular weight 45 kDa, in calf cartilage as $4\times10^{-8}\,cm^2/s$[121]. Assuming values of 0.81 and 5.15 for ϕ and K, respectively, the steady-state diffusivity estimate for avidin in immature bovine cartilage is $2.47\times10^{-8}\,cm^2/s$. Ovalbumin is a smaller molecule than avidin, so it would be expected that its diffusion would occur faster. The values reported here support that trend, although the ovalbumin is only ~1.6x faster than the avidin. One important difference between the two molecules is their charge, which could explain why the difference in diffusivity is small. The negative charge on ovalbumin could cause it to be repelled by the fixed negative charges in the cartilage ECM, effectively slowing its transport. The opposite could be true for avidin in that its positive charge could be attracted to the fixed negative charges, enhancing its transport. A study measuring the transport of serum albumin, a 69 kDa globular protein with a net negative charge, through human cartilage found a diffusivity of $2\times10^{-7}\,cm^2/s$[110] and partition coefficient of 0.01. Comparing the ϕKD_{ss} value for serum albumin to that reported here for avidin with the assumption that the porosities of the human cartilage used in the two different studies were the same, the transport of avidin is about an order of magnitude faster than that of the serum albumin. These results are consistent with the theory given the larger size of serum albumin and its negative charge compared to avidin's positive charge.

Another interesting result of the transport data was the correlation between the wet-weight normalized GAG content and thickness-normalized diffusivity for human cartilage. As GAG content increased, so did the rate of diffusion. This result supports the idea that the avidin is interacting with the GAGs, and more specifically with the fixed negative charges, in such a way as to enhance transport (i.e., partitioning and diffusion). Similar results have been reported for animal models in vivo. In rabbits, as GAG content increased, so did the half-life of avidin inside cartilage when normalized with respect to the square of the thickness[139]. In rats, GAG content was also correlated with the half-life of avidin in cartilage; however, the normalization by the square of the thickness was not necessary. The latter is likely due to the thinness of rat cartilage[11]. The GAG/diffusivity correlation was not observed for the bovine data in this work. That could be due to the pore phenomenon mentioned previously or to the vast sample-to-sample variability observed in immature bovine as their cartilage is still developing.

A puzzling result of this work was the set of transport curves that had two linear regions, each with the second having a steeper slope. Models of diffusion predict a linear region of the curve to represent steady state flux; however, they don't predict two different linear regions. The inflection points of these curves followed by a steeper slope seem to indicate the occurrence of an additional phenomenon other than the transport of avidin. One hypothesis is that the steeper slope actually represents transport of free fluorescein rather than FITC-labeled avidin. In a separate transport run, the diffusivity of free fluorescein was found to be $4.61\times10^{-7}\ cm^2/s$, only 1.05 – 1.54x faster than the values calculated using the second slopes. If, over the course of the experiment, fluorescein came off the avidin or the avidin was somehow degraded into smaller pieces, an increase in the rate of transport would be expected. The cause of this proposed breakdown is unknown at this time, but could be due to an increased temperature in the chamber. All the transport experiments were conducted above room temperature; however, this set of three curves was run at an even higher temperature than the rest, about 2 – 3˚C hotter. This increased temperature could give rise to enzymatic activity that breaks down the linkage between fluorescein and avidin or just degrade avidin itself. Additional control experiments would need to be run to confirm this hypothesis.

Previous experiments of this lab investigated the transport properties of avidin in immature bovine cartilage. Equilibrium uptake experiments produced values of $K = 5.9$, $K_D = 150.3\ \mu M$ and $N_T = 2920\ \mu M$, partition coefficient, equilibrium binding constant and binding site density, respectively. Transient transport experiments, similar to those run for this study, gave a value of $\phi K D_{ss} = 1.13\times10^{-5}\ cm^2/s$. This value is 110x faster than the reported average value of this work. The previous experiments also yielded $D_{eff} = 3.8\times10^{-7}\ cm^2/s$ based on the observed lag time in the transient experiment. Values for D_{eff} were calculated for this work as well, but not reported because the values were nearly the same as those for D_{ss} due to the very short observed lag times. Although the setups used were similar, they were not exactly the same. The previous experiments used a much larger chamber and thus bath volume. Additionally, the downstream fluorescence was not measured continually, but rather aliquots were taken from the downstream at different time points and read in a fluorescence plate reader to build up the transport curve over time. The discrepancy between the D_{eff} values could be a function of experimental setup and instrument sensitivity. The aliquot method has a decreased time resolution as compared to the continuous measurement method, which could lead to the actual lag time being shorter than observed occurs in between aliquots. Additionally, if the sensitivity of the fluorescence plate reader instrument is not as low as the spectrofluorometer, the lag time could become of function of instrument capabilities rather than tissue properties.

The transport experiments from this work provided some insight into the movement of avidin through bovine and human cartilage. They also raised some questions not able to be addressed in the scope of this work. The two different types of bovine curves seen as well as the discrepancies between values from this work compared to previously reported values warrant additional investigation into the transport properties of avidin in cartilage.

5.3 Avidin Induced Stress Relaxation

Embedded in the main hypothesis of this thesis that avidin could induce stress relaxation of cartilage, was the prediction that the time for such a relaxation would be governed by the diffusion rate of avidin into the tissue. After a perturbation to cartilage in a mechanical system, there are three main processes that follow to re-establish equilibrium. The first is

the electrical redistribution of charge, which happens on the order of nanoseconds. Because the charge re-equilibrates so rapidly, this is not a rate limiting process. The other two processes are fluid flow and ion (or other solute) concentration redistribution. Under a poroelastic model of cartilage, the characteristic time for fluid flow (Eqn. 13) depends on the square of the characteristic length (L^2), the aggregate modulus (H), the hydraulic permeability (k) and a scaling factor appropriate for the geometry of the system, in this case (radial) the first zero of the Bessel function $(\lambda \approx 2.405)$[12]. The characteristic time for radial diffusion of a solute (Eqn. 14) depends on the diffusivity (D) of the solute and also the square of the characteristic length and same scaling factor[12].

$$\tau_m = \frac{L^2}{\lambda^2 H k} \qquad (13)$$

$$\tau_D = \frac{L^2}{\lambda^2 D} \qquad (14)$$

Using the mechanical values from this thesis, τ_m ranged from 4 – 14 minutes for the different sample types and salt concentrations. The calculated diffusivities gave values of τ_D to be approximately 630 minutes for bovine cartilage and 2430 minutes for human cartilage.

In this study, cartilage samples were subjected to two types of perturbations. The first was a mechanical deformation by way of compressive strain. Experimentally, fitting a model (Eqn. 4) to the 4th strain ramp yielded relaxation times on the order of 1 minute. Extending the fit window to include an additional 2 hours past the 4th strain ramp yielded relaxation times on the order of 13 – 60 minutes. These values are on the same order of magnitude as the poroelastic times predicted above, suggesting that the governing process after compression is poroelastic fluid rearrangement. The second type of perturbation was the addition of avidin 2.5 hours after the previous compression. Fitting these data to a model (Eqn. 4) gave relaxation times of 280 – 490 minutes for bovine and 350 – 725 minutes for human; the ranges include values for both salt concentrations. These times are more on the order of the predicted characteristic diffusion times, suggesting that the stress relaxation

induced by the addition of avidin is rate-governed by the diffusion of avidin into the cartilage.

Although values for the steady-state diffusivity of avidin in bovine and human cartilage were calculated in this work, several questions remain with respect to the transport properties of avidin in cartilage. Additional experiments to better understand the whole picture of transport (e.g., partitioning, binding, etc.) could help to explain the discrepancies seen here between the predicted characteristic diffusion times and experimentally observed relaxation times.

6 SUMMARY & CONCLUSIONS

Osteoarthritis is one of the most common joint diseases affecting people worldwide. One area of research receiving significant amounts of attention in recent years is the delivery of drugs via intra-articular injection. OA is a localized disease, so administering treatment directly to the disease location rather than systemically has many benefits, including less systemic side effects and higher effective drug concentration at the treatment site. One of the main challenges associated with IA injections is the body's rapid clearance of molecules from the joint space. To combat this problem, researchers have focused on creating drug delivery systems that increase the retention time of a drug in the joint space so it can more effectively deliver its therapeutic payload.

Motivated by previous results from this lab suggesting the potential use of avidin as a drug carrier molecule for IA injection, the main goal of this thesis was to determine what effects, if any, avidin has on the mechanical properties of cartilage. One of the main functions of articular cartilage is to provide the joint with mechanical strength in compressive and shear loading. It is also one of the main tissues affected by OA, thus making it a popular target for drug therapies. Although avidin has already been shown to be non-toxic to chondrocytes, an important safety check for any drug carrier, its effects on the mechanical integrity of cartilage were not thoroughly investigated. If avidin were to cause a decrease in the mechanical strength of cartilage upon IA injection, it may not be a viable drug delivery vehicle or may at least require specific post-injection instructions to reduce the risk of

further tissue damage. Understanding this is important to guide future research with avidin and potentially to inform clinical recommendations.

For this work, mechanical stress relaxation tests were performed on immature bovine and adult human cartilage. Effects due to sample type, salt concentration and presence of avidin were assessed. Most clinically relevant was the finding that at physiologic ionic strength (1x PBS ~ 0.15 M NaCl), the addition of a high concentration of avidin (100 μM) to human cartilage had no measurable effect in the setup used. This result suggests that using avidin as a drug delivery molecule would not adversely affect the mechanical strength of cartilage post-injection. Avidin was found to have effects on cartilage in other conditions tested. In bovine cartilage at both ionic strengths and human cartilage at only low ionic strength, avidin induced stress relaxation. These findings fit with the theory that as avidin diffuses into cartilage, its positive charge interacts with and shields some of the fixed negative charges on the GAG chains of the cartilage ECM. This shielding reduces the GAG-GAG repulsion and allows the tissue to relax. Faster relaxation in both bovine and human cartilage was observed in the higher ionic strength condition, possibly due to an increased hydraulic permeability, allowing fluid to flow out of the tissue more quickly.

Real-time, one-dimensional transport experiments were also conducted. From these tests, estimates of the steady-state diffusivity of avidin in bovine and human cartilage were obtained. It was found that transport of avidin through the bovine tissue was faster than in human. This set of experiments raised many additional questions that warrant investigation, but were outside the scope of this thesis. Experiments aimed at better understanding the partitioning of avidin into cartilage as well as any processes, such as binding, that might be occurring once the avidin is inside cartilage would help to provide an overall picture of avidin's transport in cartilage. Running the transport experiment at different salt concentrations could help answer questions related to avidin's ability to weakly bind to GAG chains via electrostatic interactions. Another experiment that might be useful is a dynamic uptake measurement in which the rate of avidin leaving a bath and entering cartilage is measured. An example protocol for this type of test is described in Appendix 8.11.

The protocols developed for this thesis lay the foundation for testing of future candidate drug delivery molecules. Mechanical strength is an extremely important property of articular cartilage. Any delivery system targeted for cartilage should be assessed for its effect on the mechanical integrity of the tissue. The transport experiments, potentially with some improvements or supplemented with other measurements, can provide additional insight for the mechanical tests. Comparing the experimentally measured relaxation times with the predicted characteristic time for diffusion can help to understand what the rate-governing process is if mechanical effects are observed.

Overall, the results of this thesis suggest that avidin does not have adverse effects on the mechanical strength of human articular cartilage as it is taken up by and diffuses into the tissue. Combined with the previous results from this lab, the mechanical safety of avidin makes it a viable candidate for drug delivery via IA injection to treat OA. For completeness, additional tests at lower concentrations of avidin (e.g., 1 and 10 μM) should be run to verify these results. The concentration of avidin used for this work was much higher than what would be administered clinically, so more relevant concentrations should be assessed. Preliminary tests done by Yamini Krishnan of this lab, suggest that 10 μM avidin has no measureable effects on the equilibrium modulus and dynamic stiffness of bovine cartilage (unpublished), so it is expected that no effects would be seen in the mechanical stress relaxation tests at 10 μM or lower concentrations.

7 REFERENCES

1. The State of US Health, 1990-2010: Burden of Diseases, Injuries, and Risk Factors. *J. Am. Med. Assoc.* 310, 591–608 (2013).
2. Dieppe, P., Berenbaum, F. & Sharma, L. in *Primer on the Rheumatic Diseases* 224–240
3. Brown, T. D., Johnston, R. C., Saltzman, C. L., Marsh, J. L. & Buckwalter, J. A. Posttraumatic osteoarthritis: a first estimate of incidence, prevalence, and burden of disease. *J. Orthop. Trauma* 20, 739–744 (2006).
4. Anderson, D. D. *et al.* Post-traumatic osteoarthritis: Improved understanding and opportunities for early intervention. *J. Orthop. Res.* 29, 802–809 (2011).
5. Evans, C. H., Kraus, V. B. & Setton, L. A. Progress in intra-articular therapy. *Nat. Rev. Rheumatol.* 10, 11–22 (2014).
6. Huebner, K. D., Shrive, N. G. & Frank, C. B. Dexamethasone inhibits inflammation and cartilage damage in a new model of post-traumatic osteoarthritis. *J. Orthop. Res. Off. Publ. Orthop. Res. Soc.* 32, 566–572 (2014).
7. Heard, B. J. *et al.* A single administration of dexamethasone may protect tibial plateau cartilage in a mechanically stable surgical model of post traumatic osteoarthritis. *Osteoarthritis Cartilage* 22, S372 (2014).
8. Li, Y. *et al.* Effects of insulin-like growth factor-1 and dexamethasone on cytokine-challenged cartilage: relevance to post-traumatic osteoarthritis. *Osteoarthritis Cartilage* 23, 266–274 (2015).
9. Grodzinsky, A. J., Wang, Y., Kakar, S., Vrahas, M. S. & Evans, C. H. Intra-articular dexamethasone to inhibit the development of post-traumatic osteoarthritis. *J. Orthop. Res.* n/a–n/a (2016). doi:10.1002/jor.23295
10. Bajpayee, A. G., Wong, C. R., Bawendi, M. G., Frank, E. H. & Grodzinsky, A. J. Avidin as a model for charge driven transport into cartilage and drug delivery for treating early stage post-traumatic osteoarthritis. *Biomaterials* 35, 538–549 (2014).
11. Bajpayee, A. G., Scheu, M., Grodzinsky, A. J. & Porter, R. Electrostatic interactions enable rapid penetration, enhanced uptake and retention of intra-articular injected avidin in rat knee joints. *J. Orthop. Res.* 32, 1044–1051 (2014).
12. Eisenberg, S. R. & Grodzinsky, A. J. The Kinetics of Chemically Induced Nonequilibrium Swelling of Articular Cartilage and Corneal Stroma. *J. Biomech. Eng.* 109, 79–89 (1987).
13. Gerwin, N., Hops, C. & Lucke, A. Intraarticular drug delivery in osteoarthritis. *Adv. Drug Deliv. Rev.* 58, 226–242 (2006).
14. McCracken, T. *New atlas of human anatomy*. (MetroBooks, 2000).
15. Zhang, Z., Barman, S. & Christopher, G. F. The role of protein content on the steady and oscillatory shear rheology of model synovial fluids. *Soft Matter* 10, 5965–5973 (2014).
16. OpenStax CNX. OpenStax CNX, Synovial Joints. (2013). Available at: http://cnx.org/contents/bFtYymxt@4/Synovial-Joints. (Accessed: 29th April 2016)
17. Mansour, J. M. in *Kinesiology: the mechanics and pathomechanics of human movement* 69–83 (Lippincott Williams & Wilkins, 2009).
18. Ng, L. *et al.* Individual cartilage aggrecan macromolecules and their constituent glycosaminoglycans visualized via atomic force microscopy. *J. Struct. Biol.* 143, 242–257 (2003).

19. Sophia Fox, A. J., Bedi, A. & Rodeo, S. A. The Basic Science of Articular Cartilage. *Sports Health* 1, 461–468 (2009).
20. Buckwalter, J., Mow, V. & Ratcliffe, A. Restoration of Injured or Degenerated Articular Cartilage. *J. Am. Acad. Orthop. Surg.* 2, 192–201 (1994).
21. Felson, D. T. & Neogi, T. Osteoarthritis: Is it a disease of cartilage or of bone? *Arthritis Rheum.* 50, 341–344 (2004).
22. Hellio, L. G.-G. Disease modifying osteoarthritis drugs: Facing development challenges and choosing molecular targets. *Curr. Drug Targets* 11, 528–535 (2010).
23. Goldring, M. B. & Goldring, S. R. Articular cartilage and subchondral bone in the pathogenesis of osteoarthritis. *Ann. N. Y. Acad. Sci.* 1192, 230–237 (2010).
24. Risk Factors | Arthritis | CDC. Available at: http://www.cdc.gov/arthritis/basics/risk-factors.htm. (Accessed: 18th April 2016)
25. Spector, T. D. & MacGregor, A. J. Risk factors for osteoarthritis: genetics1. *Osteoarthritis Cartilage* 12, Supplement, 39–44 (2004).
26. Marsh, J. L., Weigel, D. P. & Dirschl, D. R. Tibial plafond fractures. How do these ankles function over time? *J. Bone Joint Surg. Am.* 85-A, 287–295 (2003).
27. Beecher, B. R., Martin, J. A., Pedersen, D. R., Heiner, A. D. & Buckwalter, J. A. Antioxidants block cyclic loading induced chondrocyte death. *Iowa Orthop. J.* 27, 1–8 (2007).
28. Martin, J. A. & Buckwalter, J. A. Post-traumatic osteoarthritis: The role of stress induced chondrocyte damage. *Biorheology* 43, 517–521 (2006).
29. Buckwalter, J. A., Saltzman, C. & Brown, T. The impact of osteoarthritis: Implications for research. *Clin. Orthop.* S6–S15 (2004). doi:10.1097/01.blo.0000143938.30681.9d
30. Gelber, A. C. *et al.* Joint injury in young adults and risk for subsequent knee and hip osteoarthritis. *Ann. Intern. Med.* 133, 321–328 (2000).
31. Gillquist, J. & Messner, K. Anterior cruciate ligament reconstruction and the long-term incidence of gonarthrosis. *Sports Med. Auckl. NZ* 27, 143–156 (1999).
32. Roos, H. *et al.* Knee osteoarthritis after meniscectomy: prevalence of radiographic changes after twenty-one years, compared with matched controls. *Arthritis Rheum.* 41, 687–693 (1998).
33. Laird, A. & Keating, J. F. Acetabular fractures: a 16-year prospective epidemiological study. *J. Bone Joint Surg. Br.* 87, 969–973 (2005).
34. Weigel, D. P. & Marsh, J. L. High-energy fractures of the tibial plateau. Knee function after longer follow-up. *J. Bone Joint Surg. Am.* 84-A, 1541–1551 (2002).
35. Olson, S. A. & Guilak, F. From articular fracture to posttraumatic arthritis: A black box that needs to be opened. *J. Orthop. Trauma* 20, 661–662 (2006).
36. Dirschl, D. R. & Adams, G. L. A critical assessment of factors influencing reliability in the classification of fractures, using fractures of the tibial plafond as a model. *J. Orthop. Trauma* 11, 471–476 (1997).
37. Jupiter, null. Complex Articular Fractures of the Distal Radius: Classification and Management. *J. Am. Acad. Orthop. Surg.* 5, 119–129 (1997).
38. Trumble, T. E., Culp, R., Hanel, D. P., Geissler, W. B. & Berger, R. A. Intra-articular fractures of the distal aspect of the radius. *J. Bone Jt. Surg. - Ser. A* 80, 582–600 (1998).
39. Burstein, D. & Gray, M. New MRI techniques for imaging cartilage. *J. Bone Jt. Surg. - Ser. A* 85, 70–77 (2003).

40. Lohmander, L. S., Ionescu, M., Jugessur, H. & Poole, A. R. Changes in joint cartilage aggrecan after knee injury and in osteoarthritis. *Arthritis Rheum.* 42, 534–544 (1999).
41. Carlson, C. S., Guilak, F., Vail, T. P., Gardin, J. F. & Kraus, V. B. Synovial fluid biomarker levels predict articular cartilage damage following complete medial meniscectomy in the canine knee. *J. Orthop. Res.* 20, 92–100 (2002).
42. Martin, J. A., McCabe, D., Walter, M., Buckwalter, J. A. & McKinley, T. O. N-acetylcysteine inhibits post-impact chondrocyte death in osteochondral explants. *J. Bone Jt. Surg. - Ser. A* 91, 1890–1897 (2009).
43. Goodwin, W. *et al.* Rotenone prevents impact-induced chondrocyte death. *J. Orthop. Res.* 28, 1057–1063 (2010).
44. Ding, L., Guo, D., Homandberg, G. A., Buckwalter, J. A. & Martin, J. A. A single blunt impact on cartilage promotes fibronectin fragmentation and upregulates cartilage degrading stromelysin-1/matrix metalloproteinase-3 in a bovine ex vivo model. *J. Orthop. Res.* 32, 811–818 (2014).
45. D'Lima, D. D., Hashimoto, S., Chen, P. C., Lotz, M. K. & Colwell, C. W. Prevention of chondrocyte apoptosis. *J. Bone Jt. Surg. - Ser. A* 83, 25–26 (2001).
46. Green, D. M. *et al.* Effect of early full weight-bearing after joint injury on inflammation and cartilage degradation. *J. Bone Jt. Surg. - Ser. A* 88, 2201–2209 (2006).
47. Guilak, F. *et al.* The role of biomechanics and inflammation in cartilage injury and repair. *Clin. Orthop.* 17–26 (2004).
48. Pelletier, J.-P. & Martel-Pelletier, J. DMOAD developments: Present and future. *Bull. NYU Hosp. Jt. Dis.* 65, 242–248 (2007).
49. Hellio, L. G.-G. OA clinical trials: current targets and trials for OA. Choosing molecular targets: what have we learned and where we are headed? *Osteoarthritis Cartilage* 17, 1393–1401 (2009).
50. Rundell, S. A., Baars, D. C., Phillips, D. M. & Haut, R. C. The limitation of acute necrosis in retro-patellar cartilage after a severe blunt impact to the in vivo rabbit patello-femoral joint. *J. Orthop. Res.* 23, 1363–1369 (2005).
51. Ramakrishnan, P. *et al.* Oxidant conditioning protects cartilage from mechanically induced damage. *J. Orthop. Res.* 28, 914–920 (2010).
52. Ding, L. *et al.* Mechanical impact induces cartilage degradation via mitogen activated protein kinases. *Osteoarthritis Cartilage* 18, 1509–1517 (2010).
53. Chubinskaya, S., Hurtig, M. & Rueger, D. C. OP-1/BMP-7 in cartilage repair. *Int. Orthop.* 31, 773–781 (2007).
54. Hurtig, M., Chubinskaya, S., Dickey, J. & Rueger, D. BMP-7 protects against progression of cartilage degeneration after impact injury. *J. Orthop. Res.* 27, 602–611 (2009).
55. Pascual, G. *et al.* Anti-apoptotic treatments prevent cartilage degradation after acute trauma to human ankle cartilage. *Osteoarthritis Cartilage* 17, 1244–1251 (2009).
56. Natoli, R. M. & Athanasiou, K. A. P188 reduces cell death and IGF-I reduces GAG release following single-impact loading of articular cartilage. *J. Biomech. Eng.* 130, (2008).
57. Osteoarthritis Treatment. *arthritis.org* Available at: http://www.arthritis.org/about-arthritis/types/osteoarthritis/treatment.php. (Accessed: 8th March 2016)
58. de Silva, M., Page, T., Hazleman, B. L. & Wraight, P. LIPOSOMES IN ARTHRITIS: A NEW APPROACH. *The Lancet* 313, 1320–1322 (1979).

59. Bonanomi, M. H. *et al.* Studies of pharmacokinetics and therapeutic effects of glucocorticoids entrapped in liposomes after intraarticular application in healthy rabbits and in rabbits with antigen-induced arthritis. *Rheumatol. Int.* 7, 203–212 (1987).
60. Thakkar, H., Sharma, R. K. & Murthy, R. S. R. Enhanced retention of celecoxib-loaded solid lipid nanoparticles after intra-articular administration. *Drugs R. D.* 8, 275–285 (2007).
61. Horisawa, E. *et al.* Prolonged anti-inflammatory action of DL-lactide/glycolide copolymer nanospheres containing betamethasone sodium phosphate for an intra-articular delivery system in antigen-induced arthritic rabbit. *Pharm. Res.* 19, 403–410 (2002).
62. Higaki, M., Ishihara, T., Izumo, N., Takatsu, M. & Mizushima, Y. Treatment of experimental arthritis with poly(D, L-lactic/glycolic acid) nanoparticles encapsulating betamethasone sodium phosphate. *Ann. Rheum. Dis.* 64, 1132–1136 (2005).
63. Liang, L. S., Wong, W. & Burt, H. M. Pharmacokinetic study of methotrexate following intra-articular injection of methotrexate loaded poly(L-lactic acid) microspheres in rabbits. *J. Pharm. Sci.* 94, 1204–1215 (2005).
64. Tunçay, M. *et al.* In vitro and in vivo evaluation of diclofenac sodium loaded albumin microspheres. *J. Microencapsul.* 17, 145–155 (2000).
65. Study of FX006 for the Treatment of Pain in Patients With Osteoarthritis of the Knee - Full Text View - ClinicalTrials.gov. Available at: https://clinicaltrials.gov/ct2/show/NCT02357459. (Accessed: 8th March 2016)
66. Floss, D. M., Schallau, K., Rose-John, S., Conrad, U. & Scheller, J. Elastin-like polypeptides revolutionize recombinant protein expression and their biomedical application. *Trends Biotechnol.* 28, 37–45 (2010).
67. Shamji, M. F. *et al.* Development and characterization of a fusion protein between thermally responsive elastin-like polypeptide and interleukin-1 receptor antagonist: Sustained release of a local antiinflammatory therapeutic. *Arthritis Rheum.* 56, 3650–3661 (2007).
68. Shamji, M. F. *et al.* Synthesis and characterization of a thermally-responsive tumor necrosis factor antagonist. *J. Controlled Release* 129, 179–186 (2008).
69. Betre, H. *et al.* A thermally responsive biopolymer for intra-articular drug delivery. *J. Controlled Release* 115, 175–182 (2006).
70. Ringdahl, E. & Sandesh, P. Treatment of Knee Osteoarthritis. *Am. Fam. Physician* 83, 1287–1292
71. Chrousos, G., Pavlaki, A. N. & Magiakou, M. A. in *Endotext* (eds. De Groot, L. J. et al.) (MDText.com, Inc., 2000).
72. Lu, Y. C. S., Evans, C. H. & Grodzinsky, A. J. Effects of short-term glucocorticoid treatment on changes in cartilage matrix degradation and chondrocyte gene expression induced by mechanical injury and inflammatory cytokines. *Arthritis Res. Ther.* 13, (2011).
73. Heard, B. J. *et al.* Single intra-articular dexamethasone injection immediately post-surgery in a rabbit model mitigates early inflammatory responses and post-traumatic osteoarthritis-like alterations. *J. Orthop. Res.* 33, 1826–1834 (2015).
74. Bajpayee, A. G., Quadir, M. A., Hammond, P. T. & Grodzinsky, A. J. Charge based intra-cartilage delivery of single dose dexamethasone using Avidin nano-carriers suppresses cytokine-induced catabolism long term. *Osteoarthritis Cartilage* 24, 71–81 (2016).
75. Helppolainen, S. H. *et al.* Rhizavidin from Rhizobium etli: the first natural dimer in the avidin protein family. *Biochem. J.* 405, 397–405 (2007).

76. Korpela, J. Avidin, a high affinity biotin-binding protein, as a tool and subject of biological research. *Med. Biol.* 62, 5–26 (1984).
77. Green, N. M. Avidin. 1. The use of [14C]biotin for kinetic studies and for assay. *Biochem. J.* 89, 585–591 (1963).
78. Berman, H. M. *et al.* The Protein Data Bank. *Nucleic Acids Res.* 28, 235–242 (2000).
79. Bajpayee, A. G. Charge-based transport and drug delivery into cartilage for localized treatment of degenerative joint diseases. (Massachusetts Institute of Technology, 2015).
80. Becher, C., Springer, J., Feil, S., Cerulli, G. & Paessler, H. H. Intra-articular temperatures of the knee in sports – An in-vivo study of jogging and alpine skiing. *BMC Musculoskelet. Disord.* 9, 46 (2008).
81. HORVATH, S. M. & HOLLANDER, J. L. Intra-articular temperature as a measure of joint reaction. *J. Clin. Invest.* 28, 469–473 (1949).
82. Kim, Y.-H., Baek, S.-S., Choi, K.-S., Lee, S.-G. & Park, S.-B. The effect of cold air application on intra-articular and skin temperature in the knee. *Yonsei Med. J.* 43, 621–626 (2002).
83. PENNEYS, R. & SMUKLER, N. M. Changes in the intra-articular temperature of the knee with cutaneous vasoconstriction and vasodilatation of the toes in normal subjects. *Ann. Rheum. Dis.* 15, 241–245 (1956).
84. Warren, T. A., McCarty, E. C., Richardson, A. L., Michener, T. & Spindler, K. P. Intra-articular Knee Temperature Changes: Ice Versus Cryotherapy Device. *Am. J. Sports Med.* 32, 441–445 (2004).
85. Ammer, K. Temperature of the human knee - A review. *Thermol. Int.* 22, 137–151 (2012).
86. HOLLANDER, J. L. & MOORE, R. Studies in osteo-arthritis using intra-articular temperature response to injection of hydrocortisone acetate and prednisone. *Ann. Rheum. Dis.* 15, 320–326 (1956).
87. Li, S.-T. & Katz, E. P. An electrostatic model for collagen fibrils. The interaction of reconstituted collagen with Ca++, Na+, and Cl−. *Biopolymers* 15, 1439–1460 (1976).
88. Mow, V. C., Ratcliffe, A. & Woo, S. L.-Y. *Biomechanics of Diarthrodial Joints*. (Springer Science & Business Media, 2012).
89. Frank, E. H., Grodzinsky, A. J., Phillips, S. L. & Grimshaw, P. E. in *Biomechanics of Diarthrodial Joints* (eds. Ratcliffe, A., Woo, S. L.-Y. & Mow, V. C.) 261–282 (Springer New York, 1990).
90. Grodzinsky, A. J. ELECTROMECHANICAL AND PHYSICOCHEMICAL PROPERTIES OF CONNECTIVE TISSUE. *Crit. Rev. Biomed. Eng.* 9, 133–199 (1983).
91. Urban, J. P. G., Maroudas, A., Bayliss, M. T. & Dillon, J. Swelling pressures of proteoglycans at the concentrations found in cartilaginous tissues. *Biorheology* 16, 447–464 (1979).
92. Fessler, J. H. A structural function of mucopolysaccharide in connective tissue. *Biochem. J.* 76, 124–132 (1960).
93. Freeman, W. D. & Maroudas, A. Charged Group Behavior in Cartilage Proteoglycans in Relation to pH. *Ann Rheum Sid Supp 2* 34, 34–35 (1975).
94. Nussbaum, J. H. & Grodzinsky, A. J. Proton diffusion reaction in a protein polyelectrolyte membrane and the kinetics of electromechanical forces. *J. Membr. Sci.* 8, 193–219 (1981).
95. Grodzinsky, A. J., Roth, V., Myers, E., Grossman, W. D. & Mow, V. C. The Significance of Electromechanical and Osmotic Forces in the Nonequilibrium Swelling Behavior of Articular Cartilage in Tension. *J. Biomech. Eng.* 103, 221–231 (1981).

96. HEDBLOM, E. E. The role of polysaccharides in corneal swelling. *Exp. Eye Res.* 1, 81–91 (1961).
97. Eisenberg, S. R. & Grodzinsky, A. J. Swelling of articular cartilage and other connective tissues: Electromechanochemical forces. *J. Orthop. Res.* 3, 148–159 (1985).
98. Myers, E. R., Lai, W. M. & Mow, V. C. A Continuum Theory and an Experiment for the Ion-Induced Swelling Behavior of Articular Cartilage. *J. Biomech. Eng.* 106, 151–158 (1984).
99. Sokoloff, L. Elasticity of articular cartilage: Effect of ions and viscous solutions. *Science* 141, 1055–1057 (1963).
100. Elmore, S. M., Sokoloff, L., Norris, G. & Carmeci, P. Nature of 'imperfect' elasticity of articular cartilage. *J. Appl. Physiol.* 18, 393–396 (1963).
101. Parsons, J. R. & Black, J. Mechanical behavior of articular cartilage: Quantitative changes with alteration of ionic environment. *J. Biomech.* 12, 765–773 (1979).
102. Maroudas, A. in *Adult Articular Cartilage* 215–290 (Pitman Medical, 1979).
103. Bodine, A. J., Brown, N., Hayes, W. C. & Jiminez, S. A. The Effect of Sodium Chloride on the Shear Modulus of Articular Cartilage. *Trans 26th Orthop Res Soc* 5, 37 (1980).
104. Biot, M. A. General theory of three-dimensional consolidation. *J. Appl. Phys.* 12, 155–164 (1941).
105. Biot, M. A. Mechanics of deformation and acoustic propagation in porous media. *J. Appl. Phys.* 33, 1482–1498 (1962).
106. Grodzinsky, A. J. & Frank, E. H. *Fields, Forces, and Flows in Biological Systems*. (Garland Science, 2011).
107. Torzilli, P. A., Adams, T. C. & Mis, R. J. Transient solute diffusion in articular cartilage. *J. Biomech.* 20, 203–214 (1987).
108. Torzilli, P. A. Effects of temperature, concentration and articular surface removal on transient solute diffusion in articular cartilage. *Med. Biol. Eng. Comput.* 31, S93–S98 (1993).
109. Torzilli, P. A., Grande, D. A. & Arduino, J. M. Diffusive properties of immature articular cartilage. *J. Biomed. Mater. Res.* 40, 132–138 (1998).
110. Maroudas, A. Transport of solutes through cartilage: permeability to large molecules. *J. Anat.* 122, 335–347 (1976).
111. Moeini, M., Lee, K.-B. & Quinn, T. M. Temperature affects transport of polysaccharides and proteins in articular cartilage explants. *J. Biomech.* 45, 1916–1923 (2012).
112. Quinn, T. M., Kocian, P. & Meister, J.-J. Static Compression Is Associated with Decreased Diffusivity of Dextrans in Cartilage Explants. *Arch. Biochem. Biophys.* 384, 327–334 (2000).
113. Quinn, T. M., Morel, V. & Meister, J. J. Static compression of articular cartilage can reduce solute diffusivity and partitioning: implications for the chondrocyte biological response. *J. Biomech.* 34, 1463–1469 (2001).
114. Quinn, T. M., Dunlop, A. E. & Evans, R. C. New Approaches to Solute Transport Measurement in Mechanically Loaded Articular Cartilage. *JSME Int. J. Ser. C Mech. Syst. Mach. Elem. Manuf.* 45, 944–951 (2002).
115. Fetter, N. L., Leddy, H. A., Guilak, F. & Nunley, J. A. Composition and transport properties of human ankle and knee cartilage. *J. Orthop. Res.* 24, 211–219 (2006).
116. Leddy, H. A. & Guilak, F. Site-specific molecular diffusion in articular cartilage measured using fluorescence recovery after photobleaching. *Ann. Biomed. Eng.* 31, 753–760 (2003).

117. Garcia, A. M. *et al.* Transport and binding of insulin-like growth factor I through articular cartilage. *Arch. Biochem. Biophys.* 415, 69–79 (2003).
118. Byun, S. *et al.* Transport and equilibrium uptake of a peptide inhibitor of PACE4 into articular cartilage is dominated by electrostatic interactions. *Arch. Biochem. Biophys.* 499, 32–39 (2010).
119. Garcia, A. M., Lark, M. W., Trippel, S. B. & Grodzinsky, A. J. Transport of tissue inhibitor of metalloproteinases-1 through cartilage: Contributions of fluid flow and electrical migration. *J. Orthop. Res.* 16, 734–742 (1998).
120. Burstein, D., Gray, M. L., Hartman, A. L., Gipe, R. & Foy, B. D. Diffusion of small solutes in cartilage as measured by nuclear magnetic resonance (NMR) spectroscopy and imaging. *J. Orthop. Res.* 11, 465–478 (1993).
121. Foy, B. D. & Blake, J. Diffusion of paramagnetically labeled proteins in cartilage: Enhancement of the 1-D NMR imaging technique. *J. Magn. Reson.* 148, 126–134 (2001).
122. Zhang, L. & Szeri, A. Z. Transportation of neutral solute in deformable, anisotropic, soft tissue. *Comput. Math. Appl.* 53, 232–243 (2007).
123. Arbabi, V., Pouran, B., Weinans, H. & Zadpoor, A. A. Transport of Neutral Solute Across Articular Cartilage: The Role of Zonal Diffusivities. *J. Biomech. Eng.* 137, 071001–071001 (2015).
124. Tandon, P. N. & Agarwal, R. A study of nutritional transport in a synovial joint. *Comput. Math. Appl.* 17, 1131–1141 (1989).
125. O'Hara, B. P., Urban, J. P. & Maroudas, A. Influence of cyclic loading on the nutrition of articular cartilage. *Ann. Rheum. Dis.* 49, 536–539 (1990).
126. Zhang, L. & Szeri, A. Z. Transport of neutral solute in articular cartilage: effects of loading and particle size. *Proc. R. Soc. Lond. Math. Phys. Eng. Sci.* 461, 2021–2042 (2005).
127. Huang, C.-Y. & Wei, Y. G. Effects of tension-compression nonlinearity on solute transport in charged hydrated fibrous tissues under dynamic unconfined compression. *J. Biomech. Eng.* 129, 423–429 (2007).
128. Mauck, R. L., Hung, C. T. & Ateshian, G. A. Modeling of Neutral Solute Transport in a Dynamically Loaded Porous Permeable Gel: Implications for Articular Cartilage Biosynthesis and Tissue Engineering. *J. Biomech. Eng.* 125, 602–614 (2003).
129. Albro, M. B., Li, R., Banerjee, R. E., Hung, C. T. & Ateshian, G. A. Validation of theoretical framework explaining active solute uptake in dynamically loaded porous media. *J. Biomech.* 43, 2267–2273 (2010).
130. Allhands, R. V., Torzilli, P. A. & Kallfelz, F. A. Measurement of diffusion of uncharged molecules in articular cartilage. *Cornell Vet.* 74, 111–123 (1984).
131. Silvast, T. S., Jurvelin, J. S., Tiitu, V., Quinn, T. M. & Töyräs, J. Bath Concentration of Anionic Contrast Agents Does Not Affect Their Diffusion and Distribution in Articular Cartilage In Vitro. *Cartilage* 4, 42–51 (2013).
132. Torzilli, P. A., Arduino, J. M., Gregory, J. D. & Bansal, M. Effect of proteoglycan removal on solute mobility in articular cartilage. *J. Biomech.* 30, 895–902 (1997).
133. Chin, H. C., Moeini, M. & Quinn, T. M. Solute transport across the articular surface of injured cartilage. *Arch. Biochem. Biophys.* 535, 241–247 (2013).
134. Moeini, M. & Quinn, T. M. Solute adsorption to surfaces of articular cartilage explants: apparent versus actual partition coefficients. *Soft Matter* 8, 11880–11888 (2012).

135. Moeini, M. *et al.* Decreased solute adsorption onto cracked surfaces of mechanically injured articular cartilage: Towards the design of cartilage-specific functional contrast agents. *Biochim. Biophys. Acta BBA - Gen. Subj.* 1840, 605–614 (2014).
136. Muehleman, C., Bareither, D., Huch, K., Cole, A. A. & Kuettner, K. E. Prevalence of degenerative morphological changes in the joints of the lower extremity. *Osteoarthritis Cartilage* 5, 23–37 (1997).
137. Sui, Y. *et al.* Mechanical injury potentiates proteoglycan catabolism induced by interleukin-6 with soluble interleukin-6 receptor and tumor necrosis factor α in immature bovine and adult human articular cartilage. *Arthritis Rheum.* 60, 2985–2996 (2009).
138. Farndale, R. W., Buttle, D. J. & Barrett, A. J. Improved quantitation and discrimination of sulphated glycosaminoglycans by use of dimethylmethylene blue. *Biochim. Biophys. Acta BBA - Gen. Subj.* 883, 173–177 (1986).
139. Bajpayee, A., Grodzinsky, A. J., Porter, R. & Scheu, M. A rabbit model demonstrates the influence of cartilage thickness on intra-articular drug delivery and retention within cartilage. *J. Orthop. Res.* 33, 660–667 (2015).
140. Khalsa, P. S. & Eisenberg, S. R. Compressive behavior of articular cartilage is not completely explained by proteoglycan osmotic pressure. *J. Biomech.* 30, 589–594 (1997).
141. Taylor, S. D. *et al.* Comparison of human and animal femoral head chondral properties and geometries. *Proc. Inst. Mech. Eng. [H]* 226, 55–62 (2012).
142. Mow, V. C., Holmes, M. H. & Michael Lai, W. Fluid transport and mechanical properties of articular cartilage: A review. *J. Biomech.* 17, 377–394 (1984).
143. Rubinstein, M. & Colby, R. H. *Polymer Physics*. (OUP Oxford, 2003).
144. Molecular Probes. Amine-Reactive Probes. (2013).
145. Molecular Probes. The best and brightest - Alexa Fluor ®488 dye. (2006).

8 APPENDICES

8.1 Commonly Used Recipes

1. *Medium*

   Dulbecco's modified eagle medium (DMEM), low-glucose (ThermoFisher Scientific, Waltham, MA)
   Non-essential amino acids (NEAA), 100x
   HEPES, 100x
   PSA, 100x
   Ascorbic acid, 250x
   Proline, 250x

   Final concentration of all concentrated components is 1x (1:100 or 1:250 dilution) and enough DMEM to achieve desired volume.

   For 50-mL of Low-Glucose Medium:
   500 µL NEAA, 100x
   500 µL HEPES, 100x
   500 µL PSA, 100x
   200 µL Ascorbic acid, 250x
   200 µL Proline, 250x
   48.1 mL DMEM, low-glucose

2. *Proteinase K*

   Proteinase K (Roche catalog # 745-723)
   Tris Buffer
   50 mM Tris-HCl
   1 mM $CaCl_2$
   pH 8.0

   Stock solution = 2 mg/mL (dissolve 100 mg protease K into 50 mL Tris buffer)
   Working concentration = 0.1 mg/mL (1:20 dilution of stock in Tris buffer

8.2 Average Mechanical and Transport Parameters of Adult Human & Immature Bovine Cartilage

Source	M/F	Age	Grade	µg GAG/mg tissue*		Initial Modulus (MPa)†		Final Modulus (MPa)†		KD_{ss} (cm^2/s)†	L (cm)#
				Mechanical	*Transport*	*0.015 M*	*0.15 M*	*0.015 M*	*0.15 M*		
H1	M	26	1	34.56 n = 3	36.62 n = 3	--	0.60 (21.18%)	--	0.83 (21.08%)	2.72E-08 (81.25%)	0.0547
H2	F	62	0	13.35 n = 4	29.09 n = 3	0.62 (22.72%)	--	0.66 (18.16%)	--	2.62E-08 (60.00%)	0.0586
*H3*ξ	M	32	0	20.00 n = 9	--	0.56 (54.75%)	0.30 (21.49%)	0.61 (44.10%)	0.51 (29.02%)	--	--
B1	--	--	--	41.78 n = 4	--	1.32 (26.24%)	--	0.91 (11.64%)	--	--	--
B2	--	--	--	45.85 n = 4	--	1.72 (27.60%)	--	1.06 (25.04%)	--	--	--
B3	--	--	--	--	43.11 n = 2	--	--	--	--	1.04E-07 (34.75%)	0.0352
B4	--	--	--	--	46.38 n = 1	--	--	--	--	1.12E-07	0.0400
B5	--	--	--	40.95 n = 4	31.34 n = 2	--	0.41 (19.25%)	--	0.44 (27.08%)	1.21E-07 (23.91%)	0.0367
B6	--	--	--	28.69 n = 2	28.10 n = 3	--	0.27 (7.86%)	--	0.30 (39.61%)	8.70E-08 (30.81%)	0.0371
B7	--	--	--	40.03 n = 7	--	0.56 n = 1	0.33 (17.18%)	0.55 n = 1	0.42 (23.83%)	--	--

* n is the number of samples for that source, applies across the columns
† Percent under the parameter value is the coefficient of variation (standard deviation ÷ mean x 100)
# Thickness of cartilage used for the transport experiments
ξ Human donor 3 was tested in both salt concentrations (n = 5 for 0.015 M and n = 4 for 0.15 M)

8.3 GAG Loss in Different Conditions

1. Varying Salt Concentrations

Purpose:

The mechanical tests run for this work were conducted in buffers of varying salt concentration. Because of this, the length of the test (24 hours) and lack of protease inhibitor in the experiment buffer, there was concern about matrix loss over the course of the experiment. Losing GAG throughout the experiment could affect the mechanical properties and ultimately cloud the results. To this end, this experiment was run to assess GAG loss in conditions used for the mechanical tests to determine whether or not GAG loss was a major factor.

Experiment:

Six different combinations of storage and experimental condition were tested for three different salt concentrations using young bovine cartilage. The plugs were stored for 18 hours and then moved to their experimental conditions for 24 hours at room temperature. At the conclusion of the experiment, the wet weight of the plugs was measured and then they were digested overnight. The plug digest as well as the experiment solution was assayed for GAG content.

Salt Concentrations = 0.1x, 1x and 10x PBS

	Storage	Experiment
1	Medium @ 37˚C	Salt solution
2	Medium @ 37˚C	Incubate 1 hour in salt solution + PI → salt solution
3	Medium @ 37˚C	Salt solution + PI
4	1x PBS+PI @ -20˚C	Salt solution
5	1x PBS+PI @ -20˚C	Salt solution + PI
6	1x PBS @ -20˚C	Incubate 1 hour in salt solution + PI → salt solution

Table 5. Summary of test conditions for salt concentration GAG loss experiment

Results:

The reported results are GAG loss as calculated by Equation 15 below.

$$\%\ GAG\ loss = \frac{solution\ GAG}{solution\ GAG + explant\ GAG} \times 100 \qquad (15)$$

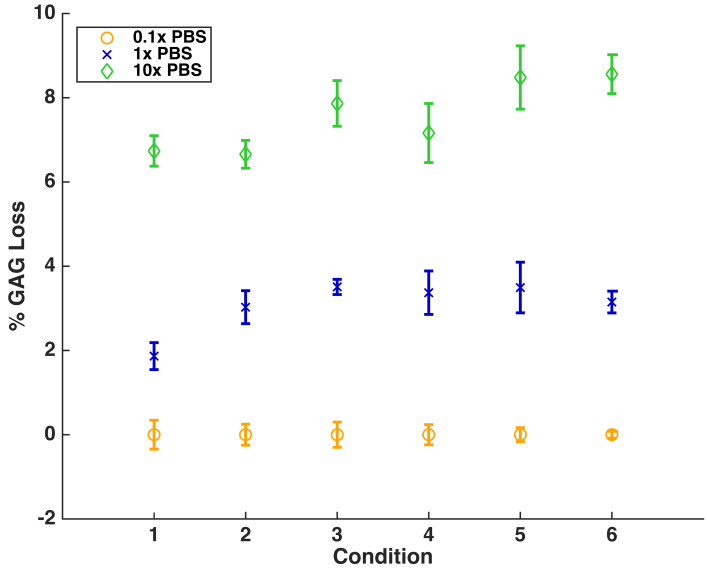

Figure 19. Percent GAG loss in different salt concentrations over 24 hours at room temperature. Error bars represent the standard error of the mean (n = 3 for each point). All experimental conditions in 0.1x PBS showed little to no GAG loss. GAG loss for all conditions in 1x PBS was significantly less than for any condition in 10x ($p \leq 0.015$). To compare conditions within a given salt concentration, ANOVA with post-hoc Tukey's range test were run. For the 10x PBS, conditions 1 and 2 had significantly less GAG loss than conditions 5 and 6 ($p < 0.05$). For the 1x PBS, condition 1 had significantly less GAG loss than conditions 3, 4 and 5. Although there were some differences within a salt concentration, as a whole, no clear trends emerged with respect to the storage (fresh vs. frozen) or experiment condition (amount of protease inhibitor). Even in the worst-case scenario, the GAG loss over 24 hours at room temperature didn't exceed 10%. The mechanical tests for this thesis were run in either 0.1x or 1x PBS. Based on the results of this experiment, GAG loss over the course of the mechanical tests was not a concern.

2. With & Without Protease Inhibitor at Two Temperatures

Purpose:

Preliminary long-term mechanical stress relaxation tests (data not shown) showed odd behavior when protease inhibitor was present in the test solution at low salt concentration. It was hypothesized that because the salt concentration was low, the ionic strength of the protease inhibitor could have a large effect on the overall solution ionic strength. The mechanical properties of cartilage are highly dependent on the ionic strength of the solution, so an unexpected change in ionic strength could cause changes to the stress relaxation behavior. An attempt was made to determine the ionic strength of the PI, but its formulation is proprietary and Roche was not willing to provide that information. Removing the PI from the test solution eliminated the odd behavior; however, then there was then concern that not inhibiting protease activity could lead to degradation of the cartilage matrix over the course of the experiment. Losing matrix affects the mechanical properties as well, so this experiment was run to assess whether or not the inclusion of PI was necessary to keep the cartilage matrix intact.

Additionally, temperature monitoring of early transport experiments revealed that the temperature inside the chamber increased to ~32˚C within the first hour of the experiment and stayed at that level for the duration. Enzyme activity is known to be affected by temperature, so there was concern about increased proteolytic activity at this increased temperature. This experiment also sought to quantify the differences in GAG loss with temperature.

Experiment:

All combinations of the following storage conditions, experimental conditions and temperatures were tested using young bovine cartilage. All plugs were stored for 24 hours before the experiment and the experiment ran for 24 hours. The wet weight of the samples was measured at the end of 24 hours and then the plugs were digested overnight. Both the plug digest and experiment solution were assayed for GAG content.

Storage Conditions:

S1 medium @ 37˚C
S2 1x PBS @ -20˚C
S3 1x PBS + PI @ -20˚C

Experiment Conditions:

C1 1x PBS
C2 incubate 1 hour in 1x PBS + PI → 1x PBS
C3 1x PBS + PI

Temperatures:

T1 30˚C
T2 37˚C

Results:

The reported results are GAG loss as calculated by Equation 15.

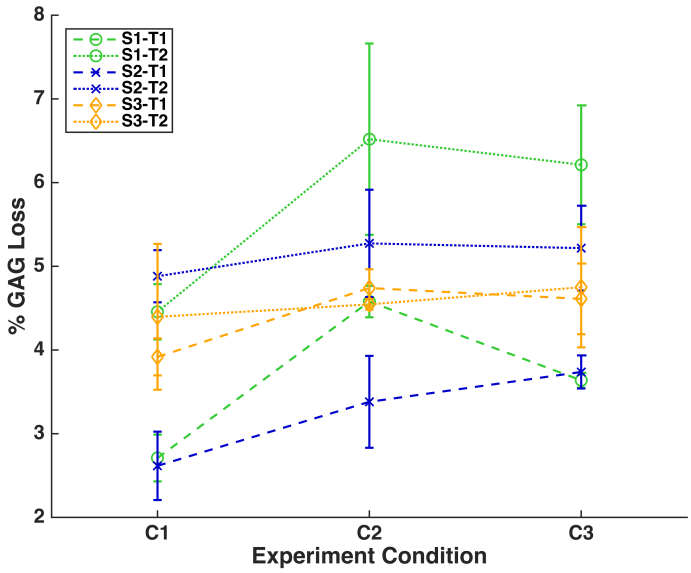

Figure 20. Percent GAG loss with and without protease inhibitor at two different temperatures. Error bars represent the standard error (n = 3 for each point). Data only represent

GAG loss during the 24 hours of the experiment, not the total GAG loss from the time of harvest. If the total GAG loss is considered, the S1 storage condition (medium at 37˚C) has significantly more GAG loss than the other two storage conditions across all experiment conditions and both temperatures (data not shown). Two-way ANOVAs were run for each storage condition with temperature and experiment condition as factors. For plugs stored at 37˚C after harvesting (S1), both the temperature and the experiment condition were significant, with temperature accounting for the majority of the variability. The S2 storage condition (1x PBS at -20˚C) was significantly affected by the temperature but not the experiment condition. GAG loss for plugs stored in 1x PBS + PI at -20˚C (S3), wasn't affect by either the temperature or the experiment condition. Overall, none of the storage/experiment/temperature combinations had greater than 8% GAG loss over the course of 24 hours. The best use of protease inhibitor, based on the findings of this experiment, is to include it in the frozen storage buffer. Doing this appeared to protect the explants against increased GAG loss at higher temperatures like what was seen in storage conditions that didn't include PI.

8.4 Temperature Measurements

1. Purpose

In early mechanical stress relaxation tests, the amount of noise observed during long static holds was unexpected. One theory on the noise was changing temperature in the dynastat room. It was thought that the building management might change the temperature in the building significantly over the course of 24 hours. Additionally, when early transport experiments were run, condensation was observed on the inside of the chamber by the end of the 24-hour experiment. For both these reasons, a temperature recording system was purchased and used to monitor the temperature over time in both the mechanical and transport experiments. The specs for the temperature monitoring system are shown below.

ONSET HOBO 4-channel Thermocouple Data Logger (#UX120-014M)
Accuracy: ±0.21˚C from 0˚ to 50˚C (±0.38˚F from 32˚F to 122˚F)
Resolution: 0.024˚C at 25˚C (0.04˚F at 77˚F)

ONSET Type K 6 ft Beaded Thermocouple Sensor (#TC6-K)
Accuracy: ±2.2˚C (±4˚F)

2. Setup

The data logger, in addition to logging data, also has a temperature sensor. This sensor was used to monitor the lab temperature over the course of the experiments. The tip of the beaded thermocouple sensor was placed inside the mechanical or transport test chambers for the duration of the experiment. In all cases, the logger was set to record temperature once every 30 seconds.

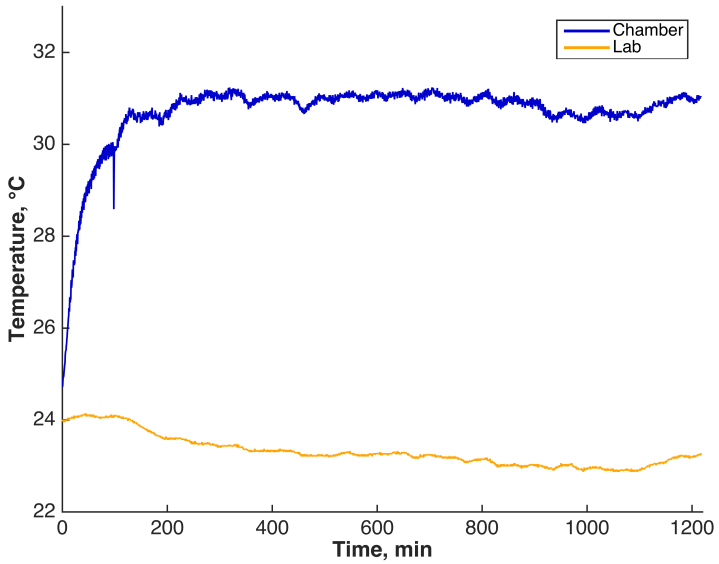

Figure 21. Temperature during a typical transport experiment. This plot shows that the temperature inside the transport chamber heats up to above room temperature. As soon as the magnetic stir plate has been turned on (t_0), the temperature inside the chamber gradually increases over about 2 hours. After that initial increase, the temperature remains steady for the remainder of the experiment, varying by less than 1˚C after the first 2 hours (30.39˚C – 31.25˚C). In the very first transport runs, the magnetic stir plate was covered with a 2.6 mm thick layer of foam rubber. These runs had chamber temperatures of about 33˚C (data not shown). In an attempt to decrease the temperature, a thick layer (23 mm) of Styrofoam was added on top of the foam rubber. The chamber temperature in this plot is representative of the temperature when the chamber is separated from the magnetic stir plate by both the foam rubber and Styrofoam. Adding the Styrofoam layer did decrease the temperature, but did not bring the chamber temperature back down to room temperature. Because of the length of the transport experiments and the logistical issues associated with trying to continually cool the chamber to room temperature, it was decided to run the experiments at the increased temperature (~31˚C). Although the temperature did increase, once it reached the higher value it remained constant and this trend was repeatable across experiments. For these reasons, combined with the fact that transport values in cartilage have been shown to scale with temperature according to the Stokes-Einstein relation (Eqn. 2)[111,108], running the experiments at an increased temperature does not compromise or cloud the data interpretation.

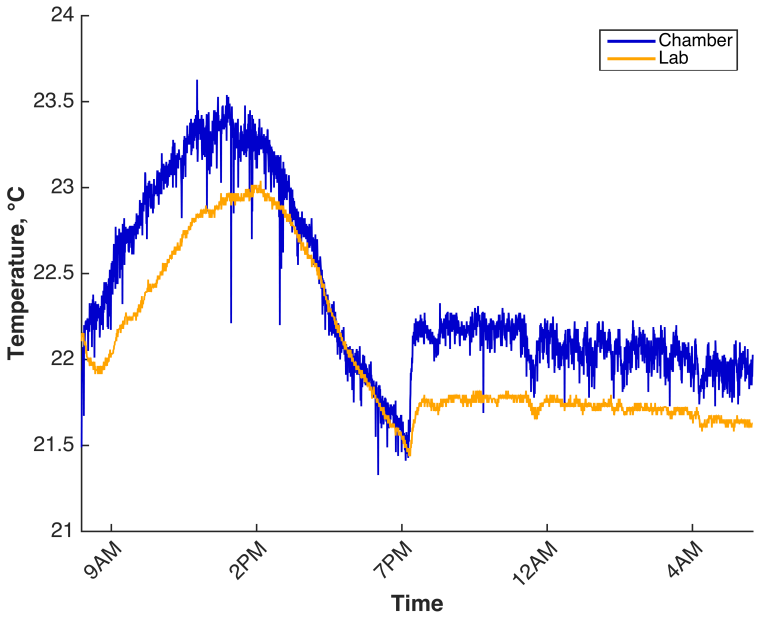

Figure 22. Temperature during a typical mechanical stress relaxation experiment. This plot shows the general trends seen in most of the temperature data collected during mechanical stress relaxation runs. At around 9 am, the temperature in the room starts to increase. The temperature peaks around 12 pm and then decreases until mid to late evening (7 – 9 pm). The jump that is seen in this graph showed up in several temperature plots at around the same time. This may be the time when the heating system of the building is programmed to kick on, causing a more sudden change in temperature. After the jump, the temperature holds steady for the remainder of the night and early morning. The temperature inside the chamber is shifted up by about 0.5˚C compared to that of the lab. This is likely due to the fact that liquid inside the chamber is being continually mixed, which creates a small amount of heat. This plot shows that the temperature in the dynastat room does change over the course of the day, however, it is only changing by about 2.1˚C (21.4˚C – 23.5˚C). The change is repeatable, but the magnitude is small. The most stable time for the temperature is during the late night and early morning hours, so if temperature is a concern for experiments, this would be the best time to conduct those experiments to minimize the effect of temperature.

8.5 Dynastat System Noise

1. Purpose

The long-term stress relaxation curves generated for this thesis exhibited noisiness. Additionally, when the temperature data for a given run was overlaid on the stress curve, there appeared to be some correlations between the shapes of the two. A small set of experiments was run to get a sense of the baseline noise inherent to the dynastat system and also to investigate a temperature/stress correlation effect. To tease out the system effects from the effects of cartilage, different materials were used in these tests.

2. Tests

Three different tests were run for this set of characterization experiments. Temperature was monitored for the duration of all these tests. The first experiment consisted of running the same protocol used for all the cartilage relaxation tests (Mechanical protocol), but with no sample in the chamber, just recirculating liquid. The second test was a simple

ramp and hold protocol using a hard plastic as the sample. The cartilage mechanical protocol couldn't be used on the plastic because it was too stiff and would have been outside the range of the load cell. The final test was to use rubber as a surrogate for cartilage in the same stress relaxation protocol.

3. Results

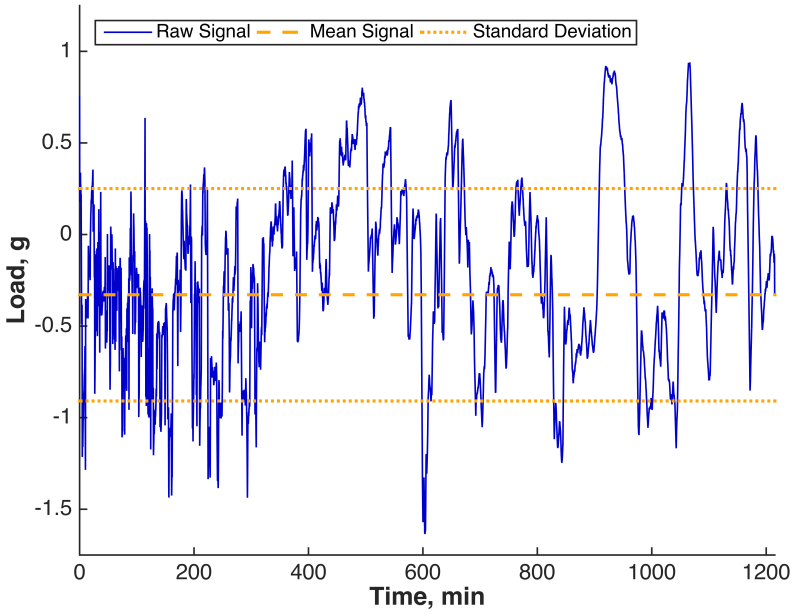

Figure 23. Dynastat system noise with no sample present. The data shown here represents the average values from two runs. During the 20¼ hours of this data collection, the platen attached to the load cell was stationary and only in contact with circulating 1x PBS; there was no sample in the test chamber. The reading of the load cell jumps around even in this negative control situation. The standard deviation of the load (shown by the dotted lines) was 0.58 g. Using Equation 3 and the area of the cartilage samples used for these tests ($7.07\times10^{-6}m^2$), the system noise in units of stress (kilopascal) is 0.8 kPa. Typical stress values for the cartilage samples during the 20¼ hour hold were 40 – 180 kPa, so the signal to noise ratio ranges from 50 to 225.

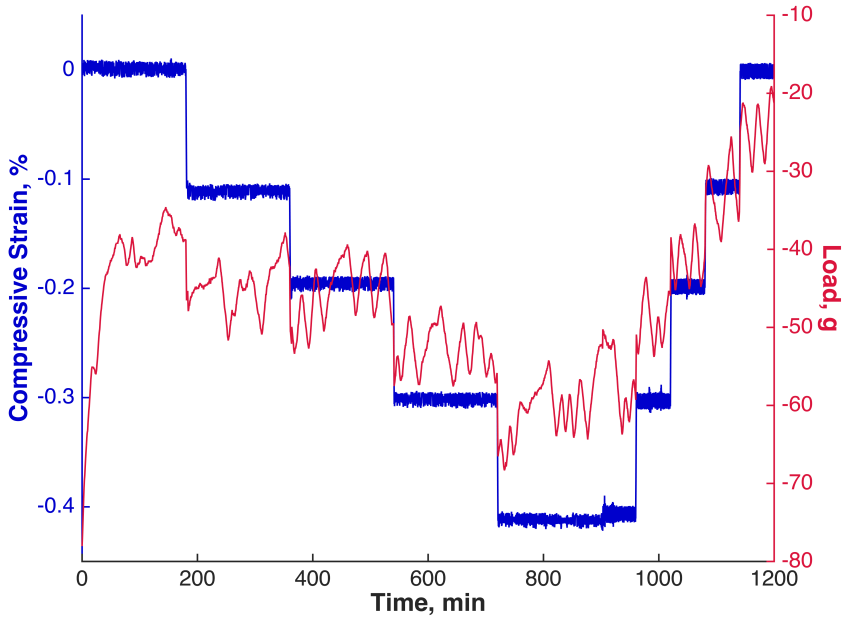

Figure 24. Strain and load values for hard plastic in the dynastat. The signal for the hard plastic in the dynastat system was noisy. For the fixed strain values, the load was expected to be constant over time, but instead the signal jumped around. No clear trend emerged showing a linear relationship between the strain and load. It is likely that even at these very small strains, the plastic is so stiff that it overwhelms the sensitive load cell and causes an unexpected response in the data.

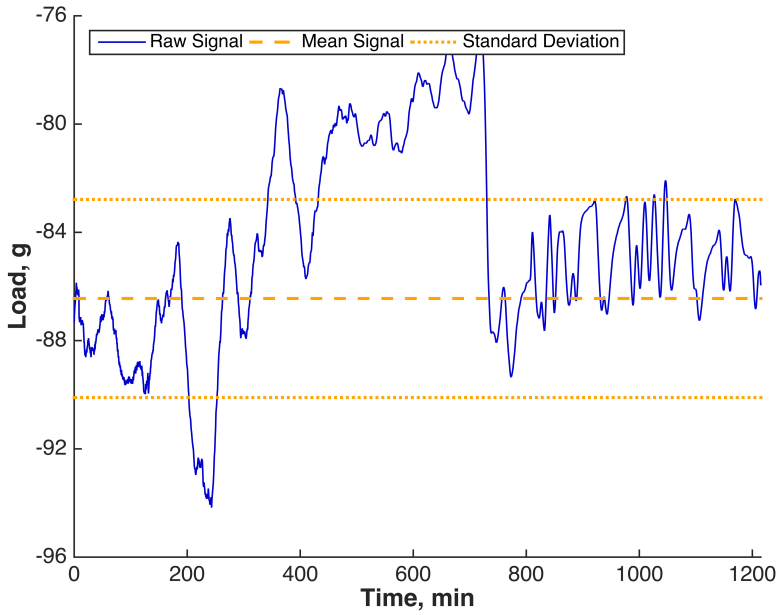

Figure 25. Load values for rubber in the dynastat system. During the 20¼ hours of this data collection, the platen attached to the load cell was held constant at 16% compressive strain of the original thickness of the rubber sample used. As with the no-sample negative control, the load signal varied even though the platen was stationary. The standard deviation for this data collection was 3.5698 g, which translates to 4.95 kPa for a sample with a diameter of 3 mm. This is an increase in noise compared to the no-sample test. The increase in noise could be due to the

dynastat system having a load-dependent noise response in which the noise increases with increasing load or it could be a product of the material properties of the rubber or a combination of both.

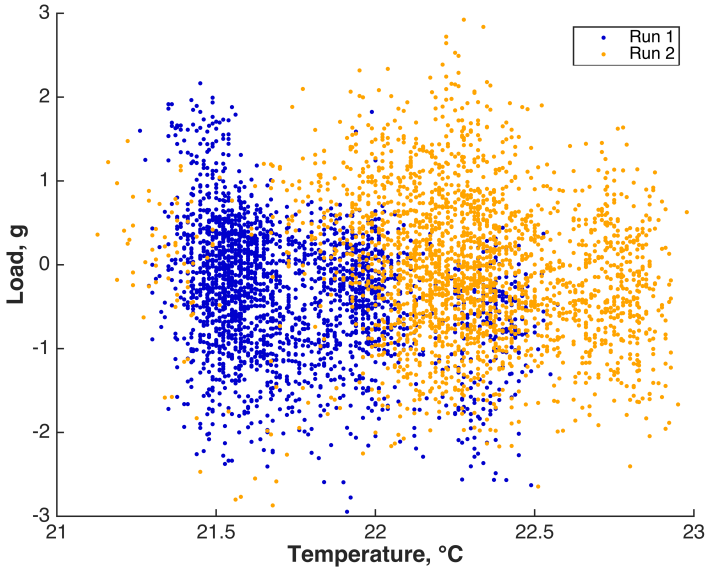

Figure 26. Load and temperature correlation for the dynastat with an empty chamber. The data from both no-sample tests are shown and represent the data collected during the 20¼ hold, shown in Figure 23. One hypothesis that was of interest for this set of experiments was to investigate whether or not an underlying correlation exists between the temperature in the room/test chamber and the reading of the load cell. This plot of temperature versus load for the empty chamber shows a cloud of data, with no clear trends of correlation. The temperature in the dynastat room does not appear to be correlated with the reading of the load cell.

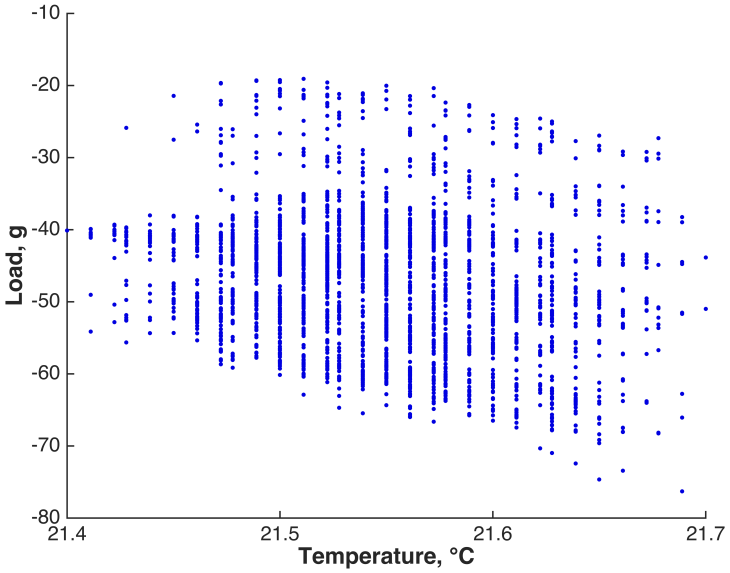

Figure 27. Load and temperature correlation for the dynastat with hard plastic. This plot shows the load and temperature data for the hard plastic over the duration of its data collection (Figure 24). Again there is no clear correlation between the temperature value and the reading of

the load cell. In the case of the hard plastic, for a given temperature the load value varies by as much as 40 g. Physically, this does not make sense if the hypothesis of temperature affecting the load value were true. If that hypothesis were true, one would expect to see load changing in a similar fashion to how the temperature changes.

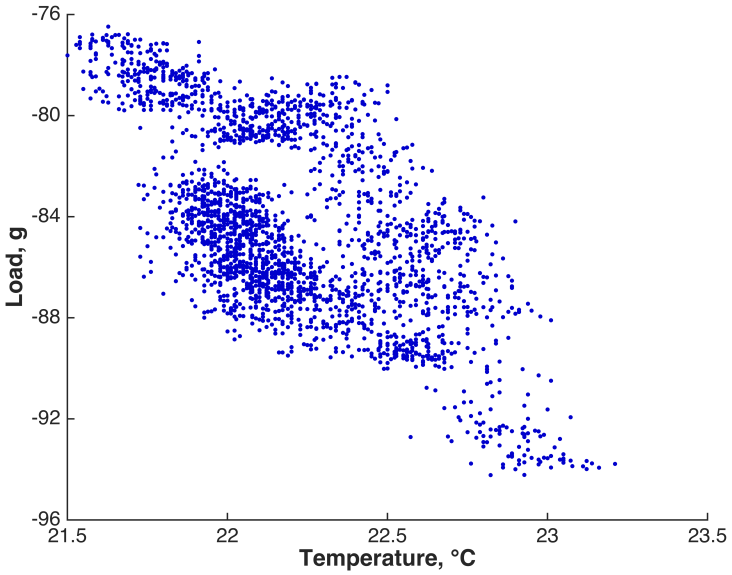

Figure 28. Load and temperature correlation for the dynastat with rubber. This plot shows temperature versus load for the rubber sample during the 20¼ hour hold at 16% compressive strain. For the rubber tested, there appears to be somewhat of a linear correlation between temperature and the load reading (correlation coefficient = 0.633). As the temperature increases, the load becomes more negative, meaning an increase in the compressive stress. The convention of the dynastat system is to assign negative values for compression, so a more negative load equates to a larger compressive stress. This correlation was anticipated as the modulus of rubber is known to depend on temperature[143]. Given the lack of correlation seen for the empty chamber and hard plastic, the correlation seen here is likely mostly a function of the material properties of the rubber rather than the response of the dynastat system.

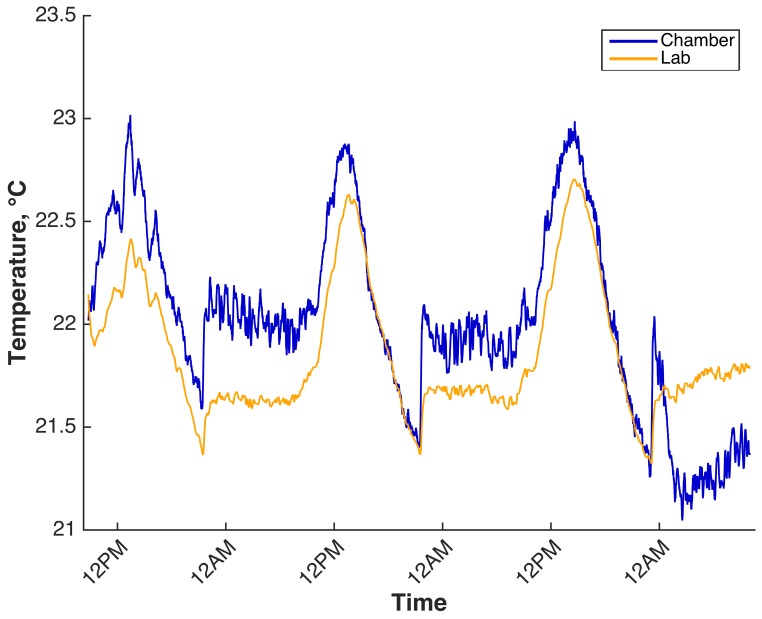

Figure 29. Temperature in the dynastat room over three days. This plot shows the continuous measurement of temperature in the dynastat room and chamber over the course of three consecutive days. Although the previously shown data for this set of experiments suggest that temperature is not correlated with the load cell reading, it is interesting to show the cyclic pattern of temperature in the dynastat room. Around 9 am each day, the temperature starts to increase. The peak temperature is around 12 pm and is followed by a steady decrease until around 9 pm when the temperature levels off for the night. The most stable period of time for the temperature occurs from around 9 pm to 9 am. It is also worth pointing out the scale on the y-axis of this graph. The temperature is only varying by about 2˚C over the course of the day.

8.6 Example Data Curves

1. Stress Relaxation

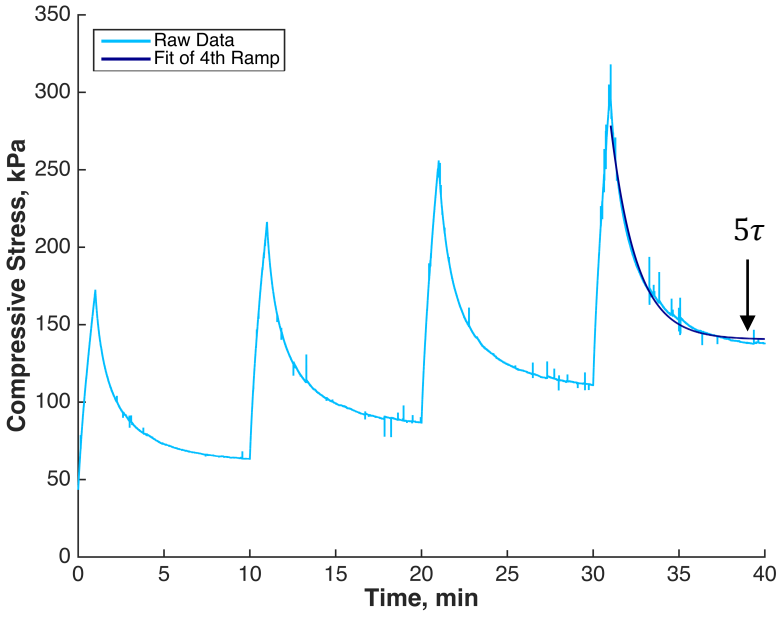

Figure 30. First four ramp and holds of mechanical protocol. The protocol used for the mechanical stress relaxation tests started out with a series of four strain ramps each followed by a relaxation period. The equilibrium stress at the end of each ramp along with its corresponding strain value were used to calculate the Young's modulus of the tissue. The 4th ramp was also used in the analysis (Data Analysis) of the long-term static hold data. A simple exponential decay model (Eqn. 4) was fit to the 4th ramp to determine the characteristic relaxation time, τ_4. The starting point for analysis of the long-term, constant strain relaxation was set at five time constants ($5\tau_4$) away from the peak of the 4th ramp, indicated by the arrow in the figure. Additionally, all the stress values of the constant strain hold were divided by the stress value at 5τ as a means of normalizing the data. The absolute stress values varied from sample to sample, so normalizing the data to range from 0 to 1 allowed for comparison between samples.

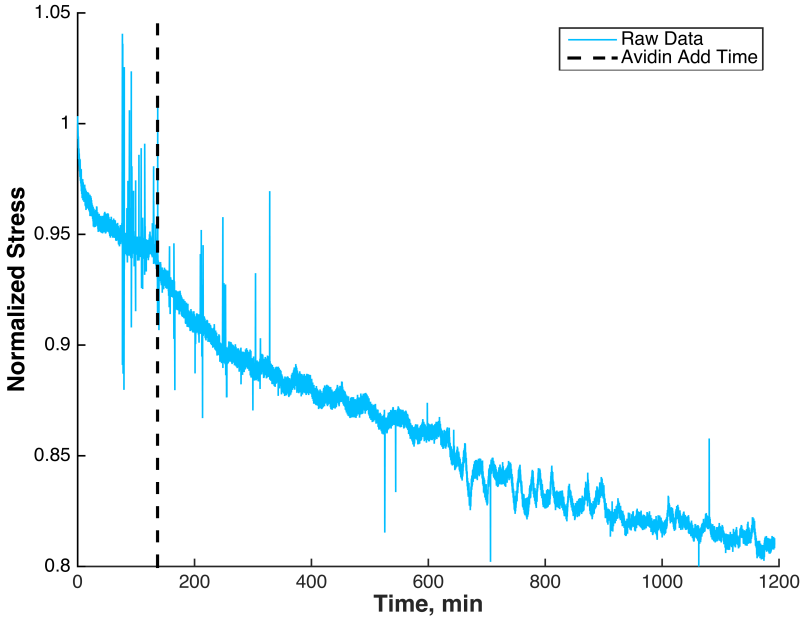

Figure 31. Raw signal of normalized compressive stress during 20-hour strain hold. After the 4th strain ramp and relaxation, the sample was held at constant strain for the next 20 hours. In negative control samples, those 20 hours were uninterrupted. For samples testing the effects of avidin, two hours into the hold, 167 µL of 100 mg/mL avidin was added to the test chamber (final concentration = 100 µM). The vertical dashed line in the figure represents the time location that avidin was added. The data in this graph starts $5\tau_4$ from the peak of the 4th ramp and the stress values have been normalized to the stress value at $5\tau_4$. This plots shows the large amount of noise that is present in the collected data. For analysis, the data was split into before and after the location of avidin addition and analyzed separately.

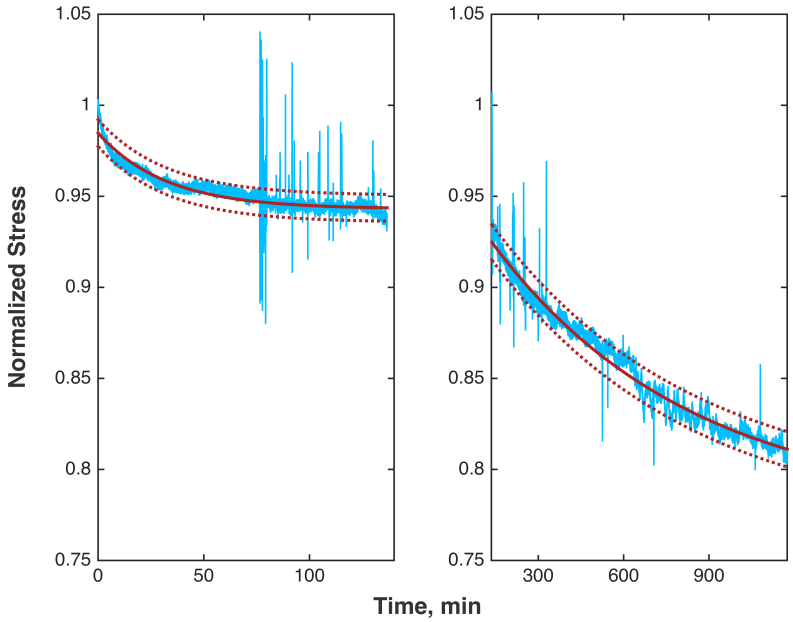

Figure 32. Before and after addition of avidin stress relaxation data. This figure shows the data from Figure 31 separated into before (left) and after (right) the addition of avidin. For the analysis of the stress relaxation data, an exponential decay model (Eqn. 4) was fit to both the before and after data. Comparisons of the parameter values from the model were made between samples at different salt concentrations and with or without avidin.

2. Transport

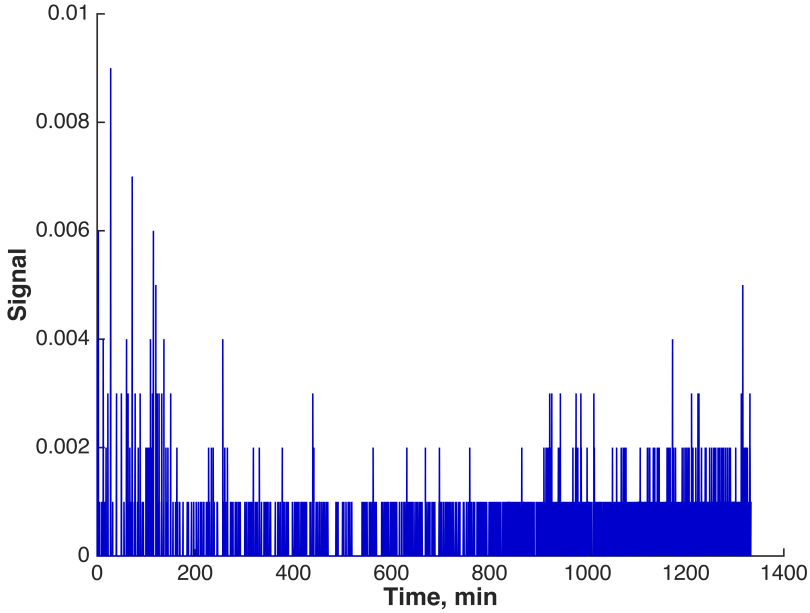

Figure 33. Transport chamber negative control, cartilage only. This plot shows the fluorescence over time in the downstream bath of the transport chamber when no FITC-avidin has been added to the upstream. This experiment was run to ensure that there was no autofluorescence in the transport setup and also that there was not an inherent linear drift in the signal of the

machine. The results indicate that there is some noise in the system, but the overall signal is very low and doesn't exhibit any clear trends or patterns.

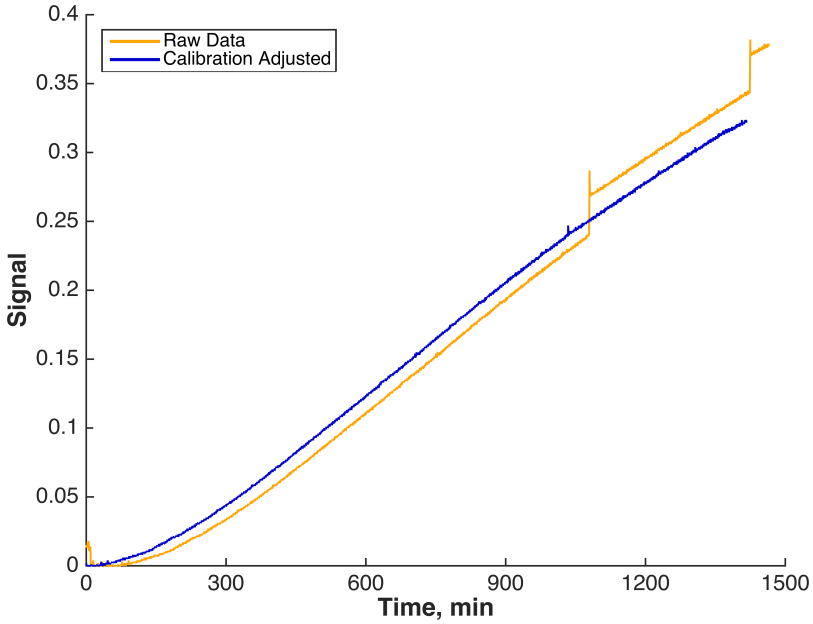

Figure 34. Example raw transport curve. This plot shows an example of a typical transport curve. The signal that is generated by the spectrofluorometer, the y-axis on this plot, is a ratio of an internal reference signal to the fluorescence signal detected by the machine. The orange curve in the graph shows the raw data from an experiment. The large jumps in the data represent calibration spikes. These spikes were done to determine the relative concentration in the downstream compared to the upstream. This was ultimately used as a measure of how much avidin passed through the cartilage. The blue curve has had the calibration spikes removed and has also been shifted to remove initial baseline data points at the beginning of the experiment. This curve was converted into a ratio of the downstream concentration to the upstream concentration and used in the determination of the transport parameters of avidin through cartilage.

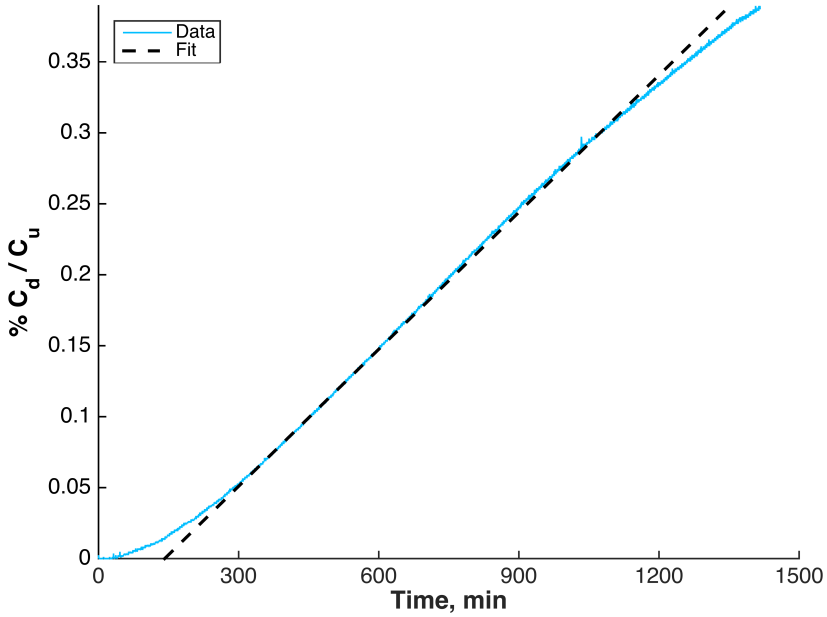

Figure 35. Example analyzed transport curve. This figure shows an example of transport data (bovine) that has ben converted into a ratio of downstream to upstream concentration. The dashed line has been fit to the linear region and its slope was used to determine the steady-state diffusivity of avidin through the tissue.

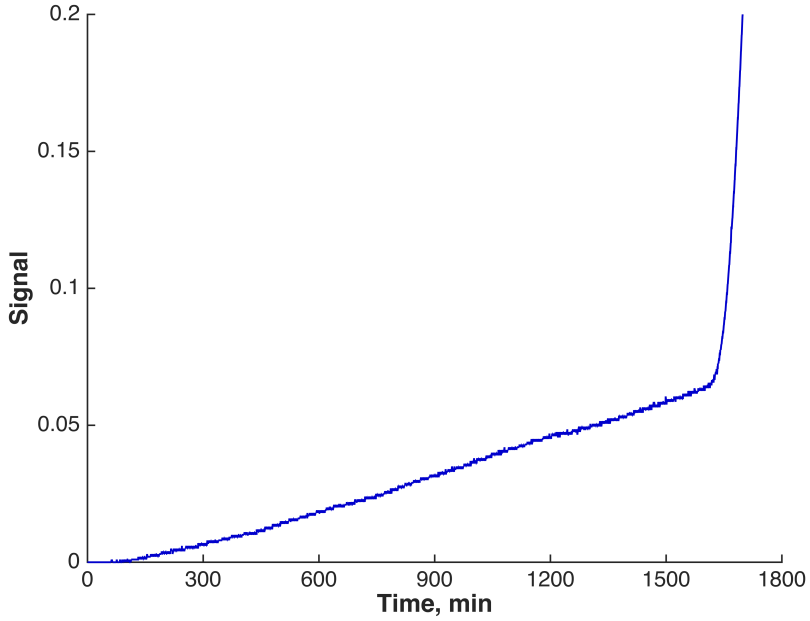

Figure 36. Addition of free fluorescein to the end of a transport experiment. To verify that the fluorescent signal being reported by the spectrofluorometer was representative of the FITC-avidin complex and not free fluorescein alone, free fluorescein was added to the upstream bath at the end of one transport experiment. The time of addition was just before the inflection point in the curve. The much steeper slope after the addition of free fluorescein represents faster diffusion, which

would be expected for the smaller, free fluorescein as compared to the FITC-avidin complex. This results suggests that the earlier signal was due predominantly to complex and not free fluorescein.

8.7 FITC-Avidin Standard Curve in Transport Chamber

1. *Purpose*

Before using the spectrofluorometer for transport experiments, a set of characterization tests was run. These tests were aimed at determining (1) whether or not the signal of the machine and the concentration of FITC-avidin were linearly related and (2) the range of detectable concentrations of the machine in the end-to-end setup.

2. *Setup*

The characterization tests were setup as if a transport experiment was being run, but a piece of rubber was placed where the cartilage would normally be to block off the upstream bath. Increasing amounts of FITC-avidin were added to the downstream bath and allowed to flow through the system until an equilibrium signal was reached. This final signal was used in the analysis.

3. *Results*

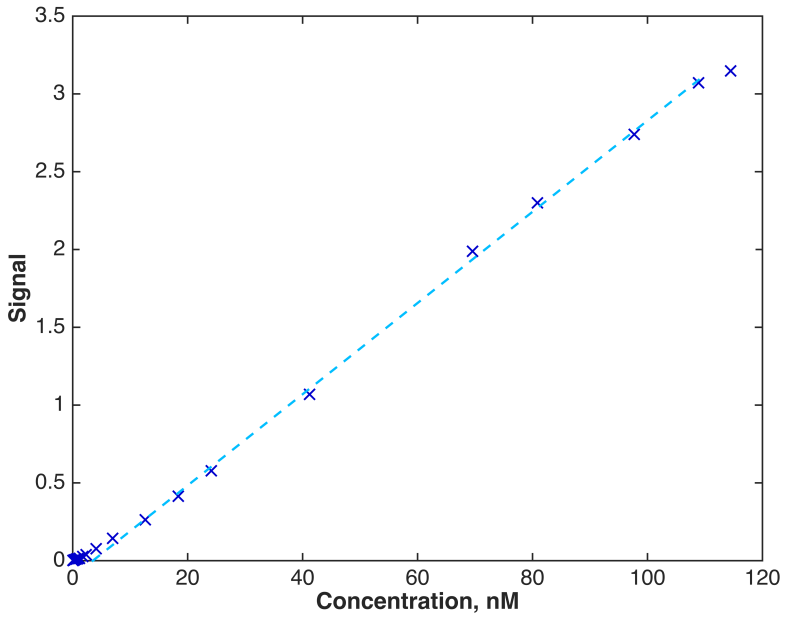

Figure 37. FITC-avidin standard curve in the transport chamber. The signal of the fluorometer and the concentration of FITC-avidin in the transport chamber have a strong linear relationship (R^2 = 0.9985). At about 110 nM of FITC-avidin, the fluorometer started to reach its saturation level as is evidenced by the flattening out of the final point in the graph. In transport experiments, the signal of the downstream bath increases over time. This linear relationship allows for that signal increase to be interpreted directly as an increase in FITC-avidin concentration. This graph shows a detection range of approximately 1 nM to 110 nM of FITC-avidin. This range is representative of the capabilities of the fluorometer, but the numbers are not absolute. Subsequent tests (data not shown) revealed that the exact signal-concentration pair of values varies from run to run. This is likely attributed to slight variations in the machine from day to day as it is zeroed for

each individual run. It is also worth noting that a similar standard curve was generated using just a cuvette inside the fluorometer (data not shown). Although experimentally this is easier, the results were quite different. The increase in signal was much steeper outside of the flow through transport setup.

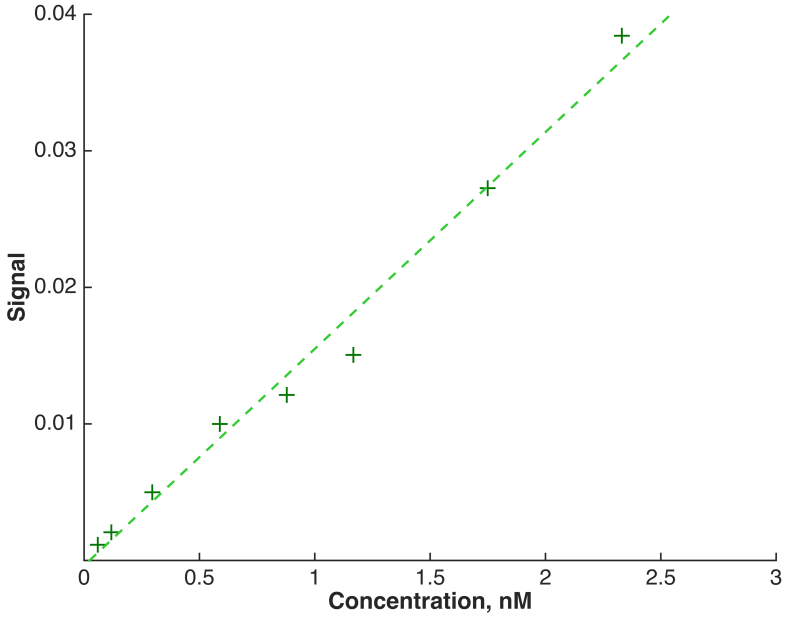

Figure 38. Zoom in on low concentrations of FITC-avidin standard curve in transport chamber. To hone in on the limit of detection, the lower end of the standard curve included many more concentrations that were spaced by smaller increments. At low concentrations, like with the whole curve, the fluorometer signal and concentration of FITC-avidin have a strong linear relationship (R^2 = 0.9855). The limit of detection of the fluorometer in the transport setup is approximately 0.06 nM. This level of sensitivity is beneficial for transport experiments because not a lot of FITC-avidin passes through the cartilage on short time scales, but this system is still able to detect that.

8.8 Dynamic Uptake Troubleshooting

1. Purpose

The transport experiments run for this thesis provided transport parameters for FITC-labeled avidin by measuring how the labeled protein moves through a slice of cartilage in 1D (see Figure 7). As an alternate measurement of these same parameters, running a set of dynamic uptake experiments was attempted. In this setup, a bath full of FITC-labeled avidin is the starting point. A baseline level of fluorescent signal is obtained and then pieces of cartilage are added to the bath. As the avidin diffuses into the cartilage, the fluorescent signal should decrease. In running these experiments, several issues were encountered and are outlined below.

2. Experiment Story & Timeline

Initially, full dynamic uptake experiments as described above were run using FITC-labeled avidin with human cartilage and then bovine cartilage. In both cases, the results

were unexpected. Several hours after the cartilage was added, the signal of the bath increased rather than decreased. The curves from these first 2 runs are shown in Figure 42.

To try to understand where the increase in signal was coming from, two negative control experiments were run. First, with the fluorometer set to the excitation and emission wavelengths of FITC, cartilage explants ***only*** were added to the bath, stirred and the fluorescence monitored. The curve of this experiment, labeled as *'Green Channel'*, is shown in Figure 39. Over the course of about 25 hours, the signal in the bath increased, suggesting that cartilage exhibits some auto-fluorescence in the green range. Although an increase was seen, its magnitude was not large enough to explain the behavior of the original two runs. A second negative control was then run to monitor the fluorescence of a bath containing ***only*** FITC-avidin, no cartilage added. This result (labeled *'Commercial'*) is shown in Figure 40. This negative control showed a large increase in signal over about 15 hours.

The main hypotheses for explaining the large signal increase in the second negative control centered on the commercial conjugation chemistry. It was learned through a conversation with a labmate that the method used (amine-isothiocyanate reaction) increases the likelihood of precipitation. The company's documentation also indicates that the linkage suffers from instability over time in water[144]. Precipitation of the FITC-labeled avidin could lead to pockets of high concentration of fluorescence that could throw off the detector reading. The instability of the conjugation could lead to FITC molecules being shed from the avidin over the course of the experiment. FITC is known to be a self-quenching fluorophore[145] and the manufacturer (ThermoFisher Scientific) reports a FITC to avidin ratio of ~4:1. If the FITC is coming off, self-quenching would no longer be occurring and the overall signal in the bath could increase. To this end, batches of in-house FITC-labeled and Rhodamine Red (RRx) labeled avidin were made using a different conjugation chemistry (EDC-NHS chemistry) and also a lower fluorophore to protein ratio.

These custom batches were first assessed in negative control tests where no cartilage was added. The results for the FITC-labeled are shown in Figure 40 and RRx-labeled are shown in Figure 41, both are designated as *'In-House'*. The FITC-labeled curve did not increase over time, instead the signal decreased by over half in 24 hours and still had not reached a visible equilibrium in that time. The hypothesis for this behavior was photo-bleaching of the fluorophore due to the constant excitation from the fluorometer. The RRx-labeled curve also decreased in signal, but leveled off after about 5 hours. An additional negative control was run to check whether or not cartilage autofluoresces in the red range. There was very little autofluorescence observed for red excitation/emission as seen in Figure 39.

The leveling off of the RRx-labeled avidin and the fact that cartilage didn't exhibit autofluorescence in the red range, led to a final attempt at the dynamic uptake experiment. In-house RRx-avidin was added to the bath and allowed to equilibrate for ~5 hours. Bovine cartilage explants were then added and the signal monitored for ~17 hours. The resulting curve is shown in Figure 42. The odd behavior of increased signal after the

addition of cartilage was seen again. Time did not allow for further investigation into this, however it seems that the combination of cartilage, fluorescently labeled avidin and aggressive mixing leads to a not yet determined interaction or reaction.

3. Results

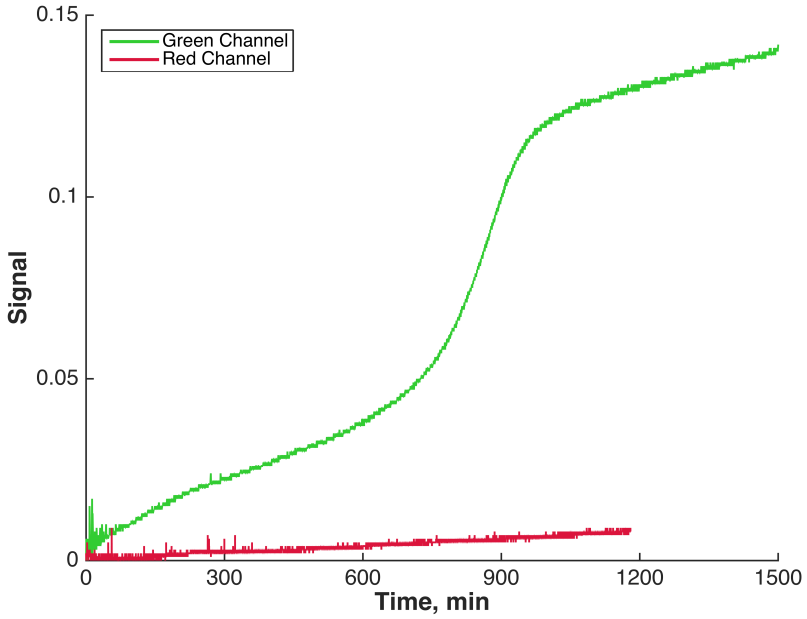

Figure 39. Autofluorescence of cartilage. Bovine cartilage was tested for autofluorescence in the dynamic uptake experimental setup. A zero baseline was first established for a bath containing only 1x PBS (no fluorescently labeled avidin). Then four explants of cartilage were added to the bath and the signal was monitored for 20-25 hours. The bath and explants were continuously mixed throughout the experiment using a magnetic stir bar as well as tubing that was circulating the liquid. This test was done in the green and red ranges (excitation/emission of 495/520 nm and 570/590 nm, respectively). Bovine cartilage exhibited autofluorescence in the green range, but not the red. The steep jump in the green range curve appears to indicate a time-dependence of the autofluorescence. During the experiment, the explants are aggressive mixed, so it is possible that they cartilage is breaking down to some degree and releasing the fluorescent signal. The cause of this signal has not been investigated in this work. The red signal did increase a little over the course of the experiment, but the overall signal was still very low by the end of 20 hours and wouldn't be expected to contribute significantly to an experiment that contained fluorescently labeled avidin.

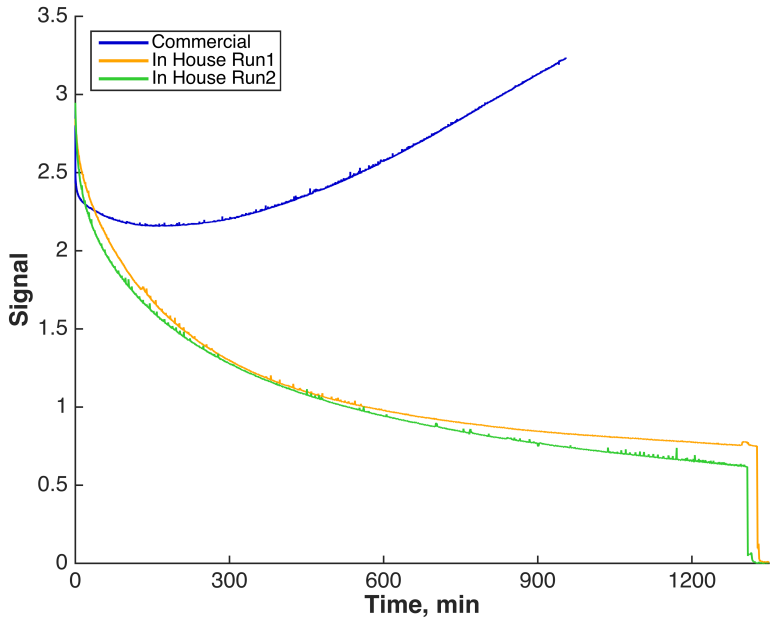

Figure 40. FITC-labeled avidin alone in dynamic uptake experimental setup. Two different types of FITC-labeled avidin were assessed in a negative control test in which the labeled avidin was added to the bath of the dynamic uptake setup, mixed and the signal monitored without any cartilage being added. The first FITC-avidin tested was a commercially-made (ThermoFisher Scientific) formulation in which ~4 FITCs were conjugated to each avidin via amine-isothiocyanate reaction chemistry. The blue curve in the plot represents the behavior of 37 nM of the commercial formulation over ~15 hours. Initially, the signal decreased as the solution was mixed, but by the end of the 15 hours, the signal increased past its starting point and reached the saturation level of the detector. Two hypotheses were developed in response to this behavior. One possible explanation for the increase in signal is that the FITC-avidin is precipitating and creating more concentrated pockets of signal that are throwing off the detector. Another idea is that FITC is being shed from the avidin and once liberated each FITC emits more strongly because other FITC molecules no longer quench it. The second FITC-avidin tested was a custom, in-house formulation (courtesy of Brett Geiger) that was made using EDC-NHS conjugation chemistry and attached ~1.75 FITC molecules per avidin. The orange and green curves in the figure show the behavior of 70 nM of the custom formulation over ~24 hours. The difference between Run1 and Run2 in the figure is that for Run2, the entire bath was vortexed after addition of the FITC-avidin before the signal was monitored. In both runs of the in-house formulation, the signal decreased for the entire experiment, with the curves not exhibiting a leveling off trend until 15 hours or longer. The drop-offs at the end of these curves represent the drop in signal that is seen as soon as the liquid is drained from the detector system. Possible causes of behavior are sticking of the FITC-avidin to the tubing between the bath and detector or photobleaching of the FITC over time due to the continual excitation. The end-to-end system was blocked with SuperBlock™ Blocking Buffer at the beginning to minimize sticking, but some could still be occurring.

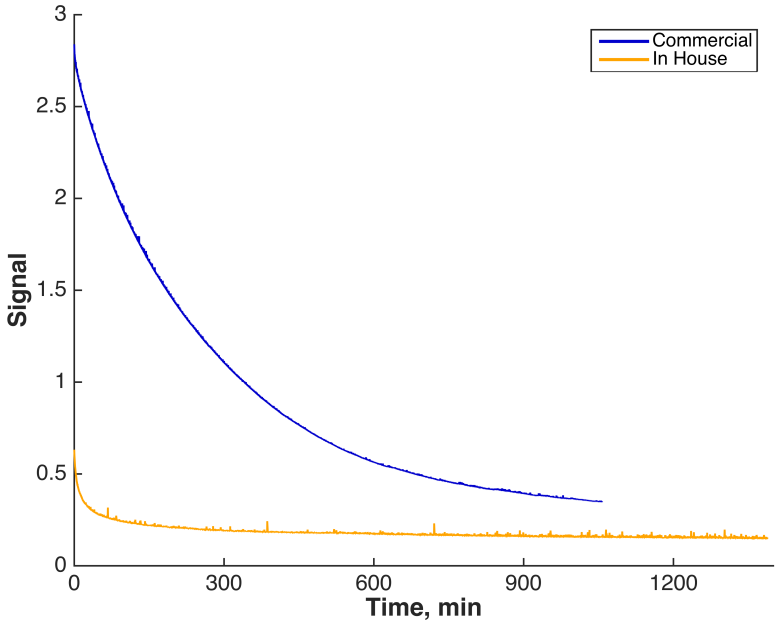

Figure 41. Red-labeled avidin alone in dynamic uptake experimental setup. This figure shows the results of the negative control experiment described above (Figure 40) for two different red-labeled avidin formulations. The commercially made formulation consisted of ~4 TexasRed (TxR) fluorophores conjugated to avidin. Shown by the blue curve, the initial signal of 250 nM of the commercial TxR-avidin was high, but dropped significantly over the 17.5 hours of monitoring and only starting exhibiting a leveling off trend near the end. This behavior could be attributed to a combined effect of mixing (the bath wasn't vortexed prior to signal monitoring) and sticking. The in-house formulation used Rhodamine Red (RRx) for the fluorophore and conjugated ~2.15 RRx per avidin using EDC-NHS chemistry. The orange curve in the figure shows the behavior of 137 nM of the in-house RRx-avidin. The starting signal is much lower than other formulations, but the signal starts to level off around 5 hours rather than 15+ like in other tests. The lower overall signal is likely due to the smaller fluorophore to avidin ratio.

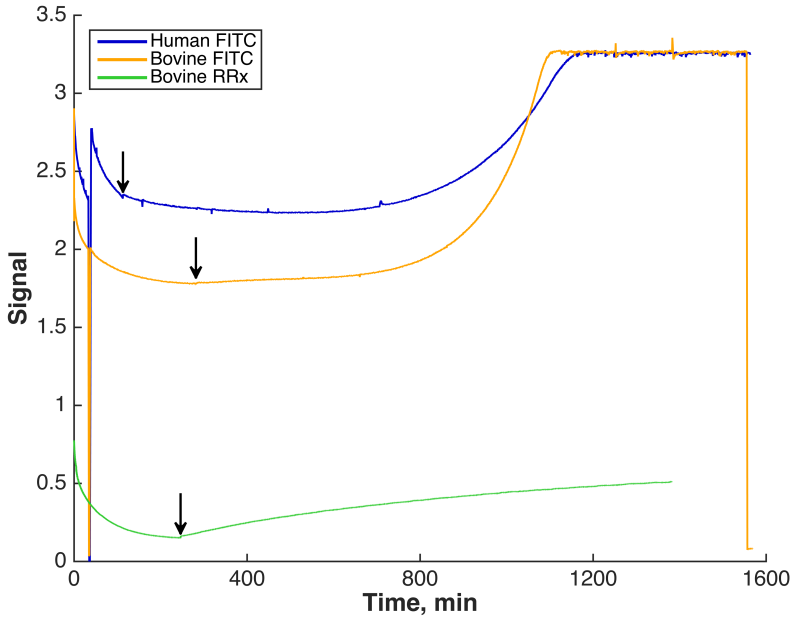

Figure 42. Three attempts at dynamic uptake experiment. This figure shows three different trials of the full dynamic uptake experiment. The blue and orange curves were the first two experiment run in this series and show what was observed using commercial FITC-avidin and human and bovine cartilage, respectively. The arrows indicate the time that the cartilage was added to the bath. The unexpected behavior of these curves prompted all the troubleshooting and control experiments shown in the preceding graphs of this section (Figure 39, Figure 40, Figure 41). The green curve shows the results of an additional attempt at the experiment after all the troubleshooting. The signal of the RRx-labeled avidin, when run alone, leveled off after about 5 hours. Also, cartilage did not show appreciable autofluorescence in the range of the RRx fluorophore. For these two reasons, a dynamic uptake experiment was attempted in these conditions. Despite the promising results of the control experiments, the same odd behavior of increased signal after the addition of cartilage was seen again. The signal didn't saturate the machine like the FITC experiments, but the overall signal started off much lower. Due to time constraints, the cause of this increase in signal was not investigated for this thesis.

8.9 Transport Parameter Measurement Methods

1. *Incubate and Slice*[107,108,109]

The incubate-and-slice setup is meant to mimic 1-dimensional diffusion of solutes into cartilage in a geometrical configuration that would be seen in a joint. Full-depth, cylindrical plugs (from cartilage superficial zone to subchondral bone) are laterally confined and a solution containing a tagged solute of interest is allowed to incubate on top of the superficial zone side of the sample for varying lengths of time. At the end of the incubation time, the same is briefly rinsed and then immediately frozen. A microtome is used to slice the sample into thin (~100 μm) disks. Each slice is then desorbed and the amount of solute in that slice is determined by measuring the solute-specific tag, typically either a radiolabel or fluorophore. Concentration-depth profiles are generated for the sample and then a transport model can be fit to the data to determine the transport properties of the solute such as diffusivity and partition coefficient.

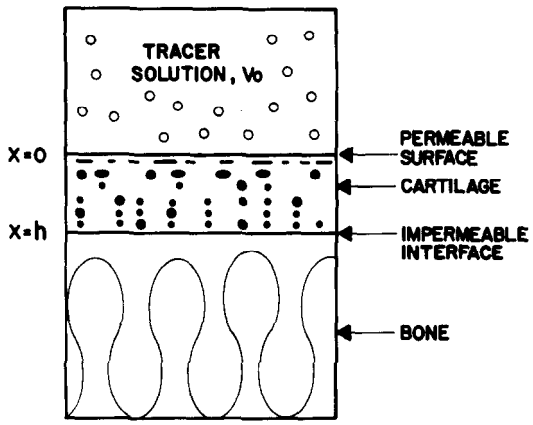

Figure 43. Setup for incubate-and-slice transport technique[107].

2. *Absorption/Desorption Bath Series*[110,111]

For this method, the cartilage sample is allowed to equilibrate in a bath containing a labeled solute for 24+ hours. After reaching equilibration, the sample is removed from the solute bath and transferred to a desorption bath(s) that contains only buffer, no additional solute. For experiments aimed at measuring diffusivity, the sample is transferred to multiple desorption baths at varying time intervals. For experiments trying to measure the partition coefficient, the sample is left in the same desorption bath until equilibrium is reached. In both cases, the amount of solute in the desorption bath(s) is measured by either counting radioactivity or measuring fluorescence intensity, depending on the label of the solute. The rate at which the solute desorbs (diffusivity) or the amount of solute in the desorption bath compared to the original absorption bath (partition coefficient) can be determined by fitting the data to transport models.

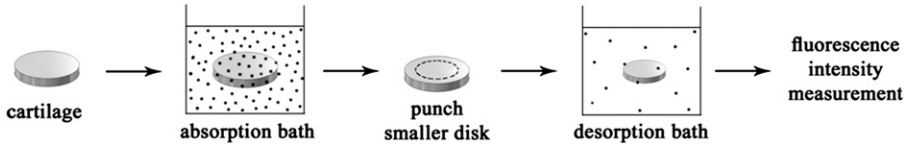

Figure 44. Procedure for absorb/desorb transport method[111]**.**

3. *Microscope and Photometer*[112,113,114]

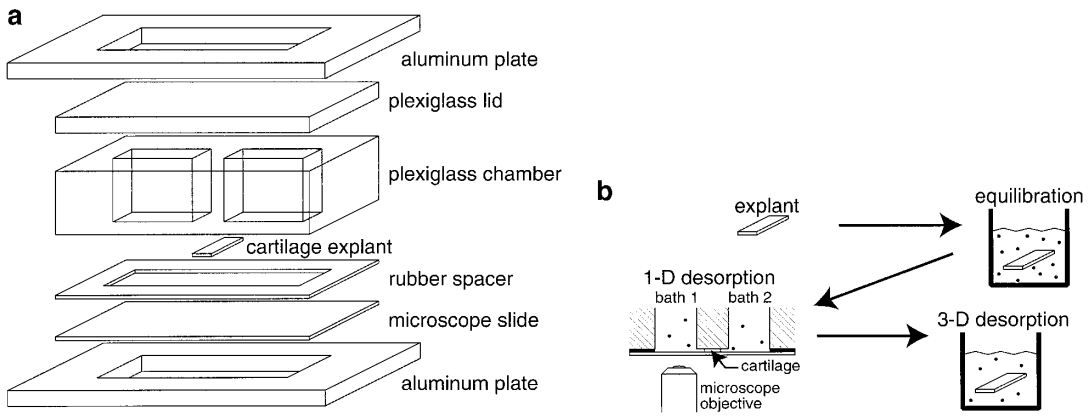

Figure 45. Microscope and photometer configuration for transport measurements[112]**.**

4. *Fluorescence Recovery After Photobleaching (FRAP)* [115,116]

Fluorescence recovery after photobleaching (FRAP) has also been used to measure diffusion of molecules in articular cartilage. Plugs of cartilage are first allowed to equilibrate (1-3 days at 4˚C) in a solution of buffer containing a fluorescently tagged molecule of interest. The sample and solute solution are brought to room temperature before the FRAP measurements are taken. The cartilage sample is loaded into a custom photobleaching/imaging chamber that is then filled with buffer (usually PBS or similar). An initial image is taken of the sample to serve as the background and starting fluorescence. A laser, set to the excitation wavelength of the fluorescent tag on the

molecule, is directed at a precise location and turned on to full power to bleach the fluorescence from that spot. A black spot, with radius equal to the radius of the laser, is visible on the sample. An image is taken immediately following the photobleaching and represents t_0 for the experiment. Subsequent images at different time points are taken to monitor fluorescence returning to the bleached location, which represents diffusion of the non-bleached molecules. The time it takes for the fluorescence to fully recover along with the radius of the bleached spot are used to determine the diffusion coefficient of the molecule.

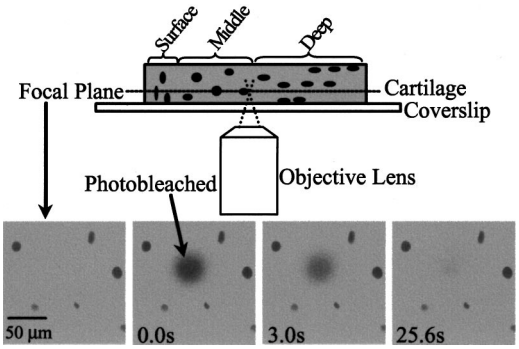

Figure 46. Setup for fluorescence recovery after photobleaching (FRAP) transport measurement method[116].

5. *Inline Downstream Bath Signal Monitoring*[117,118,119]

Another method of measuring transport properties involves the use of an inline solute detector. In this setup, thin disks (200 – 500 µm) of cartilage are sandwiched between an upstream and downstream chamber. O-rings around the circumference of the disks ensure that a seal is achieved between the two chambers and liquid can't flow freely between the chambers due to leaks in the setup. This makes it so that the only path for the solute from upstream to downstream is through the tissue. A buffer solution with no solute is put into the downstream chamber and a buffer solution containing a known amount of labeled solute is added to the upstream chamber. Both chambers are mixed and the liquid in the downstream chamber is continuously circulated between the chamber and the inline detector to monitor the flux of the solute into the downstream. The amount of label/solute in the downstream chamber is normalized to the concentration in the upstream chamber and the data can be fit to transport models to get parameters like steady-state diffusivity and effective diffusivity.

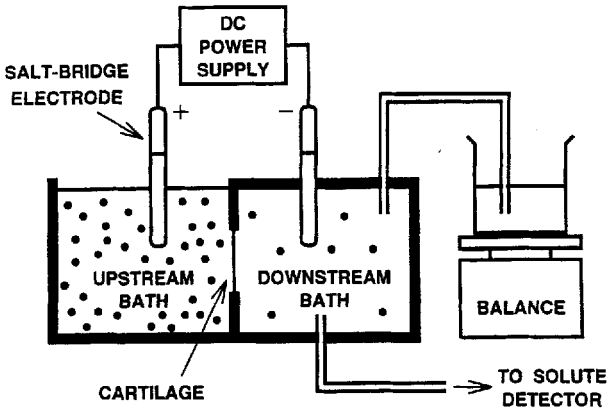

Figure 47. Inline detector transport method[119].

6. *Equilibrium Uptake*[117,118,119]

These experiments consist of allowing a cartilage sample to equilibrate (24+ hours) in a solution containing a labeled solute. The sample is then removed from that bath and the amount of solute that entered the sample is measured and compared to the starting bath concentration. The sample is also sometimes put into fresh buffer and allowed to desorb and re-equilibrate to determine how much of the solute leaves the cartilage. The purpose of the experiment is to determine the partition coefficient and also give an idea about whether or not the solute is binding inside the cartilage.

8.10 Experimental Lessons Learned

1. *Mechanical*
   - The temperature in the dynastat room varies throughout the day, but follows a fairly cyclic pattern from day to day
   - The system is very sensitive, even to movement in the room, I had more stable signals for long term holds when I timed the holds to take place during the night
2. *Transport*
   - Casein blocker is slightly negatively charged and has endogenous biotin—a bad combination for positively charged avidin
   - To get residual fluorescent signal out of transport chamber, scrub with soap and water, rinse, and repeat 2-3 times
   - Foam rubber is porous and absorbs some fluorescence that leeches out in subsequent runs if reused—use thin rubber instead and wash the same way as the chamber
   - The temperature inside the chamber increases to ~31˚C, even when elevated on 23 mm thick Styrofoam, because of the magnetic stir plate and bars
   - Technical issues: tubing can break which drains chamber (happens sometime between 24-48 hours); temperature probe can drain bath via capillary action if placed too far inside chamber; condensation can build up on top of chamber, helps to have vent holes in stoppers
3. *Dynamic Uptake*
   - Cartilage has some auto-fluorescence in the green range (FITC ex/em)

- The conjugation chemistry used by Life Technologies for FITC-Av either dissociates over time or aggregates—but either way increases in signal intensity over long time
- FITC is susceptible to photobleaching and its intensity is sensitive to changes in pH

8.11 Dynamic Uptake Protocol

What follows is the protocol that was used in the attempts at the dynamic uptake experiment. Future experiments can use this protocol as a starting point for protocol development.

Sample and setup preparation

Samples were thawed at room temperature for ≥ 30 minutes. While the samples equilibrated, all interior surfaces of the uptake tube were coated with SuperBlock™ Blocking Buffer and allowed to sit for ≥ 30 minutes. The thicknesses of the cartilage explants were measured in 2–3 locations, using digital calipers, and recorded.

Dynamic uptake

Test liquid (1x PBS) was added to the uptake tube and circulated through the spectrofluorometer using the same tubing and pump system that was used for the transport experiments for ≥ 30 minutes to establish a zero baseline. Then, FITC-labeled avidin was added to the bath, circulated through the system and allowed to come to an equilibrium signal. To ensure that the labeled avidin was not sticking to any parts in the detector, the system was quickly drained to make sure the signal dropped back to zero and then refilled. Once the signal leveled out again after refilling, 4–6 cartilage discs were added to the bath, marking time zero for the experiment. A magnetic stir bar in the bottom of the bath in combination with the tubing/pump system kept the experimental setup well mixed. The fluorescence signal was continuously monitored for the next 24 hours.

At the conclusion of the experiment, the bath liquid was saved at -20˚C and the cartilage samples underwent the same steps as previously described for the mechanical samples.